New studies on the versatile roles of Polyaniline and its composites in polymer based optoelectronic and energy storage devices

Thesis submitted to

Cochin University of Science and Technology

In partial fulfillment of the requirements for the award of

Doctor of Philosophy

By

Anand .P. B

Department of Physics,
Cochin University of Science & Technology,
Kochi- 682022, India

August 2015

New studies on the versatile roles of Polyaniline and its composites in polymer based optoelectronic and energy storage devices

Ph.D. thesis under Faculty *of Science* in the field of *Materials Science*

Author:

Anand .P.B

Ph.D. Research Scholar
Division for Research in Advanced Materials
Department of Physics
Cochin University of Science and Technology
Cochin-682022, Kerala, India
Email: anandputhirath@cusat.ac.in

Supervisor:

Dr. S. Jayalekshmi

Professor and Head, Department of Physics
Division for Research in Advanced Materials
Cochin University of Science and Technology
Cochin-682022, Kerala, India
Email: jayalekshmi@cusat.ac.in

August 2015

Department of Physics,
Cochin University of Science and Technology,
Kochi-682022, India

August 2015

Dr. S Jayalekshmi
Professor

Certificate

Certified that the work presented in the thesis entitled "*New studies on the versatile roles of Polyaniline and its composites in polymer based optoelectronic and energy storage devices*" is an authentic record of the research work done by Mr. Anand P.B. under my guidance and supervision in the Department of Physics, Cochin University of Science and Technology, Kochi-682022, and no part of it has been included in any other thesis submitted previously for the award of any degree.

Dr. S Jayalekshmi
Supervising Guide

Declaration

I hereby declare that the work presented in the thesis entitled "New studies on the versatile roles of Polyaniline and its composites in polymer based optoelectronic and energy storage devices" is based on the original research work done by me under the guidance and supervision of Dr. S Jayalekshmi, Professor, Department of Physics, Cochin University of science and Technology, Kochi-682 022 and no part of it has been included in any other thesis submitted previously for the award of any degree.

Anand .P.B

Kochi-682 022
August 2015

Department of Physics,
Cochin University of Science and Technology,
Kochi-682022, India

August 2015

Dr. S Jayalekshmi
Professor

Certificate

It is certified that all the corrections and modifications suggested during the pre-synopsis presentation, and duly recommended by the Doctoral Committee, have been incorporated in the Ph.D. thesis entitled "*New studies on the versatile roles of Polyaniline and its composites in polymer based optoelectronic and energy storage devices*" submitted by Anand .P.B, who has carried out his research work under my guidance and supervision in the Department of Physics, Cochin University of Science and Technology, Kochi-682022.

Dr. S Jayalekshmi
Supervising Guide

Nothing in life is to be feared, it is only to be understood. Now is the time to understand more, so that we may fear less.

- Marie Curie

If a man will begin with certainties, he shall end in doubts; but if he will be content to begin with doubts he shall end in certainties.

- Sir Francis Bacon

The path from dreams to reality does exist. May you have the vision to find it, the courage to get onto it, and the perseverance to follow it.

-Kalpana Chawla

Words of Gratitude…..

All through the past so many years I have been fortunate to be associated with a lot of people who have shaped my thinking and sharpened my logical understanding. From the class rooms to the research laboratory, it has been a long journey and each step has been taken with the encouragement of teachers. They have kindled in me the desire to learn and the courage to pursue my dreams. A mere 'thank you' cannot express my gratitude to them for having stood by me all these years.

Research has been an enriching experience and the able guidance of Dr. S. Jayalekshmi, Professor and Head, Department of Physics, Cochin University of Science and Technology has been my strength. Her relentless encouragement, benevolent support and scholarly sustentions have helped me at every stage of my work. She has appreciated my suggestions and boosted my confidence to take up challenging tasks. In all my walks through the dark worlds of doubts and uncertainties, she lighted the way and showed the way. I thank her profusely with the realization that no words can properly express my indebtedness to her.

I am extremely thankful to Prof. B. Pradeep and Prof. M. R. Anantharaman, former Heads of the Department of Physics for providing all the necessary facilities and environment to carry out fruitful research. I have been privileged throughout the period of research work to be associated with Prof. M. K. Jayaraj, Department of Physics. He has extended his helping hand when ever needed, and guided me through the course of research work. In fact, words are inadequate to express my sincere gratitude to Jayaraj Sir. I take this opportunity to thank all the faculty members of the Department of Physics, for their encouragement and cooperation.

I convey my sincere thanks to the administrative, library and laboratory staff of the Department of Physics for their help and assistance.

I take this opportunity to thank Dr. Gouri C, Head, Li-ion Cells Division and Dr. Bibin John, Scientist, Li-ion Cells Division of Vikram Sarabhai Space

Centre, Trivandrum for giving me the opportunity to work in the 'In Stuff Laboratories' of VSSC for making Li-ion cells and their testing. I acknowledge with gratitude the cooperation extended to me by the co-workers of Li-ion Cells Division.

I consider myself fortunate to have been associated with Dr. Reji Philip, RRI Banglore during my research work. He has been a well-wisher and a strong motivator. Thank you sir, for your generous support. The help extended by Dr. Suchand Sandeep C.S, RRI Bangalore is also gratefully acknowledged.

My special thanks to Dr. Rajive M. Tommy, Dr. Sreekanth J. Varma, Dr. Sreevalsa V.G, Dr. Sajimol Augustine, Dr. Jeeju Sukeshan, Mr. Anilkumar K. M, Mr. Manoj, Mr. Abhilash, Mrs. Jinisha B, Mrs. Saheeda, Mrs Sabira and Mrs Ranjini R Mohan, who have made the research atmosphere of the Division for Research in Advanced Materials Laboratory (DREAM Lab) fruitful and enriching. These friends, through their love, support and encouragement have made my research journey happy and comfortable.

Though I would like to acknowledge all the research scholars of the Department of Physics for their help personally, I prefer a 'thank you' due to the length of the list. Let me take this opportunity to the thank Dr. Prathapan. S. Associate Professor, Department of Applied Chemistry for his timely help and support in making conclusive remarks on certain key chemical reactions and sketching their reaction mechanisms. My wife, Mrs Nithya in the Department of Applied Chemistry deserves a special mention for her help and support with the chemical characterization procedures.

It is my pleasure to thank Prof. Ravindranathan Kartha, NIPER Chandigarh, Prof. Murukeshan Vadakkematham, NTU Singapore and Prof. Feo Kusmartev, Loborough University, UK for their constant help and encouragement throughout my research career.

The financial assistance provided by the Board of Research in Nuclear Sciences in the form of JRF-SRF is gratefully acknowledged. The travel grant support extended by the International Society for Optics and Photonics (SPIE), USA to participate in the Annual Leadership Workshop and SPIE Optics +

Photonics 2013 Conference at San Diego CA, USA and by the Department of Science and Technology (DST), Govt. of India to participate in the International Conference on Optoelectronics, Photonics and Applied Physics (OPAP-2013) held in Singapore is also acknowledged with gratitude.

I dedicate this thesis to Nithya, my sweet heart, Sarasu Anarkottle, my mother, Balan Puthirath, my father, Aravind Puthirath, my inspiring brother, Arathy Puthirath, our little squirrel and Rajesh Kumar, my brother in law, who have supported me all these years and given me the strength to fulfill my dreams. Without the unconditional love and emotional backing given by my family, I would never have been able to complete the research work in the way I wanted.

I bow in reverence before the *supreme power* for the blessings showered upon me.

Contents

Synopsis

From the early stages of the twentieth century, polyaniline (PANI), a well-known and extensively studied conducting polymer has captured the attention of scientific community owing to its interesting electrical and optical properties. Starting from its structural properties, to the currently pursued optical, electrical and electrochemical properties, extensive investigations on pure PANI and its composites are still much relevant to explore its potentialities to the maximum extent. The synthesis of highly crystalline PANI films with ordered structure and high electrical conductivity has not been pursued in depth yet. Recently, nanostructured PANI and the nanocomposites of PANI have attracted a great deal of research attention owing to the possibilities of applications in optical switching devices, optoelectronics and energy storage devices.

The work presented in the thesis is centered around the realization of highly conducting and structurally ordered PANI and its composites for applications mainly in the areas of nonlinear optics and electrochemical energy storage. Out of the vast variety of application fields of PANI, these two areas are specifically selected for the present studies, because of the following observations. The non-linear optical properties and the energy storing properties of PANI depend quite sensitively on the extent of conjugation of the polymer structure, the type and concentration of the dopants added and the type and size of the nano particles selected for making the nanocomposites. The first phase of the work is devoted to the synthesis of highly ordered and conducting films of PANI doped with various dopants and the structural, morphological and electrical characterization followed by the synthesis of metal nanoparticles incorporated PANI samples and the detailed optical characterization in the linear and nonlinear regimes.

The second phase of the work comprises the investigations on the prospects of PANI in realizing polymer based rechargeable lithium ion cells with the inherent structural flexibility of polymer systems and environmental safety

and stability. Secondary battery systems have become an inevitable part of daily life. They can be found in most of the portable electronic gadgets and recently they have started powering automobiles, although the power generated is low. The efficient storage of electrical energy generated from solar cells is achieved by using suitable secondary battery systems. The development of rechargeable battery systems having excellent charge storage capacity, cyclability, environmental friendliness and flexibility has yet to be realized in practice. Rechargeable Li-ion cells employing cathode active materials like $LiCoO_2$, $LiMn_2O_4$, $LiFePO_4$ have got remarkable charge storage capacity with least charge leakage when not in use. However, material toxicity, chance of cell explosion and lack of effective cell recycling mechanism pose significant risk factors which are to be addressed seriously. These cells also lack flexibility in their design due to the structural characteristics of the electrode materials.

Global research is directed towards identifying new class of electrode materials with less risk factors and better structural stability and flexibility. Polymer based electrode materials with inherent flexibility, stability and eco-friendliness can be a suitable choice. One of the prime drawbacks of polymer based cathode materials is the low electronic conductivity. Hence the real task with this class of materials is to get better electronic conductivity with good electrical storage capability. Electronic conductivity can be enhanced by using proper dopants. In the designing of rechargeable Li-ion cells with polymer based cathode active materials, the key issue is to identify the optimum lithiation of the polymer cathode which can ensure the highest electronic conductivity and specific charge capacity possible.

The development of conducting polymer based rechargeable Li-ion cells with high specific capacity and excellent cycling characteristics is a highly competitive area among research and development groups, worldwide. Polymer based rechargeable batteries are specifically attractive due to the environmentally benign nature and the possible constructional flexibility they offer. Among polymers having electrical transport properties suitable for rechargeable battery applications, polyaniline is the most favoured one due to

its tunable electrical conducting properties and the availability of cost effective precursor materials for its synthesis.

The performance of a battery depends significantly on the characteristics of its integral parts, the cathode, anode and the electrolyte, which in turn depend on the materials used. Many research groups are involved in developing new electrode and electrolyte materials to enhance the overall performance efficiency of the battery. Currently explored electrolytes for Li ion battery applications are in liquid or gel form, which makes well-defined sealing essential. The use of solid electrolytes eliminates the need for containment of liquid electrolytes, which will certainly simplify the cell design and improve the safety and durability. The other advantages of polymer electrolytes include dimensional stability, safety and the ability to prevent lithium dendrite formation. One of the ultimate aims of the present work is to realize all solid state, flexible and environment friendly Li-ion cells with high specific capacity and excellent cycling stability. Part of the present work is hence focused on identifying good polymer based solid electrolytes essential for realizing all solid state polymer based Li ion cells.

The present work is an attempt to study the versatile roles of polyaniline in two different fields of technological applications like nonlinear optics and energy storage. Conducting form of doped PANI films with good extent of crystallinity have been realized using a level surface assisted casting method in addition to the generally employed technique of spin coating. Metal nanoparticles embedded PANI offers a rich source for nonlinear optical studies and hence gold and silver nanoparticles have been used for making the nanocomposites in bulk and thin film forms. These PANI nanocomposites are found to exhibit quite dominant third order optical non-linearity. The highlight of these studies is the observation of the interesting phenomenon of the switching between saturable absorption (SA) and reverse saturable absorption (RSA) in the films of Ag/PANI and Au/PANI nanocomposites, which offers prospects of applications in optical switching.

The investigations on the energy storage prospects of PANI were carried out on Li enriched PANI which was used as the cathode active material for

assembling rechargeable Li-ion cells. For Li enrichment or Li doping of PANI, *n*-Butyllithium (*n*-BuLi) in hexanes was used. The Li doping as well as the Li-ion cell assembling were carried out in an argon filled glove box. Coin cells were assembled with Li doped PANI with different doping concentrations, as the cathode, $LiPF_6$ as the electrolyte and Li metal as the anode. These coin cells are found to show reasonably good specific capacity around 22mAh/g and excellent cycling stability and coulombic efficiency around 99%. To improve the specific capacity, composites of Li doped PANI with inorganic cathode active materials like $LiFePO_4$ and $LiMn_2O_4$ were synthesized and coin cells were assembled as mentioned earlier to assess the electrochemical capability. The cells assembled using the composite cathodes are found to show significant enhancement in specific capacity to around 40mAh/g. One of the other interesting observations is the complete blocking of the adverse effects of Jahn-Teller distortion, when the composite cathode, PANI-$LiMn_2O_4$ is used for assembling the Li-ion cells. This distortion is generally observed, near room temperature, when $LiMn_2O_4$ is used as the cathode, which significantly reduces the cycling stability of the cells.

In order to fulfill the aim of realizing all solid state and flexible Li-ion cells with good electrochemical performance, a Li ion conductor with appreciable ionic conductivity and structural flexibility in the solid state is essential. Polyethelene oxide (PEO) doped with *n*-Butyllithium in hexanes was synthesized and subjected to detailed investigations. The Li doped PEO could be identified as one of the best solid polymer electrolytes with quite high ionic conductivity at room temperature in the range of $1.53x10^{-3}$ S/cm, and with high prospects of application in the realization of all solid state and flexible Li-ion cells. Proto type, flexible and all solid state pouch cells using Li doped PANI as cathode, Li doped PEO as electrolyte and thin layer of graphite as anode could be assembled. The flexibility of these cells could be confirmed from the retention of the open circuit voltage of the cells with bending through various angles from the initial state.

The present thesis is divided into ten chapters. The first chapter gives an introductory approach to polyaniline (PANI), emphasizing the importance of the dopants in determining the conjugated structure, the crystallinity and the

structure related electrical, electrochemical and optical properties. An overview of nonlinear optics and Li-ion based energy storage, the two application fields of PANI addressed in the present work, is also presented in this chapter. The chapter is concluded with the highlights on the motivation and the objectives of the investigations presented in the thesis.

The second chapter gives a detailed account of the techniques employed for synthesizing highly conducting PANI, PANI-metal nanocomposites, Li doped PANI, composite cathodes based on PANI and $LiFePO_4$ and $LiMn_2O_4$ and the solid polymer electrolyte, Li doped PEO. An account of the various characterization techniques employed is also addressed in this chapter. These techniques mainly include XRD, FTIR and Raman spectroscopy for structural characterization, FESEM and AFM for morphological and surface studies and EDAX and AES for elemental composition analysis. The optical characterization in the linear and non-linear regimes has been carried out using UV-visible absorption spectroscopy and open aperture Z-scan technique. Cyclic voltammetry and charge-discharge cycling are the techniques used for analyzing the electrochemical capability and the cycling stability of the assembled Li-ion cells. Impedance measurements in the frequency range 20 Hz to 2 MHz have been employed to assess the ionic conductivity of the solid polymer electrolyte based on Li doped PEO and the four probe DC conductivity set up has been used for the electrical conductivity measurements on the various conducting PANI samples.

The third chapter is devoted to the investigations on highly crystalline PANI films showing appreciably good electrical conductivity. Emeraldine salt form of polyaniline (PANI) was synthesized by chemical oxidative polymerization method using ammonium persulfate (APS) as oxidant. Resultant emeraldine salt form of PANI was de-doped using ammonia solution and then re-doped with camphor sulphonic acid (CSA), naphthaline sulphonic acid (NSA), hydrochloric acid (HCl) and m-cresol. Thin films of these doped PANI samples were deposited on glass substrates using solution casting method with m-cresol as solvent. A level surface was employed to get homogeneous thin films of uniform thickness. Detailed X-ray diffraction studies show that these films are exceptionally crystalline. The crystalline peaks observed in the XRD

spectra can be indexed to simple monoclinic structure. The exceptional crystallinity observed in these polymer films can be confirmed from FTIR and Raman spectroscopy studies and FESEM and AFM images give better details of the surface morphology of doped PANI films. The DC electrical conductivity of the samples was measured using four point probe technique. It is seen that, the samples also exhibit quite high DC electrical conductivity, about 287 S/cm for CSA doped PANI, 67 S/cm for NSA doped PANI 65 S/cm for HCl doped PANI and just below 1 S/cm for m-cresol doped PANI. Effect of using the level surface for solution casting is studied and correlated with the observed crystallinity of PANI films.

In chapters four and five, the synthesis of gold and silver nanoparticles embedded PANI, both in bulk and thin film forms and their optical characterization in the linear and nonlinear regimes are addressed. The presence of surface plasmon resonance (SPR) and surface enhanced Raman scattering (SERS) shown by the metal nanoparticles has been established from the optical absorption studies and Raman studies. The third order optical nonlinearity has been studied in these nanoconposites in both solution and film forms using single-beam open aperture Z-scan technique. The results show that the nanocomposite films have very good optical limiting properties and can be of applications in the designing of suitable optical limiters. One of the highlights of the present work is the observation of the switching from SA to RSA in the nanocomposite films which offers prospects of applications in optical switching.

Chapter six describes the suitability of using *n*-Butyllithium, a cost effective substitute for expensive counterparts like $LiPF_6$ and $LiBF_4$, for synthesizing Li substituted polyaniline to be used as the cathode active material in rechargeable Li ion cells. Lithium substituted PANI samples were synthesized for three different concentrations of *n*-BuLi (LiPO 1, LiPO 2 and LiPO 3) and were subjected to detailed structural characterization using XRD, FTIR and SEM techniques. The structural analysis confirms the enhanced crystallinity/order in Li substituted samples compared to pure PANI. The coin cells assembled using Li substituted PANI as cathode show quite good electrochemical behaviour. Specific capacity close to the expected theoretical

capacity has been obtained for the cells with 15% lithium substitution. The specific capacity shows an increasing trend with increasing Li doping concentration. All the three assembled cells show excellent coulombic efficiency above 98% and stable charge discharge cycling behaviour up to 50 cycles. The cells are capable of showing stable cycling behaviour above 1000 cycles and it may not be surprising if these cells are found to withstand 1000-2000 charge discharge cycles without significant capacity loss.

The specific capacity of the Li-ion cells assembled using lithium doped PANI as the cathode active material is low compared to industrial standards. To improve the capacity, composite cathode materials of PANI with $LiFePO_4$ and $LiMn_2O_4$ have been synthesized and the cells assembled using these composite cathodes show pronounced enhancement in capacity, at the same time retaining the structural flexibility. One of the other important observations is the blocking of the unwanted effects of Jahn-Teller distortion, generally observed around room temperature in $LiMn_2O_4$ cathode material, by the presence of Li doped PANI in the composite cathode PANI-$LiMn_2O_4$. These investigations form the essence of chapters seven and eight.

Chapter nine gives the details of the synthesis of Li doped PEO and the investigations carried out to assess its suitability to be used as the solid polymer electrolyte in all solid state and flexible Li-ion cells. The results show that Li doped PEO is more flexible than PEO and has very good Li ion conductivity at room temperature of the order of $1.5x10^{-3}$ S/cm. The details of realization of the all solid state and flexible pouch cell, assembled using Li doped PANI as the cathode, Li doped PEO as the electrolyte and thin graphite sheet as anode are also given as the concluding part of this chapter.

The summary of the research work presented in the thesis and the conclusions arrived at are addressed in chapter ten. The future prospects of the present investigations are highlighted and the routes for fulfilling the vision of realizing all solid state, flexible and environment friendly Li-ion cells with high energy density, power density and cycling stability are envisaged.

List of Publications

<u>In Peer Reviewed Journals</u>

1. **Anand .B. Puthirath**, Bibin John, C. Gouri, S. Jayalekshmi, Lithium doped Polyaniline and its composites with $LiFePO_4$ and $LiMn_2O_4$ - Prospective cathode active materials for environment friendly and flexible Li-ion battery applications, *RSC Advances*, 2015, **5**, 69220-69228 (DOI : 10.1039/C5RA10706G).
2. **Anand .B. Puthirath**, Bibin John, C. Gouri, S. Jayalekshmi, Lithium doped PEO-a prospective solid electrolyte with high ionic conductivity, developed using n-butyl lithium in hexane as dopant, *Ionics*, 2015, **21**, 2185–2191 (DOI : 10.1007/s11581-015-1406-2).
3. **P. B. Anand**, K. Hasna, K. M. Anilkumar and S. Jayalekshmi. On the structural and optical properties of gold-polyaniline nanocomposite synthesized via a novel route, *Polymer International*, 2012 , **61**, 12, 1733–1738 (DOI 10.1002/pi.4262).
4. **P. B. Anand**, C. S. Suchand Sandeep, Kishore Sridharan, T. N. Narayanan, Senoy Thomas, Reji Philip and M. R. Anantharaman. An Optical Limiter Based on Silver-Silica Nanocomposites. *Advanced Science, Engineering and Medicine*, 2012, **4**, 33–38, (DOI:10.1166/asem.2012.1115).
5. M. Rajive Tomy , K.M. Anil Kumar, **P.B. Anand**, S. Jayalekshmi, Effect of annealing on the electrochemical properties of the Li–Mn–O thin films, prepared by high frequency RF magnetron sputtering, Journal of Physics and Chemistry of Solids, *Journal of Physics and Chemistry of Solids*, 2012 , **73** ,559–563 (DOI:10.1016/j.jpcs.2011.12.008).
6. Augustine M Sajimol, **Puthirath B Anand**, Kollery M Anilkumar and Sankaran Jayalekshmi, Exceptionally good, transparent and flexible FeS2/poly(vinyl pyrrolidone) and FeS2/poly(vinyl alcohol) nanocomposite thin films with excellent UV-shielding properties, *Polymer International*, 2012 , **62**, 4, 670–675 (DOI 10.1002/pi.4348).
7. Anas, J. Jiya, M.J. Rameez, **P.B. Anand**, M.R. Anantharaman and S. Nair, Sequential interactions of silver–silica nanocomposite (Ag–

SiO_2NC) with cell wall, metabolism and genetic stability of Pseudomonas aeruginosa, a multiple antibiotic-resistant bacterium, *Letters in Applied Microbiology*, 2012, **56(1)**,57-62 (DOI:10.1111/lam.12015).

8. Rajive Tomy , K.M. Anil Kumar, **P.B. Anand**, S. Jayalekshmi, Effect of annealing on structural and electrical properties of the Li–Mn–O thin films, prepared by high frequency RF magnetron sputtering, *Journal of Physics and Chemistry of Solids*, 2011, **72** 1251–1255 (DOI:10.1016/j.jpcs.2011.07.018).

Book Chapter Contributed

1. S Jayalekshmi and **Anand Puthirath**, Supercapacitors-Fundamental Aspects, Nanostructured Ceramic Oxides for Supercapacitor Applications, *CRC Press*, 21st February 2014.

Published abstracts and professional presentations

1. **Anand B. Puthirath**, Bibin John, C. Gouri, S. Jayalekshmi, Role of polyaniline towards realizing polymer based, flexible and environment friendly energy storage devices, *International Conference on Energy Harvesting, Storage and Conversion(IC-EEE 2015)*, Kochi, India.
2. **Anand B. Puthirath**, K. M. Anilkumar and S. Jayalekshmi, Electrochemical Characteristics of Li-Ion Cells Using Polyaniline-LiMn2O4 Composite as Cathode Active Material , *2nd International Conference on Advanced Functional Materials (ICAFM 2014),* Trivandrum, India.
3. **Anand B. Puthirath**, K. M. Anilkumar and S. Jayalekshmi, Electrochemical Characteristics of Li-Ion Cells Using Polyaniline-$LiFePO_4$ Composite as Cathode Active Material, *26th Kerala Science Congress, 2014*, Pokkode, India.
4. **P. B. Anand** and S. Jayalekshmi, Observation of switching between SA and RSA in silver/gold-polyaniline nanocomposite films, Proc. SPIE 8809, Plasmonics: Metallic Nanostructures and Their Optical

Properties XI, 88092B (September 11, 2013); *SPIE-Optics+Photonics 2013*, San Diego, CA, United States.

5. **P. B. Anand**, Ann Mary Jose, Dhanya Rajan, S. Jayalekshmi , On the structural and nonlinear optical properties of polyaniline/silver nanocomposites and its thin films, synthesized via a simple route, *Fifth edition of International Symposium for Research Scholars on Metallurgy, Materials Science and Engineering (ISRS 2013) 13-15*, IIT Madras, India.
6. **P.B. Anand**, S. Jayalekshmi, On the structural and impedance characteristics of Li- doped PEO, using n-butyl lithium in hexane as dopant, *2nd International conference on Optoelectronic Materials and Thin films for Advanced Technology (OMTAT 2013)*, Kochi, India.
7. **Anand P B**, Rajive M. Tomy, Anilkumar K. M. and Jayalekshmi S, On the structural and electrochemical properties of Li-ion cells based on Lithium doped (n-Butyllithium as dopant) polyaniline as cathode active material, *Annual International Conference on Optoelectronics, Photonics & Applied Physics* (OPAP 2013), Singapore.
8. **P.B. Anand**, Sreekanth. J. Varma, S. Jayalekshmi, Structural And Electrical Characterisation Of Exceptionally Crystalline CSA, NSA And HCl Doped Polyaniline (Pani) Thin Films, *Fifth International Conference On Electroactive Polymers: Materials and Devices (ICEP 2012)*, Varanasi, India.
9. K.K. James, **P.B Anand**, S. Jayalekshmi and M. K. Jayaraj, Electrical and Di-electric properties of Fe doped $BaSnO_3$, *International Seminar on Advanced Materials (ICAM 2011)*, Coimbatore, India.
10. Jiya Jose, Bina Jose, **Anand. P .B**, Anas Abdulaziz, M.R. Anantharaman and Shanta Nair, Effect of Ag Nanoparticles on multiple metal –and antibiotic resistant pathogenic bacteria from cochin estuary, Invited Talk, *Cochin Nano 2011*, Kochi, India.

Personal Achievements

1. Won the **Best Poster Award** in Physical Sciences at the *26th Kerala Science Congress* held at Kerala Veterinary and Animal Sciences University, Pookode, Wayanad during 28th to 31st January, 2014.

2. SPIE Official **Travel Grant winner** for participating in the Annual Leadership Workshop and *SPIE Optics + Photonics 2013* Conference at San Diego CA, USA.
3. Won the **Best Student Paper Award** at the *International Conference on Optoelectronics, Photonics and Applied Physics (OPAP-2013)* held in Singapore during 4-5, February 2013, organized by the Global Science and Technology Forum.

Chapter 1

Introduction to Relevant Fundamental Aspects

Abstract: Introductory ideas related to the present research work are addressed in this chapter. The chapter begins with a brief historical background of the evolution of polymers from the status of passive insulating materials to that of functional electronic materials, endowed with tunable characteristics suitable for a host of technological applications. The present stature of polyaniline among the category of electrically conducting polymers is highlighted, on the basis of its unique structural aspects, intriguing material characteristics and the application prospects crossing vast frontiers of research arenas. As the title of the thesis illustrates, the versatile roles of polyaniline and its composites in two different perspectives are addressed in the present work and all the relevant fundamental aspects are considered in this chapter. The brief discussion on the objectives of the present studies and the motivation behind initiating the present line of investigations also forms an integral part of the first chapter.

1.1 Conducting Polymers

The pioneering work of Alan Heeger, Alan G. MacDiarmid and Hideki Shirakawa during the 1970's which culminated in the Nobel Prize in Chemistry for unveiling the unprecedented merits of the class of conducting polymers, was the mile stone for identifying the potential of this class of materials in a wide variety of technological applications. The surprising

discovery of the metallic properties in the linear conjugated organic polymer ,polyacetylene and the additional surprises related to the possibilities of tuning the electrical conducting properties of this polymer from insulating to superconducting, based on the doping strategies adopted, triggered a surge of worldwide research activity to identify more categories of polymers with enhanced electrically conducting properties. A variety of approaches for the synthesis of conducting polymers was soon identified and based on both chemical and electrochemical routes different types of conducting polymers with impressive characteristics could be realized. The prime members of this group of conducting polymers with potential application prospects include polyacetylene, polyaniline, polypyrrole, polythiophene, polyphenylene vinylene and their group of substituted polymers, co-polymers and hybrid polymers.

Among those polymers endowed with electrical conducting properties suitable for applications in active devices, polyaniline (PANI) is one of the highly sought after material, because of its unique material characteristics, and exceptionally good environmental stability, not observed in any of the other polymers. Polyaniline is highly stable in air and is an ecofriendly material, possessing quite fascinating electronic and optoelectronic properties with excellent application prospects in the emerging technological fields. The current advances in nanotechnology have triggered another phase of activity, centered around nanostructured polyaniline systems and the nanocomposites of polyaniline.[1-4]

1.1.1 Polyaniline -Historical Background

Historically, polyaniline was first known in 1835 as "aniline black", a term used for any product obtained by the oxidation of aniline. A few years later, Fritzche carried out the tentative analysis of the products obtained by the chemical oxidation of this aromatic amine. Later Letheby discovered that the final product of anodic oxidation of aniline at a platinum electrode, in aqueous sulphuric acid solution, is a dark brown precipitate. Subsequent investigators have verified these results, and similar observations have been made during the oxidation of aqueous hydrochloric acid solutions of aniline. Green and co-

workers [15-20] proposed a linear octameric structure, of the quinone-imine type in the para -position, for the product obtained by the chemical oxidation of aniline. The base of the octamer is leucoemeraldine which exhibits four distinct states of oxidation. They are protoemeraldine, emeraldine, nigraniline and pernigraniline which are shown schematicall in figure 1.1.

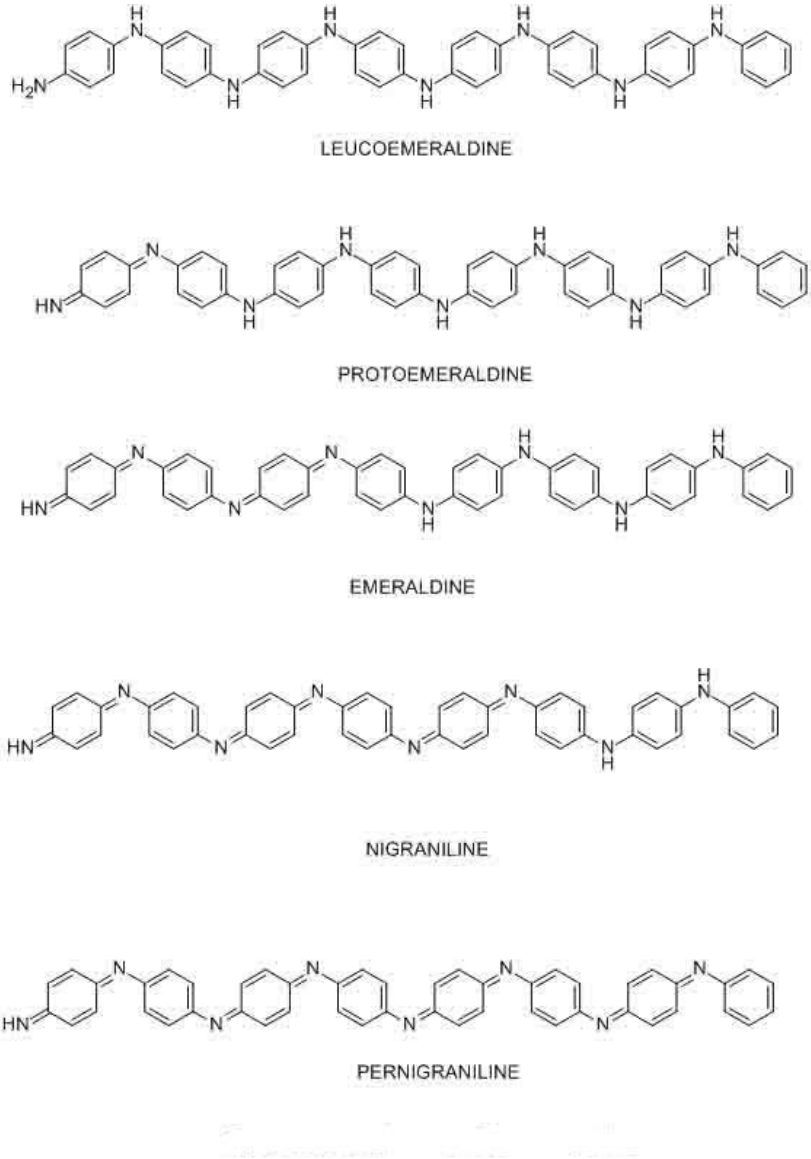

Figure 1.1: Four oxidation states of leucoemeraldine

In 1935, Yasui suggested a reaction scheme for the anodic oxidation of aniline at a carbon electrode. No further research was carried out until the middle of

the 20th century when Khomutov and Gorbachev re-examined the previous results, and verified the earlier observation about the green precipitate as the acid doped, conducting form of polyaniline. It seems that pursuit of the earlier lines of research on oxidative condensation of aniline will help to obtain a better understanding of aniline polymerization and the possible chemical structures of doped PANI which are of current relevance.[5-7]

1.1.2 Constitution and Nomenclature

Since the resurgence of PANI, there has been considerable confusion regarding its constitution. Studies since then have resulted in the formulation of a proposed structure for the polyanilines, together with a modification of the nomenclature based on the older concepts.

As mentioned earlier, Green and Woodhead gave various trivial names to PANI, but they did not know the structure of the polymer at that time, believing it to be an octameric molecule. Polyaniline may be described as a combination of any desired relative ratio of the idealized repeating units depending on the experimental conditions to which the polymer is subjected. Different names have been proposed in the literature and for the sake of simplicity one can summarize them as follows.

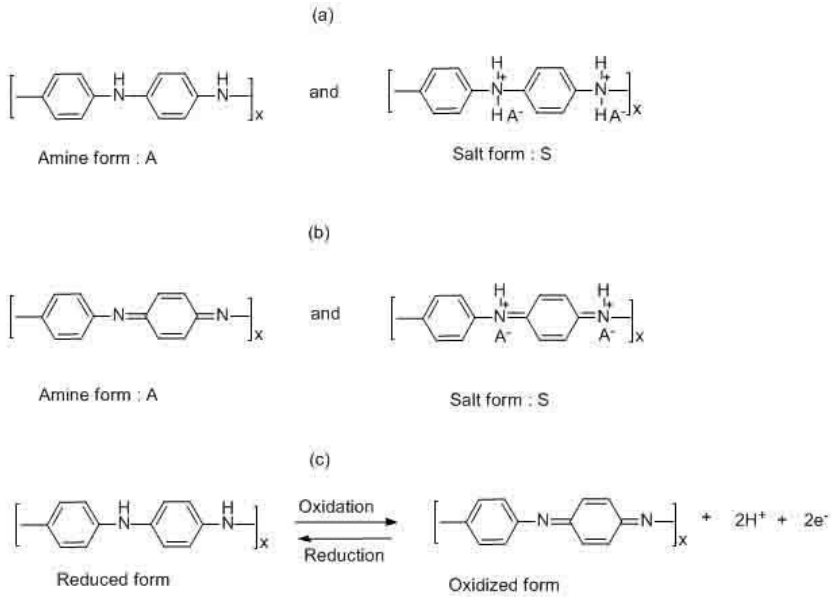

Figure 1.2: Chemical structures of polyaniline

In general, PANI contains two principal units, one of them being the completely reduced form of a repeat unit containing two benzenoid rings and the other, the partially oxidized form of a repeat unit containing one benzenoid ring and one quinonoid ring which are shown in figures 1.2a, and 1.2b respectively. In both cases, either one or both, of the nitrogen atoms in a repeat unit may be protonated, depending on the pH of the solution to which the polymer has been exposed. The base and protonated forms are referred to as the amine (A) and the salt (S) forms respectively as illustrated in figures 1.2a and 1.2b.

Proto-emeraldine, emeraldine and nigaraniline are the intermediate oxidation states of the above mentioned forms of PANI. However, it is interesting to note that the smallest number of reduced and/or oxidized repeat units which can be used, and which will permit inter-conversion between the above compositions, is eight- a finding which is in full agreement with the structure proposed by Green and co-workers for polyaniline. The conversion of the completely reduced form to the completely oxidized state involves a loss of electrons and protons, as illustrated in figure 1.2c. Out of the five oxidation states of PANI, the emeraldine form, with the structure shown in figure 1.1 has been most widely studied.[8-11]

1.1.3 Synthesis

Polyaniline may be synthesized by two principal methods. One of them is by the direct oxidation of aniline using chemical oxidants and the second one by anodic oxidation of aniline on an inert electrode.

1.1.3.1 Chemical synthesis

In the chemical polymerisation of aniline, the polymer is obtained as a precipitated product from a solution containing typical reagents like the oxidant, ammonium peroxydisulphate (persulphate), acids like hydrochloric, sulphuric, nitric or per- chloric, and aniline. This direct route represents the classical approach to polyaniline synthesis in which, aniline, the monomer, is converted directly to a conjugated polymer by a condensation process. One of the disadvantages of this direct approach stems from the experimental observation that an excess amount of the oxidant and higher ionic strength of

the medium lead to materials that are essentially intractable. It is not possible to polymerize the ortho and meta-substituted aniline derivatives, due to the steric and weak inductance effects of the substituents. The para-position should be kept free for radical coupling. During oxidative condensation of aniline, the solution progressively becomes coloured and yields a black precipitate. The colouration of the solvent is probably due to the presence of soluble oligomers. The intensity of colouration depends on the nature of the medium and the concentration of the oxidant.

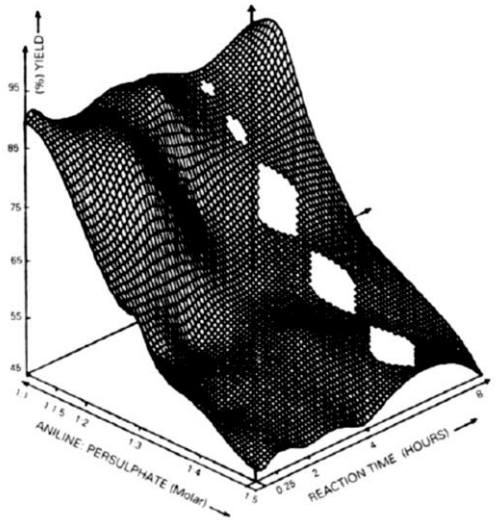

Figure 1.3: Chemical Synthesis of polyaniline. Three dimensional diagram

Many variations of the synthesis of PANI have appeared in the literature. The four major parameters that affect the course of the reaction and the nature of the final product are (1) the nature of the medium, (2) concentration of the oxidant, (3) duration of the reaction and (4) the temperature of the medium. Besides these, the combined effect of the concentration of the oxidant, ammonium persulphate and the duration of the polymerization reaction on the percentage yield of polyaniline has been investigated and the results are displayed in a three-dimensional diagram shown in figure 1.3.

Generally, one may state that polyaniline can be obtained as an insoluble residue during the oxidative condensation of aniline, which has to be separated by filtration and washed with a copious amount of the acidic solution of desired ionic strength to remove oligomers, and dried under dynamic vacuum

for 48 hours. The resulting dark powder is generally transferred to a soxhlet apparatus to remove low-molecular-weight species, and extracted with CH_3CN until the extract becomes colourless. The material has to be dried under dynamic vacuum.

Table 1.1: Chemical synthesis of PANI using different oxidants and varied reaction conditions

Oxidant	Time of reaction Hours	Temperature (^oC)	Reaction Medium	Normalized aniline/oxidant ratio	Yield (%)
*KIO_3	15	Zero	2M HCl	0.61	100.0
*KIO_3	3	Zero	2M HCl	0.61	48.5
*$(NH_4)_2S_20_8$	1.5	Zero	2M HCl	0.61	82.4
*H_2O_2	15	Room temp.	4M HCl	0.61	60.0
$(NH_4)_2S_20_8$	1	Room temp.	1M H_2SO_4	1.00	99.0
$Ce(SO_4)_2$	1	Room temp.	1M H_2SO_4	1.00	75.4
$K_2Cr_2O_7$	1	Room temp.	1M H_2SO_4	1.00	96.0
$NaVO_3$	1	Room temp.	1M H_2SO_4	1.00	94.0
$K_3[Fe(CN)_6]$	1	Room temp.	1M H_2SO_4	1.00	2.1

* Data from Pron and co-workers

Chemical synthesis of emeraldine hydrochloride and emeraldine base: The method used for the synthesis of emeraldine hydrochloride is summarized as follows. An aqueous solution of ammonium persulphate is added slowly to a solution of aniline in hydrochloric acid. The reaction mixture is stirred for about an hour at -5°C. The precipitate formed is removed by filtration, and washed repeatedly with 1M hydrochloric acid, and dried under dynamic vacuum for 48 hours. The material thus obtained is identified as emeraldine hydrochloride or emeraldine salt.

1.1.3.2 Electrochemical polymerization

There is at present a two-fold interest in the electrochemical polymerization (ECP) process for the synthesis of PANI. Generally, ECP reactions provide a viable method of polymerization with a fine control of the initiation and

termination steps and have technological significance. One of the important features found in ECP reactions of conducting polymers is that they proceed with electrochemical stoichiometry. This is because electrochemical reactions are often much cleaner, with respect to possible pollutants, than chemical reactions. One can see that electrons, as reagents, are inherently pollution-free.

Electrochemical methods generally employed for ECP of aniline are, constant current or galvanostatic technique, constant potential or potentiostatic technique and potential scanning/cycling or sweeping methods. The first method essentially consists of a two-electrode assembly dipped in an electrolyte solution containing the monomer. Passing a current of 1 mA/cm^2 will lead to the deposition of a PANI film on the surface of a platinum foil electrode. Polymerization of aniline at constant potential yields powder samples which adhere poorly to the electrode. On the other hand, electro-oxidation of aniline by continuous cycling between the predetermined potentials results in homogenous polymeric films with strong adhesion to the electrode surface. These thin films can be cycled between oxidized and reduced states which are generally conducting. Thicker films can be produced and can be peeled off from the electrode surface to yield free-standing, electrically conducting films. As these films are in the oxidized state, they represent polyaniline cations, and their overall charge balance is achieved by incorporation of counter anions from the electrolyte solution. Some of the well-known counter anions include, F^-, $C1^-$, ClO_4^-, SO_2^{-1} and BF_4^{-1}.

The anodic oxidation of aniline is generally carried out on an inert electrode. Though the usual anode material would be platinum, or conducting glass, many metals such as Fe, Cu and Au have also been employed. Metals such as Ag or Al, which get oxidized more readily than aniline monomer, would obviously not be a good choice for the anode. Until recently, it was believed that polyaniline deposited from aprotic solutions such as CH_3CN is electro-inactive, and, therefore, it was thought that electro active polyaniline could be formed only from acidic aqueous solutions. However, it has been demonstrated that electro active polyaniline can be synthesized in an aprotic solvent, such as propylene carbonate solution containing an organic acid, CF_3COOH and an electrolyte, lithium perchlorate.

Electrochemical methods have definite advantages over chemical methods of synthesis of polyaniline, mostly because of the reliability of the techniques. The results show that the stoichiometric electro chemical polymerization reaction can be a general procedure for the synthesis of organic polymer films, with electro active properties and good electrode behavior and polyaniline is one such example.[16-20]

1.1.4 Mechanisms of Polyaniline Formation

The numerous methods employed to synthesize PANI have given rise to several products which differ in their nature and properties and must represent the results of a multitude of polymerization mechanisms of aniline. In general, polymerization proceeds via the radical cation of the monomer, which then reacts with a second radical cation of the monomer to give a dimer by eliminating two protons. At the potential required to oxidize the monomer, the dimer or higher oligomer would also be oxidized, and thus could react further with the radical cation of the monomer to build up the aniline chain.

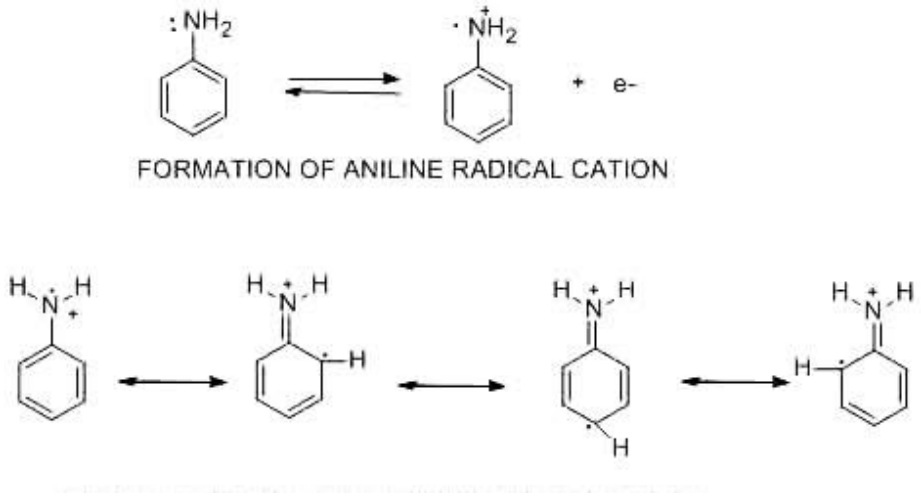

Figure 1.4: Formation of aniline radical cation and the resonance forms of aniline radical cation

Mohilner., Breitenbach and Heckner, Hand and Nelson, and Genies and coworkers have proposed mechanisms for electro chemical polymerization of aniline. The point of agreement in the proposed mechanisms is the first step of oxidation of aniline, related to the formation of the radical cation. This radical

cation gives three different resonance forms as shown in figure 1.4. Two mechanisms for the anodic oxidation of aniline in acidic and alkaline media have been reported. The mechanism in acidic media was proposed by Mohilner et al., based on the measurement of the kinetic parameters for the initial charge transfer step, and upon direct comparison of the properties, including infrared studies of the precipitate formed on the anode. On the basis of their experimental evidence, it has been suggested that p-aminodiphenylamine is one of the intermediates in the electrochemical oxidation of aniline. The mechanism of polymerization of aniline in a basic medium, like acetonitrile-pyridine, proceeds in a way essentially similar to that proposed earlier in the acid medium. The possible mechanism is schematically shown in figure 1.5.[20-25]

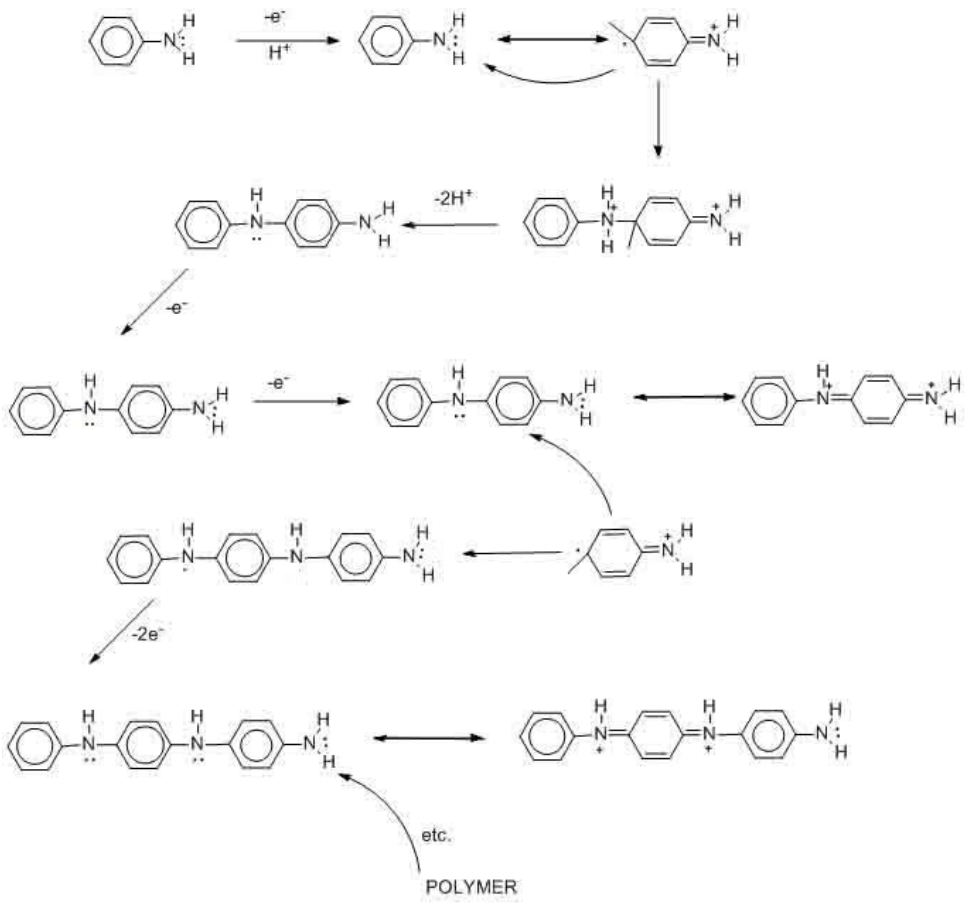

Figure 1.5: Mechanism of formation of polyaniline

1.1.5 General considerations of "doping" in conjugated polymers

The treatment of a conjugated polymer with ionizing agents (charge-transfer agents) leads to a concomitant increase in electrical conductivity. This process was named "doping", by analogy with the treatment of silicon with such elements as arsenic, boron and phosphorus. In crystalline silicon, which is tetravalent, the tri or pentavalent element replaces silicon at a lattice site to produce a "hole" or "electron", respectively. These dopants as they are called are added only at ppm levels as the mobility of the carriers is quite high, whereas, the dopants of the polymers under discussion have to be added at much higher concentrations, since they have lower mobility. The polymers derived from organic compounds, with high extent of electron conjugation and high "dopant" concentration, are termed as conducting organic polymers. The nature of the dopant decides the type of conduction in the resulting conducting polymer chain. Positive charge carriers in an acceptor doped polymer bring about p-type conduction and negative charge carriers in a donor doped polymer, n-type conduction.

The presence of the "dopant" in conducting polymers is to balance the charges created by electron removal or addition in the polymer chain, by a redox process, unlike that in inorganic semiconductors. The dopants are added at ppm levels to an inorganic material to make it semiconducting. But the amount of counter-ions in conducting polymers is in the range of 50% by weight of the material composition. In inorganic semiconductors, the dopants are metals, whereas in organic polymers they are generally non-metallic species. In spite of these differences, the word "doping" is still in use, related to polymers as well, probably because it helps to demonstrate similarities between conducting polymers and inorganic semiconductors. In both cases, doping changes the state of oxidation without changing the structure. In conducting polymers, doping changes only the packing order, and the 1-dimensional charge transport properties are exhibited along the polymer chains. The required higher concentration of dopants in conducting polymers is to attain the desired mobility of the charge carriers on par with inorganic semiconductors. Even though conjugated polymers have backbone structures well suited for conduction with high carrier mobilities, the inherent low carrier

concentration results in lower conductivity which has to be compensated by increasing the dopant concentration to achieve the desired carrier mobility and conductivity. In polymers, it is assumed that the dopant "dissolves" in the polymer matrix, until the doping level exceeds a certain limit of solubility, which is perhaps in the vicinity of a few per cent. This assumption does not contradict the available structural data and is supported by the experimental results on the temperature dependence of the electrical conductivity in the low doping regime. [26-29]

1.1.5.1 Doping in polyaniline: A new concept

The novelty of polyaniline is mainly due to its symmetrical conjugated structure, having extensive charge delocalization, resulting from a new type of doping rather than just oxidation which occurs in the p-doping of all other conducting polymer systems. Polyaniline differs from earlier studied conducting polymers such as polyacetylene and polypyrrole in that the electronic state of PANI can be controlled through variations in the number of electrons and in the number of protons per repeat unit as illustrated in figure 1.6.

The redox activity of PANI is pH-dependent in aqueous medium. It has been established that the electro activity of PANI ceases in aqueous media of pH > 4. On the other hand, the electrochemical behaviour of PANI, investigated in an aprotic solvent, such as propylene carbonate, in the presence of 1M lithium perchlorate as supporting electrolyte, demonstrates two purely electronic processes.

However, these redox processes vanish, if a small amount of 2, 4, 6-trimethyl pyridine (a strong base) is added to the system. The dramatic effect of variation of pH (changing pH from 0 to 6 decreases the electrical conductivity, σ, by six orders of magnitude) upon the conductivity of PANI clearly demonstrates that besides the dopants (counterions), the presence of protons invariably has a pronounced effect on the conductivity. Studies show that the emeraldine base form of polyaniline can be doped by protonic acids to be elated to the metallic conducting regime by a process involving neither oxidation nor reduction of the polymer, thereby introducing a new concept of

doping to the conducting polymer field. The proton-induced conductivity in polyaniline is a remarkable physical phenomenon demanding in depth studies and convincing explanation.[30-31]

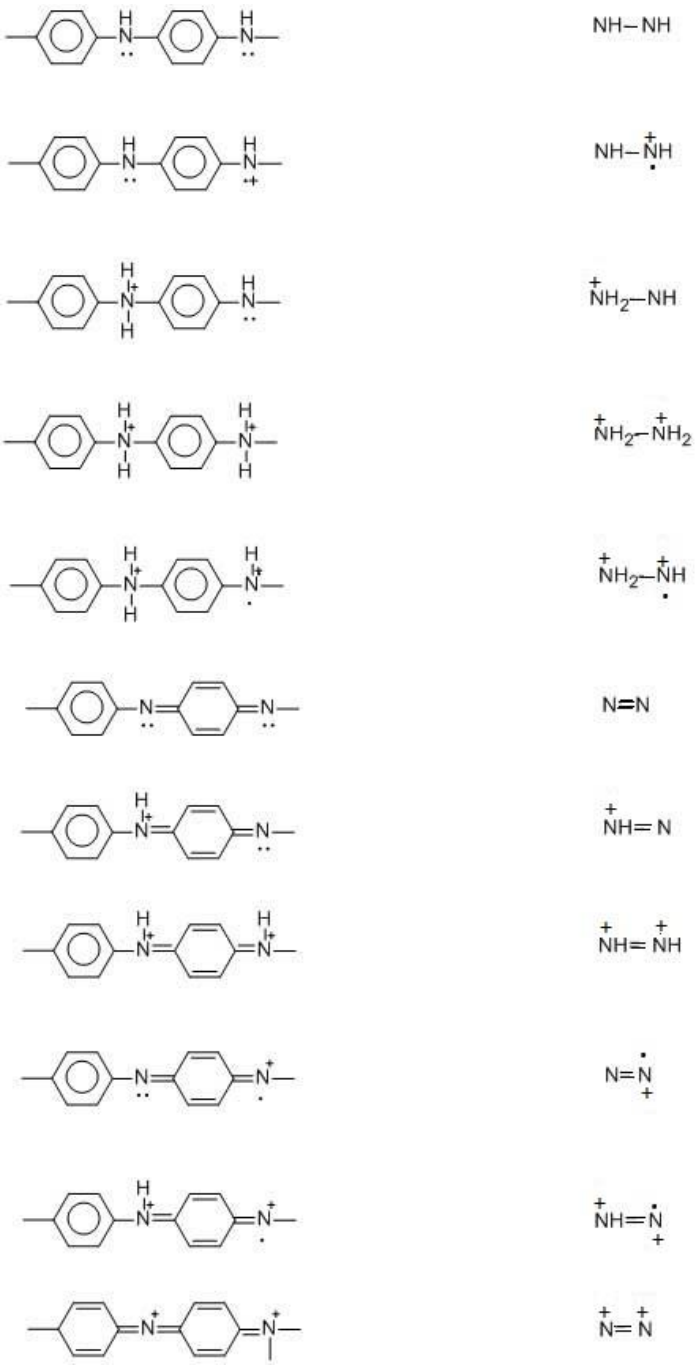

Figure 1.6: Electro-active molecular structures in polyaniline

1.1.6 Factors affecting the conductivity of polyaniline

The DC electrical conductivity (henceforth referred to as conductivity) of chemically and electrochemically synthesized PANI is dependent on a number of parameters. Temperature, protonation/pH, humidity, oxidation state and counter ions exert major influences on the conductivity of PANI. Besides these, temperature of synthesis, pressure, and the duration of compression of PANI powders also have a considerable influence on the conductivity of PANI.[32-40]

1.1.6.1 Temperature

It is well known that the effect of temperature on the conductivity of metallic conductors and semiconductors is quite different. In metals, or metal-like substances an increase in temperature causes a gradual decrease in conductivity, while the heating of a semiconductor results in a sharp increase in conductivity. The conductivity of PANI has been studied over a wide range of temperatures including 5-300 K, 20-340 K and 80-300 K. The results reveal the metallic character of the polymer in the above temperature range for protonic acid doped samples. The temperature dependence of the dielectric constant of the semiconducting PANI samples indicates an increase of the coherence length with increasing temperature.

1.1.6.2 Protonation

The interesting phenomenon of insulator-to-metal transition in polyaniline, effected via protonation, was first reported in 1985. Since then, extensive investigations have been carried out to establish proton induced insulator-to-metal transition phenomenon through electrical, magnetic, optical, thermo-power and ESR studies. The earlier studies have led to the proposal that the electronic structure of insulator polyaniline (also referred to as emeraldine base) is transformed to that of a granular polaron metal upon protonation (also referred to as emeraldine salt form). Recent studies on protonic acid doping of the emeraldine salt form of polyaniline give support to the idea that the distribution of protons between polymer and bathing solution takes place in thermodynamic equilibrium.

The conductivity of polyaniline is a function of the extent of protonation. The proton induced insulator to metal ($\sigma \cong 10^{-10}\ \Omega^{-1}\ cm^{-1} - \cong 10^{0}\ \Omega^{-1}\ cm^{-1}$) transition is an interesting phenomenon in polyaniline. This is not observed in other conducting polymers such as polythiophene and polypyrrole. This unique behavior of polyaniline can be ascribed to three important aspects. First of all, polyaniline does not have a symmetric charge conjugation. That is, the Fermi level and band gap are not formed at the centre of the band, so that valence and conduction bands are quite asymmetric. Another notable criterion is that both the carbon rings and nitrogen atoms lie within the conjugation path. This configuration differs, for example, from polypyrrole, whose heteroatoms do not contribute significantly to the k-band formation. Thirdly, the electronic state of the polymer can be changed through variations in the number of electrons and the number of protons.

1.1.6.3 Oxidation state

Polyaniline exists in many forms classified as (1) fully reduced and neutralized PANI (NH),(2) the one with protonated species (NH_2^+),(3) the first oxidized, neutral and/or protonated forms, N= and NH^+; and (4) the fully oxidized state, N^+. These forms are in thermodynamic relation to each other according to a classical “square scheme”. Based on the hypothesis concerning the relative thermodynamic potential and pK values for electron transfer, some interesting potential against pH diagrams are reported in the literature. These diagrams have contributed to a better understanding of the fact that quinonic imine is more basic than the corresponding aromatic amine in the polymer chain. A novel method of representing the “state” of polyaniline in a three dimensional diagram was first reported by Salaneck et al. Later Genies and Vieil proposed a three-dimensional surface diagram for the charge and conductivity to enable convenient and unambiguous description of the electrically conducting states of polyaniline based systems. These diagrams are useful, for example, in battery applications and electromagnetic interference (EMI) shielding.

1.1.6.4 Counter-ion

The dependence of resistivity of electrochemically synthesized polyaniline (PANIE) on the nature of the counter-ion was first observed by Paul, Ricco and Wrighton. This resistivity shows typical U-type functional dependence on the electrochemical potential. The experiment was repeated by Fock and coworkers who used different anions, which include hydrion buffer, paratoluene sulphonate (CH_3-C_6H_4-SO_3^-), tetrafluoroborate ($BF_4^{-)}$, trifluoroacetate(CF_3COO-) and chloride (Cl^-)] at pH 2. They also observed a similar U-type functional dependence.

Proton assisted, doping-induced conductivity in PANI is a remarkable phenomenon, which offers ample scope for in depth investigations.

1.1.7 Conduction Mechanisms

The charge transfer in the "emeraldine" form of polyaniline has become the subject of increased study because of the interesting discovery of insulator-to-metal transition as a function of protonation. The proposal of the transition from the electronic structure for insulator PANI (base form of emeraldine) to a polaronic, metallic structure of PANI (salt form of emeraldine) upon protonation is supported by a series of optical, magnetic and band structure studies. Much of the work on conduction mechanisms of polyaniline is centred around French and American groups. The French group of researchers have proposed a conduction mechanism based on electron hopping between localized states, with a proton-exchange-assisted conduction of electrons, which they enthusiastically refer to as PEACE. On the other hand, the American group, after extensive studies, have concluded that a charging-energy-limited-tunneling theory is most suitable for the explanation of transport phenomena in the emeraldine form of polyaniline.

The American group has carried out an extensive set of optical, photo induced optical, magnetic, transport, electrochemical and mechanical studies on polyaniline systems. Their study is focused- on the essential role of molecular excitons and polarons. Photo-excitation of the exciton absorption in the insulator form leads to the occurrence of polaron absorption features. Insulator-to-metal transition causes a transformation of the electronic structure

of the chain into a polaron lattice. These results are in agreement with the charging-energy-limited tunneling theory. The presence of metallic islands of about 100-200 Å size and average charging energy, E, of about 20 meV and the presence of structural defects, broken bonds, chain links, excess protonation etc., are responsible for sizable barriers between metallic islands.

In summary, the broad range of optical, magnetic and transport studies show that polyaniline is a system with physics substantially different from that of polyacetylene and polypyrole. The present theories certainly account for conduction mechanisms which are interesting, but not conclusive. It is essential to further elucidate the various phenomena associated with this novel conducting polymer to make more use of its vast application prospects.[41-45]

1.1.8 Applications

Polyaniline, modified polyaniline and their composites have immense applications in a variety of technological fields. Polyaniline films are found to have excellent catalytic activity and this observation has led to the identification of modified polyaniline as a possible fuel cell electrode. In an interesting study, electrodeposition of platinum microparticles onto polyaniline film has been demonstrated. The resultant film exhibits catalytic activity for hydrogen evolution and methanol oxidation. In another communication, polyaniline-nafion composite films have been shown to display better reversibility than the polyaniline films alone. Catalytic and electrocatalytic capabilities of polyaniline are of great importance and further research will certainly lead to newer applications.

Polyaniline films have been used as indicators by virtue of the multiple colour changes of PANI films on electrodes and chromatic reactions of PANI solutions in different pH ranges. Unlike other conducting polymers such as polypyrrole and polythiophene, PANI has a unique feature that the equilibration by acid solution imposes the anion in the polymer. This has been the basis for the use of PANI as an anion exchange polymer. The mixtures of halide ions can also be separated on polyaniline.

A large change in electronic conductivity of PANI with a change in electrochemical potential is the basis for the development of PANI-based

electronic devices. In practice, PANI deposited on to a gold microelectrode array has been shown to behave like a diode and a transistor. These polymer-based, transistor-like devices can be turned 'on' and 'off' by electrical or chemical signals that oxidize and reduce the polymer.

The optical characteristics of the PANI films undergo changes with the corresponding changes in electrical conductivity. In the oxidized state, PANI films are coloured and highly conductive and in the reduced state, they are optically transparent with low conductivity. In fact, colouration and conductivity are associated with the doping of the films.

Kobayashi and co-workers were the first to report the mechanism of the electro chromic reactions of PANI films and their applications to practical electro chromic display devices with liquid electrolytes. The colour of PANI films is reversibly changed to green by oxidation and to transparent yellow by reduction in 1M hydrochloric acid, in the potential range from -0.2 V to +0.6 V against Standard Calomel Electrode (SCE). The reversibility of the colour change can be observed more than 10^6 times in the aforesaid potential range, with rapid response of less than 100 millisecond. In an interesting study, it has been demonstrated that the surface of an oxidized PANI electrochromic film, in contact with pure water, is more hydrophilic than that of a reduced surface. Furthermore, hydrophilicity is directly related to the conductivity of the film and the higher the conductivity, the greater the hydrophilicity of the surface.

The conversion of solar energy to chemical or electrical energy by photo-electrochemical cells (PECs) has attracted considerable attention during the last decade. This is because of their inherent simplicity of manufacture and consequently reduced cost. However, the susceptibility of narrow band-gap semiconductors to photodegradation has been a serious limitation on its wide popularity.

Two applications of PANI in PECs have been studied to date which include the protection against photo-corrosion of inorganic semiconductors and the photo response of junction PANI films. In the former case, the polyaniline-coated semiconducting electrodes (Cd-chalcogenides, Si, GaAs, GaP) are found to exhibit enhanced stability of the photocurrent when compared to the

current of the naked electrodes and in the latter case, the photocurrent is induced when visible light from a 500 W, xenon lamp is, allowed to fall on a PANI film coated on platinum. Subsequent development in this field has resulted in a fast photo response of junction polyaniline films.

Conjugated polymers are expected to exhibit nonlinear optical properties (NLO) due to the presence of delocalized π-electrons along the polymer backbone. Investigations on the optical characteristics of conjugated polymers may open ways to identify potential NLO active materials useful in advanced photonic devices.

During the last decade, intense research activity has been focused in the direction of developing polyaniline based rechargeable batteries. Polyaniline has many advantages over other conducting polymers, such as simplicity and rapidity of synthesis of the polymer by chemical or electrochemical methods, and chemical durability against aerial oxidation and moisture. The ability of polyaniline to store considerable amount of charge through the redox process has led to proposals for both non-aqueous and aqueous batteries.

It is reported that the use of polyaniline as cathode material, in conjunction with lithium-doped aluminium as anode material, in propylene carbonate containing 1M lithium perchlorate, results in an open circuit voltage of 3.7 V. The massive capacity of 145 Ah/kg, and the self-discharge (with separator) rate of about 8% after 90 days make the polyaniline-lithium battery more attractive for new types of technological applications.

In a recent communication, PANI has been shown to have a maximum discharge capacity of 164 Ah/kg, a low rate of self-discharge, and a long life, as a positive active material in a secondary lithium battery. The larger massive capacity of PANI is attributed to its fibrous structure which is generated galvanostatically, in an aqueous 1M perchloric acid solution containing 0.5M aniline at room temperature, at the current density of 5 mA/cm^2. Propylene carbonate is a good electrolyte solvent, extensively employed in secondary lithium batteries, to ensure longer life and lower self-discharge for PANI.

Polyaniline has been identified as a promising material for both aqueous and non-aqueous storage batteries. The question whether non-aqueous or aqueous

electrolytes would be preferable for a specific purpose cannot be answered until much more information has been gathered. The use of aqueous electrolytes will, in general, be accepted to result in cells having a smaller potential, and hence, a smaller energy density than cells employing a non-aqueous electrolyte. Real long-term advances in the field can only be accomplished by detailed studies on chemical and electrochemical reactions, occurring during storage and recycling, under a wide variety of experimental conditions.[46-60]

1.2 Towards Nonlinear Optics

Electromagnetic radiation interacts with matter primarily through the valence electrons in the outer orbitals. This interaction creates electric dipoles leading to a macroscopic polarization of the medium. For small field strengths, this induced polarization is proportional to the applied electric field. When an electromagnetic wave propagates through a dielectric medium, the electric displacement can be written as,

$$D = \varepsilon E \tag{1.1}$$

where ε is the permittivity tensor and E is the electric field. (The electric displacement, electric field and polarization are vector quantities. However for the sake of simplicity, they are considered as scalar quantities in the following discussion). The permittivity tensor can be written in terms of the permittivity of free space (ε_0) and relative permittivity (ε_r) as,

$$\varepsilon = \varepsilon_0 \varepsilon_r \tag{1.2}$$

The electric displacement can also be written as,

$$D = \varepsilon_0 E + P \tag{1.3}$$

where P is the electric polarization (electric dipole moment density). From the above equations, one can write,

$$P = \varepsilon_0 (\varepsilon_r - 1)E = \varepsilon_0 \chi E \tag{1.4}$$

where, $\chi = \varepsilon_r - 1$ is called the electric susceptibility tensor (or simply electric susceptibility) of the medium. In the nonlinear regime, the expression for the polarization should be modified to a power series as,

$$P = \varepsilon_0 (\chi^1 E + \chi^2 EE + \chi^3 EEE + \ldots\ldots \tag{1.5}$$

where, χ^1 , χ^2 and χ^3 are the linear, quadratic (second-order), and cubic (third-order) susceptibility tensors, respectively. Substitution of equation 1.5 into Maxwell's equations leads to a set of nonlinear differential equations that involve terms with higher-order-powers of the optical electric field strength. These terms are responsible for various, observed coherent optical frequency-mixing effects. In other words, in the nonlinear regime, the re-radiation coming from the dipoles does not faithfully reproduce the sinusoidal electric field that generates them. As a result, the distorted re-radiated wave contains frequencies different from those of the original wave. [61-63]

1.2.1 Second-order nonlinearities

The second-order susceptibility χ^2 is responsible for second harmonic generation, sum and difference frequency generation, and optical parametric amplification. The above-mentioned second-order nonlinear effects are produced by two waves, which interact to produce a third wave. Conservation of momentum and photon energy are always required in these processes. The optical fields of these waves are coupled to one another through the second-order susceptibility. The coupling provides the mechanism for the exchange of energy among the interacting fields. In centro-symmetric crystals, $\chi^{(2)}$ is zero. Hence second-order nonlinear processes are generally possible only in materials that lack inversion symmetry.[64]

1.2.1.1 Sum and difference frequency generation

In this process, two waves of frequencies ω_1 and ω_2 with comparable intensity interact nonlinearly to produce a wave at a third frequencyω_3 . The polarization in this case can be written as,

$$P(\omega) = \epsilon_0 \chi^2 E(\omega_1) E(\omega_2) \qquad (1.6)$$

where $\omega_3 = \omega_1 + \omega_2$. Similarly a wave at the difference frequency $\omega_3 = \omega_1 - \omega_2$ may also be generated ($\omega_3 > \omega_2 > \omega_3$).

1.2.1.2 Second harmonic generation (SHG)

This is a special case of frequency mixing in which the initial waves have the same frequency, $\omega = \omega_1 = \omega_2$ and $\omega_3 = 2\omega$. The induced polarization takes the form

$$P = \varepsilon_0(\chi^1 E\, Sin\,(\omega t) + \frac{1}{2}\chi^2 EE\,(1 - Cos\,2\omega t) + \ldots\ldots \qquad (1.7)$$

according to equation 1.5, with $E = E_0\, Sin\,(\omega t)$. The presence of the second term involving 2ω in the above expression shows that a wave having twice the fundamental frequency can be generated during the nonlinear process.

1.2.2 Third-order nonlinearities

Third-order nonlinearities involve the nonlinear susceptibility tensor $\chi^{(3)}$ in equation 1.5. This term governs many nonlinear phenomena like third harmonic generation, optical Kerr effect, stimulated Raman scattering and stimulated Brillouin scattering. In general, $\chi^{(3)}$ couples together four frequency components. In other words, three fields interact to produce a fourth field.

$$P(\omega_4) = \varepsilon_0\, \chi^{(3)} E(\omega_3) E(\omega_2) E(\omega_1)$$

In a lossless medium the susceptibility coefficients of $\chi^{(3)}$ are real. In this case, the primary nonlinear optical effects are the generation of new frequency components and the intensity dependent refractive index change (Kerr effect). In third-order interactions involving absorption, the imaginary part of $\chi^{(3)}$) describes Raman and Brillouin scattering and two-photon absorption.[65-67]

1.2.2.1 The nonlinear light transmission phenomenon

Depending on the characteristic response of a medium to the frequency of light, the transmission of light gets affected by the scattering, refraction or absorption by the medium. For instance, when the intensity of the input light is such that the corresponding electric field is sufficient to evoke the otherwise small nonlinear terms in the dipole oscillation, it modifies the properties of the medium, affecting light transmission. The change in transmittance of a medium as a function of the input light intensity or fluence is referred to as nonlinear light absorption or nonlinear light transmission. At sufficiently high intensities, the probability of an absorber absorbing more than one photon before relaxing to the ground state can be enhanced. A few major mechanisms that control nonlinear light transmission are discussed in the following sections.

1.2.2.1.1 Saturable absorption

Saturable absorption is a property of materials where the absorption of light decreases with increasing light intensity. At sufficiently high incident light intensity, atoms or molecules in the ground state of a saturable absorber material become excited into an upper energy state at such a rate that there is insufficient time for them to decay back to the ground state before the ground state becomes depleted, and the absorption subsequently saturates.[68-70]

1.2.2.1.2 Two-photon absorption (2PA)

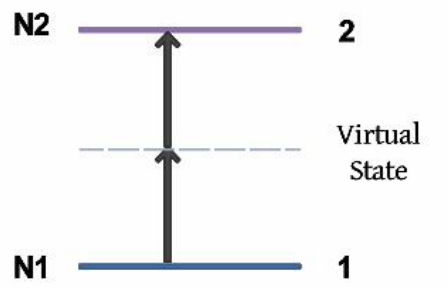

Figure 1.7: Schematic representation of two-photon absorption

The process of the transition of a system from the ground state to a higher level by the simultaneous absorption of two photons from an incident radiation field is termed as two-photon absorption. Two photons of frequency ω of the incident field are simultaneously absorbed by the system to make the transition to a state that is approximately resonant at 2ω. A schematic representation of two-photon absorption can be found in figure 1.7.[71]

1.2.2.1.3 Three-photon absorption (3PA)

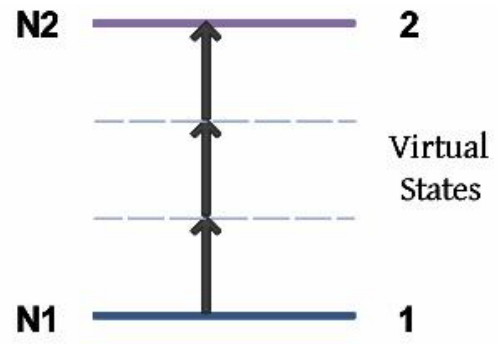

Figure 1.8: Schematic representation of three-photon absorption.

The process of the transition of a system from the ground state to a higher level by the simultaneous absorption of three photons from an incident radiation field is termed as three-photon absorption (3PA). The schematic representation is given in figure 1.8.[71]

1.2.2.1.4 Reverse saturable absorption (RSA)

Reverse saturable absorption (RSA) is a two-step, sequential one-photon absorption process, shown schematically in figure 1.9.

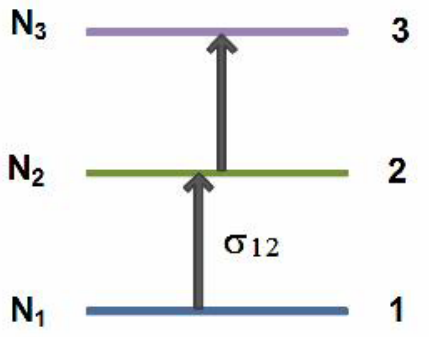

Figure 1.9: Schematic representation of reverse saturable absorption

In this case the medium has a resonant linear absorption for the incident laser beam, and some of the molecules in the ground state are excited to the higher energy level 2. For a properly chosen medium, it is possible that the excited molecules make another transition from the excited state 2 to a higher excited state 3 via another one-photon absorption. (In polyatomic molecules in fact a 5-level model may be considered, which involves both singlet and triplet states).[71]

1.2.2.1.5 Free carrier absorption

Once free carriers are generated by linear absorption in semiconductors, they may experience phonon-assisted absorption to higher-lying (lower-lying) states in the conduction (valence) band. This process is called free carrier absorption.[71]

1.3 Rechargeable Li-ion Cells: An Overview

The development of efficient technologies for sustainable energy generation and its storage is one of the prime challenges of the present century.

Renewable and sustainable energy harvesting strategies specifically based on solar and wind power generation schemes require, state of the art techniques for energy storage as well since, the energy generated is often intermittent. Developing energy storage installations that balance intermittent supply with consumer demand is one of the prime goals to be accomplished.

Among the energy storage systems, rechargeable batteries constitute the category of the most useful and attractive devices mainly because of the possibility of repeated use, many hundreds of times, without capacity loss. Primary batteries, on the other hand are disposed after the energy is consumed. Lead-acid, nickel cadmium (NiCd), nickel metal hydride (NiMH), lithium ion (Li-ion), redox flow and Na/S are all rechargeable batteries and are, with the exception of the redox flow and Na/S batteries, commonly used in electronic devices. The nickel-cadmium, and nickel metal hydride batteries are used in large storage capacity applications such as UPS (uninterruptible power supply), HEV (Hybrid Electric Vehicle), and stationary storage.

Among the commercial battery systems the rechargeable lithium battery stands out with superior merits and high demand and is commonly used in portable devices that require comparatively lower volume and weight, such as laptop computers and mobile phones. The demand for miniature sized secondary batteries has more than doubled between 1995 and 2006, from 180 million to 380 million units having been sold. The market share of lithium rechargeable batteries has grown from 47% in 2006 to 70% in 2010. The lithium rechargeable batteries are prospective power sources for hybrid electric vehicles (HEVs) and electric vehicles (EVs) due to the high power and energy densities. The EV is a good solution to limit CO_2 exhaust and to tackle the limited resource of fossil fuels. After Toyota opened the HEV market in 1997, the trend has moved to Plug-in Hybrid Electric Vehicle (PHEV) and to some extent to EV. Much effort has been put in to develop large size lithium batteries that satisfy the requirements for mileage, fast charging time, low cost, and safety. To meet the milestones, novel electrode and electrolyte materials are being identified and developed, and considered for commercial lithium batteries.

Poly(ethylene oxide) (PEO) based polymer electrolytes have been investigated for applications in high safety lithium batteries since they were first reported in 1973 by Fenton et al. The ion transfer in PEO occurs through complexation between the polymer and alkali metal salts, which enables its use as a solid polymer electrolyte (SPE) for electrochemical systems, such as batteries, capacitors, and sensors. The SPE has many advantages which include safety, flexibility, and the required material density. One of the drawbacks of SPE is the low ionic conductivity at low temperatures, which is the main hindrance for commercialization. In PEO-based SPEs the mobility of lithium ions decreases with increasing molecular weight. To solve the problem of PEO-based electrolytes, the use of branched polymers, cross-linked polymers, block copolymers, and incorporation of ceramic fillers into the PEO matrix have been investigated. The use of gel polymer electrolytes, prepared by incorporating organic liquid electrolytes in a porous membrane of a host polymer, has been suggested to improve the electrochemical properties, since they possess high ionic conductivity and sufficient mechanical integrity for handling. The latter systems are commercially well established even though the liquid electrolyte solvents are volatile and thermally unstable and thus cause safety problems in batteries. As a result, there has been much interest in recent years to replace organic solvents with room-temperature ionic liquids (RTILs), which are non-volatile and non-flammable molten salts with low melting points. The RTILs generally exhibit high ionic conductivity, high thermal and chemical stability, a wide electrochemical window, and low toxicity.

Another goal of lithium rechargeable battery development is attaining the mechanical flexibility demanded for weight sensitive applications and various forms of soft, portable electronic devices. To convert such potentials into reality, one paramount challenge is the goal of making flexible electrodes with robust mechanical properties and excellent electrochemical performance. Also, such batteries should fit to the life cycles of the applications and should be disposable or recyclable. For the flexible lithium battery applications, organic conducting materials such as 2, 2, 6, 6-tetramethyl-1- piperidinyloxy (TEMPO)-based polymers, sulfide-based polymers, and carbonyl-based

polymers and conducting polymers including polyaniline and polypyrrole have been investigated as possible electrode materials.[81-82]

1.3.1 Lithium rechargeable battery

One of the most viable candidates as a sustainable energy conversion and storage system is the rechargeable lithium ion battery (LIB), which was commercialized by Sony in the early 1990s. The main componets of a rechargeable Li-ion cell are the cathode and the anode, which have the property of reversible insertion and extraction of lithium ions. Transfer of lithium ions between the electrodes is enabled by the presence of suitable electrolyte and a mechanical separator between the anode (negative electrode) and the cathode (positive electrode). When the lithium ion is inserted in to the cathode and extracted from the anode, electrical energy is generated by electrochemical oxidation and reduction as shown in figure 1.10.

In the commercial LIBs lithium is introduced as lithiated carbon (i.e. as LiC_6) in the anode, although there is hope in future to utilize pure lithium metal anodes for ultimate power density. Carbon as anode material marked the turnaround for the lithium ion rechargeable batteries in the early 1990`s because it prevents the dendrite formation, which short-circuits the battery when lithium metal is used as the anode. Carbon based anode material has high reversibility and a reaction potential close to the oxidation/reduction of lithium metal, resulting in a high energy density. It is also considered environment-friendly and economically efficient.

On the cathode side transition metal oxides ($LiMO_2$), such as $LiCoO_2$, act as electron and Li-ion acceptors during the discharge process. However, the cathode material has to be replaced by cheaper and more environmentally friendly materials for electric vehicle (EV) applications. Many compounds such as transition metal oxides, sulfides, and organic materials (polymers) have been proposed as replacements. Oxide and sulfide materials have been extensively studied because of their high theoretical capacity. More recently $LiFePO_4$ has attracted much attention and has been even introduced in the commercial market, as a cathode material to replace $LiCo_2$ and $LiMO_2$, due to high cycle stability, low cost, high thermal stability and lack of toxicity.

Polymer-based cathodes are also studied for applications in flexible lithium batteries.[83-85]

The electrolyte between the anode and cathode has to be an ionic conductor, electronic insulator and is responsible for the transport of lithium ions. The optimal electrolyte should combine the conduction properties of a liquid and the mechanical stability of a solid with high chemical stability. Even though liquid electrolytes are commonly used, due to high ionic conductivity, application of polymer and ionic liquid electrolytes are also being investigated since they might improve the safety of lithium ion batteries.

A membrane (separator) is an important component of a battery, as it prevents short circuit by separating the anode from the cathode. In the LIB, the membrane is required to be capable of effecting battery shutdown at a temperature below that at which thermal runaway occurs, and the shutdown should not result in loss of mechanical integrity. Shutdown is an important trait of a good membrane for the safety of lithium batteries. The promising membranes are those with high electrolyte permeability and mechanical strength, as well as good thermal, chemical, and electrochemical stability.

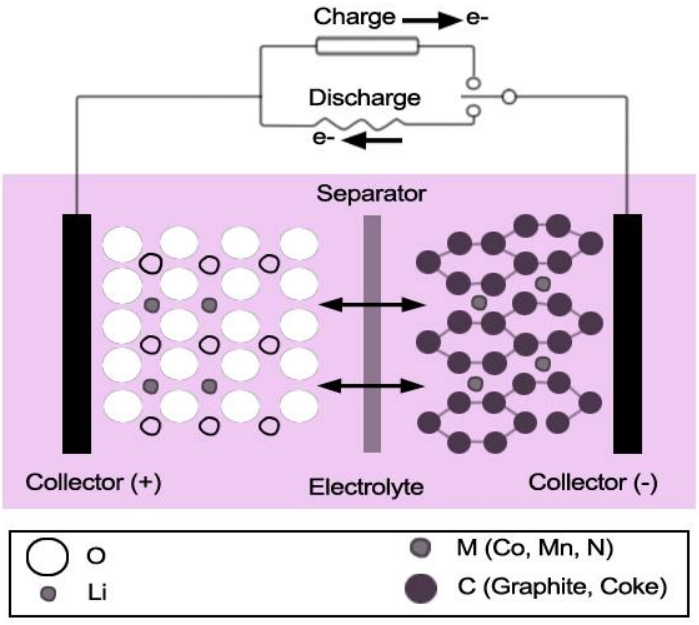

Figure 1.10: Working of a rechargeable lithium ion cell

The electrochemical reactions at a typical Li-ion cell are:

$$\text{Cathode : } LiMO_2 \xleftrightarrow{charge\text{-}discharge} Li_{1-x}MO_2 + xLi^- + xe$$

$$\text{Anode: } C + xLi^+ + xe \xleftrightarrow{charge\text{-}discharge} Li_xC$$

$$\text{Overall: } LiMO_2 + C \xleftrightarrow{charge\text{-}discharge} Li_xC + Li_{1-x}MO_2$$

Each component of a Li-ion cells (the anode, the cathode, the electrolyte and the separator membrane) has to be compatible with each other to provide high safety, cyclability, high capacity, and high rate capability. The LIB is quite suitable for application in Electric Vehicles with improved safety as the main concern. At the same time, much efforts to overcome the 250 Wh/kg limitation of the energy density of lithium batteries is in progress, with the identification of novel types of electrode and electrolyte materials. [86-90]

1.3.2 Cathode

Since 1980 when the $LiCoO_2$, with a 274 mAh/g theoretical capacity, was first demonstrated as a possible cathode material for rechargeable lithium ion cells, the transition metal intercalation oxides have caught the major attention as cathode materials. The conventional cathode materials belong to layered compounds $LiMO_2$ (M=Co, Ni, Mn, etc.), spinel compounds LiM_2O_4 (M=Mn, Fe, etc.), and olivine compounds $LiMPO_4$ (M=Fe, Co, Mn, etc.). The spinel structure of LiM_2O_4 is displayed in figure 1.11.

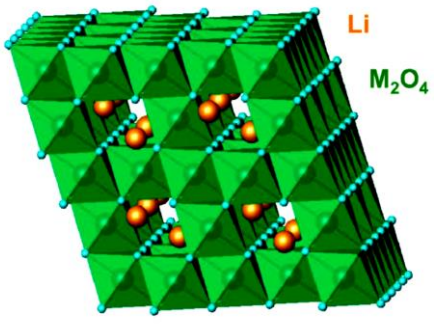

Figure 1.11: Crystal structure of spinel LiM_2O_4 (green: transition metal ions, gold: Li ions) (Courtesy: Prof Petkov)

The cations (M) occupy the octahedral sites but 1/4 of them are located in the Li layer, leaving 1/4 of the sites in transition metal layer vacant. The Li ions occupy the tetrahedral sites that share faces with the empty octahedral sites in the transition metal layer. The structure is based on a three-dimensional MO_2 host and the vacancies in transition metal layer ensure three-dimensional Li diffusion pathways.

Cathode materials for Li ion cells are designed to optimize two important factors, energy density and cyclability. The energy density is determined by the reversible capacity and operating voltage, which are mostly influenced by the material's intrinsic chemistry, such as the effective redox couples and maximum lithium ion concentration in the active material. For good cycling performances, electronic and ionic mobility are important determining factors, though particle morphologies are also significant due to the anisotropic nature of the structures.

Al though Co is expensive and toxic, $LiCoO_2$ is still used in most lithium batteries designed for portable devices due to the high energy density and the good cycle performance. The spinel $LiMn_2O_4$ (120 mAh/g practical capacity) is a non-toxic, safer alternative with good electrochemical characteristics. But this has a drawback, due the dissolution of manganese and destruction of crystal structure at high temperatures. The capacity fading associated with the transformation of the cubic phase to tetragonal phase on repeated cycling of the $LiMn_2O_4$ based cells, termed as the Jahn Teller distortion is another inherent drawback of the $LiMn_2O_4$ cathode material. This defect can be arrested to a significant extent by using composites of $LiMn_2O_4$ with suitable materials. The metal oxide electrode materials are still potentially dangerous because they provide oxygen that might be released and induce a battery explosion at harsh conditions.

Around 1997, Armand et al. and Goodenough et al. independently found that lithium metal phosphate ($LiMPO_4$) has a very stable structure, due to covalent bonding between oxygen and phosphorous, and $LiFePO_4$ was developed as a response to economic and environmental concerns. The olivine structured $LiFePO_4$ offers several advantages, which include theoretical specific capacity

of 170 mAh/g and a high flat voltage versus charge characteristic at 3.4 V against lithium. The latter provides a wider safety margin for use with organic electrolytes and good reversibility of the cathode reactions. High thermal and chemical stability, low material costs, low toxicity, and stable cycling performance are the additional advantages of related to $LiFePO_4$ based Li ion cells. The important characteristics of the commonly used cathode materials for Li ion cells are detailed in table 1.2.

Table 1.2: Properties of cathode materials for rechargeable lithium batteries

	$LiCoO_2$	$LiNiO_2$	$LiMn_2O_4$	$Li[Ni_{1/3}Co_{1/3}Mn_{1/3}]O_2$	$Li[Ni_{1/2}Mn_{1/2}]o_2$	$LiFePO_4$
Theoretical Capacity	274 mAh/g	275 mAh/g	148 mAh/g	285 mAh/g	285 mAh/g	170 mAh/g
Available Capacity	145 mAh/g	185 mAh/g	120 mAh/g	170 mAh/g	170 mAh/g	150 mAh/g
Voltage	3.7 V	3.6 V	3.8 V	3.7 V	3.7 V	3.45 V
Advantages	-High Conductivity. -Easy Synthesis route.	-High Capacity. -Stability of Electrolyte.	-Low Price. -Non Toxic.	-High Capacity -Nontoxic -Good thermal Stability	-High Capacity -Low Price -Good thermal stability	-Low Price -Environ--ment friendly
Disadvanta-ges	-High Cost -Toxic	-Difficult synthesis route -Thermal Instability	-Low Capacity. -Capaci-ty fading at high temperatures	-Low tap density compared to $LiCoO_2$	-Low conductivity ($<10^{-5}$ S/cm)	-Low conductivity ($<10^{-5}$ S/cm)

Inorganic cathode materials are synthesized using a number of techniques such as solid-state, sol-gel, mechanical activation, hydrothermal, co-precipitation, spray, microwave, and supercritical methods. The synthesis conditions are very important for the final properties of the cathode materials. Therefore, the synthesis parameters have been optimized by numerous groups to enhance the electrochemical performance.

For flexible electronic devices, there is a high demand for thin and flexible batteries, driven by their potential applications in micro- and nano-electronic systems. To meet this demand, many attempts have been made to synthesize novel active electrode materials. For this purpose cathodes based on organic/polymeric materials are more advantageous, compared to the conventional cathode materials based on transition metal oxides, since the former are light, environment-friendly and easily processed to thin films with good flexibility. The polyaniline (PANI), polypyrrole (PPy), and organic radical PTMA (poly(2,2,6,6-tetramethylpiperidinyloxy-4-yl methacrylate)) have gained much attention as active cathode materials for flexible batteries(figure 1.12). [91-96]

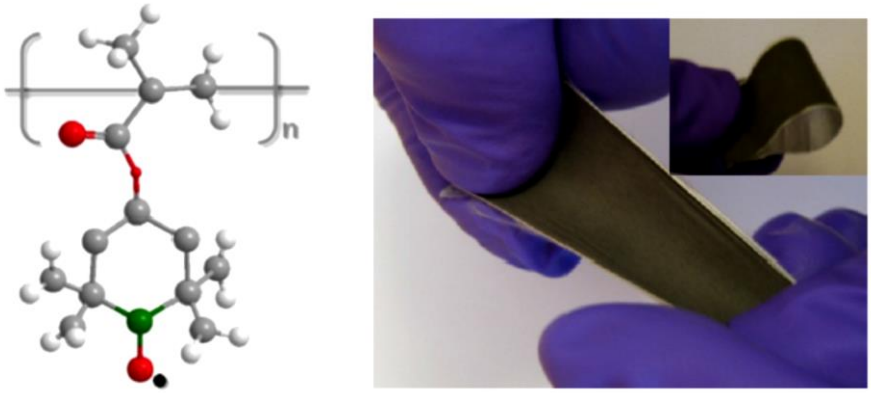

Figure 1.12: Structure of PTMA (left) and a flexible electrode based on the PTMA (right)

1.3.3 Anode

The active anode material occupies 10 weight percent of lithium ion cells and releases electrons during the oxidation stage. In the early attempts, pure lithium was directly used as anode in lithium metal batteries, but it was later substituted by lithiated carbon because of safety problems due to dendrite formation. An ideal anode material should have the electrode potentials close to that of lithium, high energy densities per volume and weight, operational safety during charge discharge processes, perseverance of high current densities, and high thermal stability.

Table 1.3: Properties of anode materials for lithium rechargeable batteries

	Li Metal	Graphite	Si ($Li_{22}Si_5$)	Sn($Li_{22}Sn_5$)	SnO, SnO_2, Al, Pb, Ge, Nano-Co, Nano-Ni
Characteristics	-High Energy Density -High Activity -Not suitable for Flexible Battery Applications	-Low Theoretical Capacity (372 mAh/g) -Low Cost -Low Irreversible Capacity	-High Theoretical Capacity (4200 mAh/g) -Large Irreversible Capacity -Poor Cyclability	-High Theoretical Capacity (990 mAh/g) -Large Volume Expansion (670%) -Large irreversible capacity -Poor Cyclability	-High Capacity (2200 mAh/g) -Large Volume Expansion -Large Irreversible Capacity -Poor Cyclability

Among the carbon materials generally used as anodes, Graphite has the most satisfying anode properties and has been widely used in commercial lithium batteries. The characteristics of anode materials generally used for Li ion cells are summarized in table 1.3.[97-100]

1.3.4 Membrane and Electrolytes

The separator membrane in a typical Li ion cell is a porous film between the anode and the cathode that prevents the possibility of any electrical shorting. Polyethylene (PE) and polypropylene (PP) belong to the class of polyolefin and are the most common membrane materials for rechargeable lithium batteries. Porous polyolefin membranes are suitable,for rechargeable Li ion cells since they can be used for hundreds of cycles without any chemical or physical degradation. A collapse of the pores occurs when the temperature approaches the melting point (around 130°C) of the material, which then forms a nonporous insulated film with a sharp increase in impedance. Since

the increase in the impedance of a PP separator is less than that of a PE separator, the impedance of the PP membrane may not be large enough for complete shutdown in the vicinity of a thermal runaway. Hence, porous PE is the most preferred membrane material for most Li ion cell applications.

The main disadvantages of polyolefin membranes are poor thermal stability at high temperatures and danger of internal short, due to the weak mechanical strength which lead to thermal runaway and even explosions in the extreme case. Ceramic based membranes are being investigated to resolve the disadvantages associated with polyolefin membranes. The ceramic membranes are prepared with inorganic sub-micron sized particles and a small amount of polymer binder, which have dimensional stability at high temperature as well as wettability. Ceramic membranes that improve the thermal and mechanical stability, are also made by ceramic coating of hybrid forms of polyolefin. This type of separator is highly desirable for the development of large-size lithium batteries, especially those installed in electric vehicles and power tools. The membranes used should usually meet the following requirements summarized in the table 1.4.

The electrolyte provides a pathway for ion transfer between the cathode and anode. It should have a high ionic conductivity, good compatibility with the electrode materials and should not react with lithium ions. The electrolyte is usually a liquid where a lithium salt is dissolved in an organic solvent. Aqueous electrolytes are not suitable in rechargeable lithium batteries because they get decomposed at a voltage of 4.2 V. Organic solvents which are more stable in this voltage range are generally used in lithium batteries.

Currently, commercial lithium battery electrolytes use organic carbonate based solvents, such as propylene carbonate (PC) and ethylene carbonate (EC), and $LiPF_6$, $LiBF_4$, and $LiAsF_6$ as lithium salts. The use of these electrolytes allows the realization of high performance batteries. However, since the solvents are flammable, their use poses serious safety risks and strongly reduces the batteries operational temperature range of the batteries. For this reason, alternative electrolytes have been proposed and studied. Among the alternative electrolytes, ionic liquid-based electrolytes and polymer electrolytes appear to be the most promising.

Table 1.4: Required properties of membranes swollen with an electrolyte for rechargeable Li ion batteries

Parameter	Unit	Goal
Conductivity	S/cm	$>10^{-4}$
Thickness	µm	<25
Electrical Resistance	Ω cm^{-2}	<2
Pore Size	µm	<1
Porosity	(%)	~40
Puncture Strength	(kg/S^2)	$>1x10^8$
Mix Penetration Strength	(kg/S^2)	$>4x10^7$
Tensile Strength	(%)	< 2% offset at 1000 psi
Shut Down Temperature	(^oC)	~130
High-temperature, Melt Integrity	(^oC)	>150
Chemical Stability		Stable in battery for a long period of time
Dimensional Stability		Separator should lay flat; must be stable in electrolyte

The solid polymer electrolyte is one of the most promising alternative electrolytes suggested decades ago in order to improve the safety of rechargeable lithium ion cells. The solid polymer electrolyte is synthesized by dissolving a lithium salt in a polar polymer. The poly(ethylene oxide) (PEO) based electrolyte is still one of the most promising and widely studied solid polymer electrolytes because of its good mechanical and thermal properties, and interfacial stability towards lithium metal. The transport of lithium ions within the solid electrolyte has been associated with the local relaxation and segmental motion of the amorphous regions in the PEO chains. These polymers often show high crystallinity at low temperatures and the electrolytes thus exhibit low ionic conductivity at room temperature (typically 10^{-5} S/cm). This drawback of the solid polymer electrolytes necessitates operation at high temperatures (generally, >70 °C) for successful utilization in practical applications.

Gel polymer electrolytes (GPEs) have attracted much attention since they show high ionic conductivities at room temperature. GPEs are made by immobilizing large amount of liquid electrolyte in a polymer host. Porous polymer hosts have been developed to fit GPEs. In porous polymer

electrolytes, the polymer host is a membrane with pores of nanometer to micrometer size that retain the liquid electrolyte. The membrane should have the capability to absorb the liquid electrolyte without leakage, be chemically compatible with electrode materials, and adhere well to the electrodes. Poly(vinylidene fluoride) (PVdF), poly(vinylidene-fluoride-co-hexafluoropropylene){P(VdF-HFP)}, polyacrylonitr-ile (PAN), PEO, and poly(methyl methacrylate) (PMMA) (figure 1.13) have been widely studied as host polymers for preparing GPEs. Poly(vinylidene fluoride) and its copolymer P(VdF-HFP), are particularly preferred as polymer hosts for GPEs because of their thermal and electrochemical stability. The porous membranes are prepared by different methods that include solution casting, phase inversion, plasticizer extraction, and electrospinning. The size and distribution of the pores are important factors that determine the membrane's ability for electrolyte uptake. The process of electrospinning is particularly suitable for producing thin and homogenous polymer membranes with pores in the nano to micrometer size range. Since the membranes possess high porosity, they also exhibit a high electrolyte uptake that results in an ionic conductivity almost comparable with that of liquid electrolytes. [101-105]

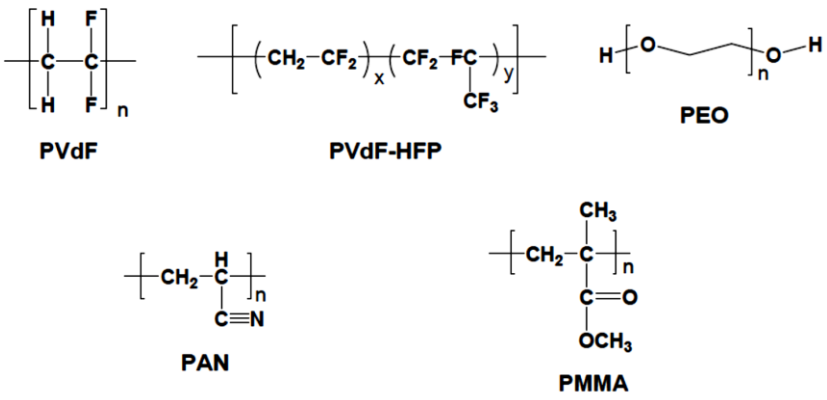

Figure 1.13: Structure of host polymers for gel polymer electrolytes

1.4 Motivation and Objectives of the Present Investigations

Polyaniline is conventionally synthesized using chemical or electrochemical techniques. The effects of dopants and oxidants on the structural and charge transport properties of polyaniline samples have been studied by different

research groups. Recently, some researchers have studied the relationship between the crystallinity of PANI and its charge transport properties and have found that the electrical conductivity of PANI samples strongly depends on the degree of crystallinity. However the synthesis of highly crystalline PANI films with ordered structure and high electrical conductivity has not been pursued in depth.

- In the first phase of the present work, attempts have been made to synthesize, PANI films with high extent of structural order, crystallinity and high electrical conductivity, by chemical oxidative polymerization followed by de-doping and re-doping processes, using m-cresol as solvent. As a new approach, a level surface assisted solution casting technique has been employed to grow homogenous films with uniform thickness on glass substrates .One of the advantages of this technique is that it is a cost effective technique compared to the more expensive spin coating method and thicker films having micrometer order thickness can also be grown using this technique on a variety of substrates. There also exists the possibility of obtaining free standing, conducting films of PANI, which can be rolled into the form of conducting wires for applications in electrical circuits.

Conjugated polymers having good extent of electron delocalization are expected to exhibit significant nonlinear optical (NLO) properties with substantial application prospects. The NLO characteristics can be quite captivating in nanostructured polymer systems and polymer nanocomposites embedded with metal nanoparticles. The phenomena of surface plasmon resonance (SPR) and surface enhanced Raman scattering (SERS) associated with metal-polymer nanocomposite systems are of significant applications in optical limiting and sensor protection, in the design of plasmon waveguides and as nanoprobes in the medical field.

- In the pursuit of assessing the application prospects of PANI in the perceptive of photonics and light based technologies, the first phase of the present work has been devoted to synthesize highly stable PANI-silver/gold nanocomposite samples both in bulk and thin film forms using a modified oxidative polymerization method with monomer

aniline and silver/gold colloidal samples as precursors and investigate the optical properties in the linear and nonlinear regimes. Generally it is not easy to get good, stable films of polymer-metal nanocomposites with the required transparency to pursue the NLO properties. The studies on the NLO characteristics of polyaniline-metal nanocomposite films are significant in this perspective.

Development of sustainable and pollution free energy harvesting schemes in the cost effective way is one of the inevitable requisites of the present century. This calls for the need of accomplishing relevant technologies for energy storage as well, since energy generation is generally intermittent and not continuous. Global research is directed towards identifying new class of component materials with less risk factors and better structural stability and flexibility for assembling energy storage devices with the desired characteristics. Polymer-based electrode materials with inherent flexibility, stability and eco-friendliness can be a suitable choice for secondary batteries and supercapacitors which encompass the important class of energy storage devices. Electronically conducting polymers including polyaniline (PANI), polypyrrole (PPy), their substituted equivalents and their composites with nanostructured filler materials are being investigated to assess their suitability as cathode active materials, specifically in lithium ion batteries. In the designing of rechargeable Li ion cells with polymer-based cathode active materials, the key issue is to identify the optimum lithiation of the polymer cathode which can ensure the highest electronic conductivity and specific charge capacity possible.

- In earlier studies, using lithium substituted (lithiated) PANI as cathode, the lithiation has been achieved by treating PANI with $LiPF_6$ or $LiBF_4$. In the present work, a novel approach of lithiation has been attempted,by treating PANI with *n*-butyllithium(*n*-BuLi) in hexanes which is a more economical method to achieve lithium substitution in PANI.

- The ultimate aim is to assemble Li ion cells employing Li substituted polyaniline and its composites with conventional inorganic cathode

materials like $LiFePO_4$ and $LiMn_2O_4$ as the cathode active materials, lithium foil as anode and lithium hexafluorophosphate ($LiPF_6$) in ethylene carbonate (EC): dimethyl carbonate (DMC) (1:1) as electrolyte, with expected specific capacity over 50mAh/g, coulombic efficiency around 98% and excellent cycling stability over 100 cycles. The possibilities of arresting the inherent Jahn-Teller distortion of $LiMn_2O_4$ cathode, due to the presence of PANI in the composite cathode material will also be investigated.

- With a view to assess the prospects of lithium enriched polyethylene oxide (PEO) as a suitable substitute for the conventionally used liquid electrolytes in Li ion cells, attempts have been made to investigate in detail the Li ion transport properties in this solid electrolyte. Identifying suitable solid electrolytes with the desired electrochemical characteristics is a pre-requisite to fulfill the vision of having all solid state, polymer-based lithium ion cells with flexibility in cell design and construction. The present investigations are eventually oriented in the direction of assembling eco-friendly, polymer-based, flexible, solid state Li ion cells with excellent cycling stability and desired charge storage capability.

References

1. R. L. Greene, G. B. Street and L. J. Suter, *Phys. Rev. Lett*., **34**, 577 (1975).
2. 2. H. Shirakawa, E. J. Louis, A. G. MacDiarmid, C. K. Chiang and A. J. Heeger, *J. Chem. Soc. Chem. Commun*., 578 (1977).
3. C. K. Chiang, C. R. Fincher, Jr., Y. W. Park, A. J. Heeger, H. Shirakawa, E. J. Louis, S. C. Gau and G. MacDiarmid, *Phys. Rev. Lett*., **39**, 1098 (1977).
4. A. F. Diaz and J. A. Logan, *J. E/ectroanal. Chem*., **111**, 111 (1980).
5. L. Gilchrist, *J. Phys. Chem.*, **8**, 539 (1904).
6. H. T. Bucherer, *Ber,*, **40**, 3412 (1907).

7. Akheel A. Syed and Maravattickal K. Dinfsan, *Review-Ta/anta*, **38**, 8, 815-837, (1991)
8. Idem, *Sovehsch. Electrokhim*., **579.** Izdat. Akad. Nauk SSSR, Moscow, (1953).
9. W.-S. Huang, B. D. Humphrey and A. G. MacDiannid, *J. Chem. Soc*., Faraday Trans. I, **82**, 2385 (1986).
10. R. de Surville, M. Jozefowicz, L. T. Yu, J. Perichon and R. Buvet, *E/ectrochimica Acta*,, **13**, 1451 (1968).
11. M. Jozefowicz, J. H. Perichon, L. T. Yu and R. Buvet, *Br. Patent*, , No. 1216569(1970).
12. S. P. Armes and M. Aldissi, *J. Chem. Soc. Chem. Commun*., **88** (1989).
13. J. C. Chiang and A. G. MacDiarmid, *Synth. Met*., **13**, 193 (1986).
14. J. C. Chiang, *Ph. D. Thesis*, University of Pennsylvania, (1987).
15. Idem, *ibid.* **200**, 127 (1986).
16. A. G. MacDiannid, J. C. Chiang, M. Halpern, W. S. Huang, S. L. Mu, N. L. D. Somasiri, W. Wu and S. I. Yaniger, *Mo/. Cryst. Liq. Cryst*., **121**, 173 (1985).
17. G. Mengoli, M. T. Munari, P. Bianco and M. M. Musiani, *J. Appl. Polym. Sci*., **26**, 4247 (1981).
18. M. M. Musiani, G. Mengoli and F. Furlanetto, *ibid*, **29**, 4433 (1984).
19. D. W. DeBerry, J. Electrochem. Soc., **132**, 1022 (1985).
20. G. Mengoli, M.-T. Munari and C. Folonari, *J. Electro- anal. Chem*., **124**, 237(1981).
21. R. Noufi, A. J. Nozik, J. White and L. F. Warren, *ibid*. **129**, 2261 (1982).
22. T. Osaka, S. Ogano and K. Naoi, *ibid*, **135**, 539 (1988).
23. D. M. Mohilner, R. N. Adams and W. J. Argersinger, Jr., *J. Am. Chem. Soc*., **84**, 3618 (1962).
24. J. Bacon and R. N. Adams, *J. Am. Chem. Soc*., **90**, 6596 (1968).
25. M. Breitenbach and K.-H. Beckner, *J. Electroanal. Chem.,* **29**, 309 (1971).
26. Idem, *ibid*. **33**, 45 (1971).

27. E. M. Genies, J. F. Penneau and M. Lapkowski, *J. E/ectroana/. Chem*., **260**, 145 (1989).
28. E. M. Genies, J. F. Penneau, M. Lapkowski and A. Boyle, *ibid*. **269**, 63 (1989).
29. J. P. Travers, J. Chroboczek, F. Devreux, F. Genoud, M. Nechtschein, A. A. Syed, E. M. Genies and C. Tsintavis, *Mo/. Cryst. Liq. Cryst.*, **121**, 195 (1985).
30. W.-S. Huang, A. G. MacDiarmid and A. J. Epstein, *J. Chem. Soc. Chem. Commun*., 1784 (1987).
31. L. T. Yu and M. Josefowicz, *Rev. Gen. E/ec*., **75**, 1014(1966).
32. M. Doriomedoff, F. H. Cristofini, R. de Surville, M. Josefowicz, L. T. Yu and R. Duvet, *J. Chim. Phys*., **68**, 1055 (1971).
33. L. J. van der Pauw, *Philips Tech. Rev*.,, **20**, 220 (1958/59).
34. F.-R. F. Fan, T. V. Shea and A. J. Bard, *J. E/ectro- chem. Soc*., **131**, 828 (1984).
35. M. Gholamian, T. N. S. Kumar and A. Q. Contractor, *Proc. Indian Acad, Sci., Chem. Sci*., **97**, 457 (1986).
36. 8. Lundberg, W. R. Salaneck and I. Lundstr, *Synth. Met*., **21** 143 (1987).
37. H. H. S. Javadi, F. Zuo, K. R. Cromack, M. Angelopoulos, A. G. MacDiarmid and A. J. Epstein, *ibid*., **29**, E409(1989).
38. A. J. Epstein, J.- M. Ginder, F. Zuo, R. W. Bigelow, H.-S. Woo, D. 8. Tanner, A. F. Richter, W. S. Huang and A. G. MacDiarmid, ibid., **18**, 303 (1987).
39. W. W. Focke, G. E. Wnek and Y. Wei, *J. Phys. Chem.*, **91**, 5813(1987).
40. W. W. Focke and G. E. Wnek, *J. Electroana/. Chem.*, **256**, 343 (1988).
41. M. Angelopoulos, A. Ray, A. G. MacDiarmid and A. J. Epstein, *ibid.*, **21**, 21(1987).
42. J. P. Travers and M. Nechtschein, *ibid.*, , 21, 135 (1987).
43. A. Kitani, M. Kaya, J. Yano, K. Yoshikawa and K. Sasaki, *ibid*. **18**, 341(1987).
44. H. Kuzmany, N. S. Sariciftci, H. Neugebauer and Neckel, *Phys. Rev. Lett*., **60**, 212 (1988).

45. A. Ray, G. E. Asturias, D. L. Kershner, A. F. Richter, G. MacDiarmid and A. J. Epstein, Synth. Met., **29**, El41 (1989).
46. A. Kitani, M. Kaya and S. Sasaki, *J. E/ectrochem. Soc.*, **133**, 1069(1986).
47. A. G. MacDiarmid, S. L. Mu, N. L. D. Somasiri and W. Wu, *Mo/. Cryst. Liq. Cryst.*, **121**, 187(1985).
48. M. Akhtar, H. A. Weakliem, R. M. Paiste and K. Gaughan, *Synth. Met.*, **26**, 203 (1988).
49. M. A. Habib, *Langmuir*, **4**, 1302 (1988).
50. S. Gottesfeld, A. Redondo and S. W. Feldberg, *J. Electrochem. Soc*., **134**, 271 (1987).
51. A. J. Nozik, *Annual Rev. Phys. Chem*., **29**, 189 (1978).
52. S. Chandra and R. K. Pandey, *Phys. Stat. Sol. A*, **72**, 415(1982).
53. M. Kaneko and H. Nakamura, *J. Chem. Soc. Chem. Commun*., **346** (1985).
54. S. Chao and M. S. Wrighton, *J. Am. Chem. Soc*., **109**, 6627 (1987).
55. M. Gholamian, J. Sundaram and A. Q. Contractor, *Langmuir*, **3**, 741 (1987).
56. T. Hirai, S. Kuwabata and H. Yoneyama, J. Electro- chem. Soc.: Electrochem. Sci. Technol., **13**, 1132(1988).
57. G. Bidan, E. M. Genies and M. Lapkowski, *J. Chem. Soc. Chem. Commun*., **533**. (1988).
58. K. M. Kost, D. E. Bartak, B. Kazee and T. Kuwana, *Anal. Chem*., **60**, 2379 (1988).
59. R. Jiang and S. Dong, *J. Chem. Soc. Faraday Trans.1*, **SS**, 1585 (1989).
60. A. A. Syed and M. K. Dinesan, *Synth. Met*., **36**, 209 (1990).
61. Handbook of Nonlinear Optics, R. L. Sutherland, Second Edition, *Marcel Dekke*r New York (2003).
62. Solid-State Lasers, W. Koechner and M. Bass, *Springer-Verlag*, New York (2003).
63. Suchand Sandeep C.S., *Phd Thesis,* Raman Research Institute, March (2010)

64. Ultrafast Optics (Wiley Series in Pure and Applied Optics), A. Weiner, *Wiley, Hoboken* (2009).
65. Physics of Nonlinear Optics, Gung S. He and Song H. Liu, *World Scientific*, Singapore (1999).
66. Laser Spectroscopy: Volume 2: Experimental Techniques, W. Demtroder, Fourth Edition, *Springer-Verlag*, Berlin Heidelberg (2008).
67. Lasers, A. E. Seigman, *University Science Books*, California (1986)
68. Lasers, A. E. Siegman, University Science, *Mill Valley*, CA. (1986).
69. Strong-field saturation effects in laser media, D. H. Close, *Phys. Rev*., **153**, 360 (1966).
70. An analysis of saturable absorbers, M. Hercher, *Appl. Opt*. **6**, 947 (1967).
71. Handbook of Nonlinear Optics, R. L. Sutherland, Second Edition, *Marcel Dekker*, New York (2003).
72. Handbook of Batteries, 2nd edition, D. Linden, Ed., *McGraw-Hill*, Inc., NewYork (1995).
73. Modern Batteries: An introduction to Power sources Colin A. et.al *Edward Arnold* (1984).
74. "Advanced Secondary Batteries" A review. R.M Dell U.K. *Atomic Energy Authority* (1979).
75. M. Armand, J.-M. Tarascon, *Nature*, **451**, 652–657(2008).
76. C. Daniel, *JOM*, **60** (9) 43–48(2008).
77. M.S. Whittingham, *MRS Bull*. **33** (4), 411–419(2008).
78. A. Patil, V. Patil, D.W. Shin, J.-W. Choi, D.-S. Paik, S.-J. Yoon, Issue a, *Mater. Res. Bull.* **43,** 1913–1942 (2008).
79. J. Hassoun, P. Reale, B. Scrosati, *J. Mater. Chem.* **17,** 3668–3677 (2007).
80. A.K. Shukla, T.P. Kumar, *Curr. Sci.* **94,** 314–331(2008).
81. M.S. Whittingham, , *Dalton Trans*. 40 (2008) 5424–5431.
82. P.G. Bruce, B. Scrosati, J.-M. Tarascon, *Angew. Chem. Int. Ed*. **47**, 2930–2946 (2008).
83. M.S. Whittingham, *Chem. Rev*. **104**, 4271–4301 (2004).
84. Y.-G. Guo, J.-S. Hu, L.-J. Wan, *Adv. Mater*. **20**, 2878–2887(2008).
85. Y. Wang, G. Cao, *Adv. Mater*. **20**, 2251–2269 (2008).

86. M.S. Whittingham,, Dalton Trans. **40**,5424–5431(2008).
87. P.G. Bruce, B. Scrosati, J.-M. Tarascan,, *Angew. Chem. Int. Ed*. **47**, 2930–2946(2008).
88. Y.-G. Guo, J.-S. Hu, L.-J. Wan, Adv. Mater. **20**, 2878–2887(2008).
89. Y. Wang, G. Cao,, Adv. Mater. **20**, 2251–2269 (2008).
90. White, C.G. Vayenas, M.E. Gamboa-Aldeco (Eds.), **8**, *Springer*, New York, NY, pp. 75–126 (2007).
91. D. Belov, M.-H. Yang, *Solid State Ionics* **179**, 1816–1821(2008).
92. D. Belov, M.-H. Yang, J. *Solid State Electrochem.* 12, 885–894(2008).
93. C.-H. Doh, D.-H. Kim, H.-S. Kim, H.-M. Shin, Y.-D. Jeong, S.-I. Moon, B.-S. Jin, S.W. Eom, H.-S. Kim, K.-W. Kim, D.-H. Oh, A. Veluchamy, *J. Power Sources* **175**, 881–885(2008).
94. Y. Takahashi, S. Tode, A. Kinoshita, H. Fujimoto, I. Nakane, S. Fujitani, *J. Electrochem. Soc*. **155 (7)**, A537–A541 (2008).
95. G.G. Amatucci, J.M. Tarascon, L.C. Klein, *Solid State Ionics* **83**, 167–173(1996).
96. G.G. Amatucci, J.M. Tarascon, L.C. Klein, J. *Electrochem. Soc*. **143 (3)**, 1114–1123 (1996).
97. Poizot, P.; Laruelle, S.; Grugeon, S.; Dupont, L.; Tarascon, J-M. *Nature*, **407**, 496-499 (2000).
98. Nam, K. T.; Kim, D. P.; Yoo, J.; Chiang, C.; Meethong, N.; Hammond, P. T.; Chiang, Y.; Belcher, A. M. *Science*, **312**, 885-888 (2006).
99. Lou, X. W.; Deng, D.; Lee, J. Y.; Feng, J.; Archer, L. A. *Adv. Mater*., **20**, 258–262 (2008).
100. Li, Y.; Tan, B.; Wu, Y. *Nano Lett*. **8**, 265–270 (2008).
101. M.Wakihara, O. Yamamoto (Eds.), Lithium Ion Batteries, *Wiley–VCH* (1998).
102. F.M. Gray, Solid Polymer Electrolytes, *VCH*, (1991).
103. R.D. Rogers, K. Seddon (Eds.), Ionic Liquids: Industrial Applications to Green Chemistry, *ACS Symposium Series* **818** (2002).
104. M. Galin´ ski, A. Lewandowski, I. Ste¸pniak, *Electrochim. Acta*, **51**, 5567(2006).
105. Andrzej Lewandowski, Agnieszka S´widerska-Mocek, *Journal of Power Sources* **194**, 601–609 (2009).

Chapter 2

Materials and Methods

Abstract: A lot of research grade chemicals and sophisticated instruments for material synthesis and analysis have been utilized to carry out the investigations detailed in the present work. The important chemicals and materials used and the characterization techniques employed are summarized below.

2.1 Materials Used

Consumables	**Source**
n-Butyllithium solution ~1.6 M in hexanes	Sigma- Aldrich
Poly(ethylene oxide)	Sigma- Aldrich
Lithium per chlorate	Sigma- Aldrich
Gold foil	Vision Scientific
Silver Nitrate	Sigma- Aldrich
Aniline	Alfa –Aesor
m-Cresol	Alfa –Aesor
Ammonium Peroxy-disulphate	Alfa – Aesor
PVDF	Sigma – Aldrich
$LiPF_6$ in DMC and MC	MTI Corporation
Aluminum and Copper Foil	MTI Corporation
Camphor Sulphonic Acid (CSA)	Alfa- Aesor
Naphthalene Sulphonic Acid (NSA)	Alfa- Aesor
Hydrochloric Acid (HCl)	Alfa- Aesor

2.2 Characterization Techniques:

2.2.1 X-ray Powder Diffraction (XRD)

X-ray powder diffraction (XRD) is a rapid analytical technique primarily used for phase identification of a crystalline material and can provide information on unit cell dimensions. The materials to be analyzed are finely ground, homogenized, and average bulk composition is determined.

Max von Laue, in 1912, discovered that crystalline substances act as three-dimensional diffraction gratings for X-ray wavelengths similar to the spacing of planes in a crystal lattice. X-ray diffraction is now a common technique for the study of crystal structures and atomic spacing.

X-ray diffraction is based on constructive interference of monochromatic X-rays and a crystalline sample. These X-rays are generated by a cathode ray tube, filtered to produce monochromatic radiation, collimated to concentrate, and directed toward the sample. The interaction of the incident rays with the sample produces constructive interference (and a diffracted ray) when conditions satisfy Bragg's Law ($n\lambda = 2d\ sin\ \theta$). This law relates the wavelength of electromagnetic radiation to the diffraction angle and the lattice spacing in a crystalline sample. These diffracted X-rays are then detected, processed and counted. By scanning the sample through a range of 2θ angles, all possible diffraction directions of the lattice should be attained due to the random orientation of the powdered material. Conversion of the diffraction peaks to d-spacing allows identification of the material because each material has a set of unique d-spacing. Typically, this is achieved by comparison of d-spacing with standard reference patterns.[1, 2]

All diffraction methods are based on generation of X-rays in an X-ray tube. These X-rays are directed at the sample, and the diffracted rays are collected. A key component of all diffraction is the angle between the incident and diffracted rays. Powder and single crystal diffraction techniques vary in instrumentation design, beyond this.

X-ray diffractometers consist of three basic elements: an X-ray tube, a sample holder, and an X-ray detector. X-rays are generated in a cathode ray tube by

heating a filament to produce electrons, accelerating the electrons toward a target by applying a voltage, and bombarding the target material with electrons. When electrons have sufficient energy to dislodge inner shell electrons of the target material, characteristic X-rays are generated, which consist of several components, the most common being K_α and K_β. K_α consists of $K_{\alpha1}$ and $K_{\alpha2}$. $K_{\alpha1}$ has a slightly shorter wavelength and twice the intensity of $K_{\alpha2}$. The specific wavelengths are characteristic of the target material (Cu, Fe, Mo, Cr). Filtering, by foils or crystal monochromater, is required to produce monochromatic X-rays needed for diffraction. The radiations $K_{\alpha1}$ and $K_{\alpha2}$ are sufficiently close in wavelength so that a weighted average of the two is used. Copper is the most common target material for single-crystal diffraction, with a wavelength of 1.5418 Å for CuK_α radiation.

Figure 2.1: The PANalytical's X'Pert Pro high resolution diffractometer with $Cu\ K_\alpha$ radiation of 1.542 Å

In a typical experiment, X-rays are collimated and directed onto the sample. As the sample and detector are rotated, the intensity of the reflected X-rays is

recorded. When the geometry of the incident X-rays impinging the sample satisfies the Bragg equation, constructive interference occurs, resulting in a peak in intensity. A detector records and processes this X-ray signal and converts the signal to a count rate which is then output to a device such as a printer or computer monitor.

The geometry of an X-ray diffractometer is such that the sample rotates in the path of the collimated X-ray beam at an angle θ while the X-ray detector is mounted on an arm to collect the diffracted X-rays and rotates at an angle of 2θ. The instrument used to maintain the angle and rotate the sample is termed a goniometer. For typical powder patterns, data is collected at 2θ from ~5° to 70°, which are the angles that are preset in the X-ray scan. In the present work PANalytical's X'Pert Pro high resolution diffractometer (Figure 2.1) with Cu Kα radiation of 1.542 Å was used for structural characterisations.[3-4]

2.2.2 Fourier Transform Infra-Red Spectroscopy (FTIR)

In infrared spectroscopy, IR radiation is passed through a sample. Some of the infrared radiation is absorbed by the sample and some of it is passed through (transmitted). The resulting spectrum represents the molecular absorption and transmission, creating a molecular fingerprint of the sample. Like a fingerprint, two unique molecular structures will not produce the same infrared spectrum. This makes infrared spectroscopy useful for several types of analysis.

Infrared spectroscopy has been a workhorse technique for material analysis in the laboratory for over seventy years. An infrared spectrum represents a fingerprint of a sample with absorption peaks which correspond to the frequencies of vibrations between the bonds of the atoms making up the material. Since every compound is a unique combination of atoms, no two compounds can produce exactly same infrared spectrum. Therefore, infrared spectroscopy is quite effective in the identification (qualitative analysis) of every kind of material. In addition, the size of the peaks in the spectrum is a direct indication of the amount of material present in the sample. With modern software algorithms, infrared spectroscopy is an excellent tool for quantitative analysis.[5-6]

Fourier Transform Infrared (FT-IR) spectrometry was developed in order to overcome the limitations encountered with dispersive instruments. The main difficulty was the slow scanning process. A method for measuring all of the infrared frequencies simultaneously, rather than individually, was needed. A solution was developed which employed a very simple optical device called an interferometer. The interferometer produces a unique type of signal which has all of the infrared frequencies "encoded" into it. The signal can be measured very quickly, usually on the order of one second or so. Thus, the time element per sample is reduced to a matter of a few seconds rather than several minutes.

Figure 2.2: Thermo Nicolete Avatar 100 DTGS model FTIR spectrophotometer

Most interferometers employ a beam splitter which takes the incoming infrared beam and divides it into two optical beams. One beam gets reflected from a flat mirror which is fixed in place and the other from another flat mirror, which is mechanically allowed to move a very short distance (typically a few millimeters) away from the beam splitter. The two beams get reflected off from their respective mirrors and are recombined when they meet back at the beam splitter. Because the path that one beam travels is fixed and the other is constantly changing as its mirror moves, the signal which exits the interferometer is the result of these two beams "interfering" with each other. The resulting signal is called an interferogram which has the unique property that every data point (a function of the moving mirror position) which makes up the signal has information about every infrared frequency which comes from the source.

This means that as the interferogram is collected, all frequencies are being acquired simultaneously. Thus, the use of the interferometer results in extremely fast measurements. Because the analyst requires a frequency spectrum (a plot of the intensity at each individual frequency), a means of "decoding" the individual frequencies is required. This can be accomplished via a well-known mathematical technique called the Fourier transformation. This transformation is performed by the computer which then presents the user with the desired spectral information for analysis.[7-8]

2.2.3 Raman Spectroscopy

Raman spectroscopy is a technique based on inelastic scattering of monochromatic light, usually from a laser source. Inelastic scattering means that the frequency of photons in the monochromatic source changes upon interaction with a sample. Frequency of the scattered photons is shifted up or down in comparison with original monochromatic frequency and this phenomenon is called the Raman Effect. This shift provides information about vibrational, rotational and other low frequency transitions in molecules. Raman spectroscopy can be used to study solid, liquid and gaseous samples.

The Raman effect is based on molecular deformations in the presence of an electric field E determined by molecular polarizability. The laser beam can be considered as an oscillating electromagnetic wave with electrical vector E. Upon interaction with the sample it induces electric dipole moment $P = \alpha E$ which deforms the sample. Because of periodical deformation, the molecules of the samples start vibrating with characteristic frequency ν_m.

Amplitude of vibration is called a displacement. In other words, monochromatic laser light with frequency υ_0 excites molecules and transforms them into oscillating dipoles. If the substance being studied is illuminated by monochromatic light, for example from a laser, the spectrum of the scattered light consists of a strong line (the exciting line) of the same frequency as the incident illumination together with weaker lines on either side shifted from the strong line by frequencies ranging from a few to about 3500 cm^{-1}. The lines of the scattered radiation having frequency less than that of the exciting radiation are called Stokes lines, and the others anti-Stokes lines.[9-10]

About 99.999% of all incident photons undergo elastic Rayleigh scattering. This type of signal is useless for practical purposes of molecular characterization. Only about 0.001% of the incident light produces inelastic Raman signal with frequencies $v_0 \pm v_m$. Spontaneous Raman scattering is very weak and special measures should be taken to distinguish it from the predominant Rayleigh scattering. Instruments such as notch filters, tunable filters, laser stop apertures and double and triple spectrometric systems are used to reduce Rayleigh scattering and obtain high-quality Raman spectra.

Figure 2.3: High resolution Raman spectrometer (Horiba JY)

Raman signal is normally quite weak and attempts are being carried out to improve Raman spectroscopy techniques. Many different ways of sample preparation, sample illumination and scattered light detection have been implemented to enhance intensity of Raman signal.

2.2.3.1 Surface Enhanced Raman Scattering (SERS)

Surface-Enhanced Raman Spectroscopy utilizes the following effect. Raman signal from molecules adsorbed on certain metal surfaces can be five to six orders of magnitude stronger than the Raman signal from the same molecules in bulk volume. The exact reason for such dramatic improvement in signal intensity is still under discussion. Since the intensity of Raman signal is proportional to the square of electric dipole moment $P = \alpha E$, there are two possible reasons - the enhancement of polarizability α, and the enhancement of electrical field E.

The enhancement of polarizability may occur because of a charge-transfer effect or chemical bond formation between metal surfaces and molecules under observation. This is called chemical enhancement.

The second one takes into account the interaction of the laser beam with irregularities on the metal surface such as metal micro-particles or roughness profile. It is believed that laser light excites conduction electrons at the metal surface leading to surface plasmon resonance and strong enhancement of electric field E. It is called electromagnetic enhancement.[11-12]

In all cases choice of appropriate substrate is very important. The most popular and universal substrates used for SERS are electrochemically etched silver electrodes as well as silver and gold colloids with average particle size below 20 nm.

2.2.4 Stylus Profiler

The stylus profiler is commonly used to measure the thickness of film samples. A diamond stylus or probe in contact with the sample surface is moved laterally to detect and measure small vertical variations. The lateral resolution is dependent on probe size (radius), speed, scan length, and the force applied. The profiler can be used to determine film thickness, average surface roughness (RMS), depth of etch pits or holes and the thickness of film samples can be determined in the range of a few nanometers to micrometers. Its limitations include the possibilities of sample damage due to the scratching of the sample surfaces as the tip touches the sample during the measurement. The stylus profiler generally does single line scans.[13-14]

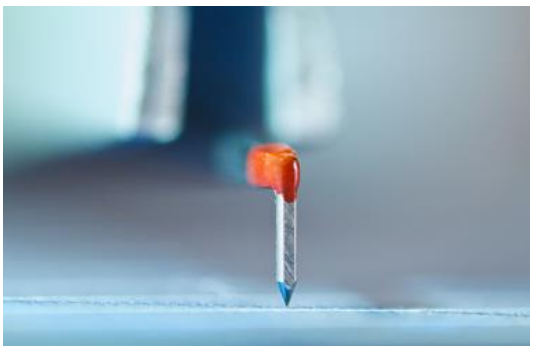

Figure 2.4: Probe of a stylus profiler

2.2.5 Atomic Force Microscopy (AFM)

Atomic Force Microscopy provides a 3D profile of the sample surface on a nanoscale, by measuring forces between a sharp probe (tip size <10 nm) and the surface at very short distances of the order of 0.2-10 nm (probe-sample separation). The probe is supported on a flexible cantilever. The AFM tip "gently" touches the sample surface and records the small forces between the probe and the surface.

The probe is placed at the end of a cantilever (which one can think of as a spring). The amount of force between the probe and the sample is dependent on the spring constant (stiffness of the cantilever) and the distance between the probe and the sample surface. This force can be described using Hooke's Law, [15-16]

$$F = -k.x \tag{2.1}$$

F = Force
k = spring constant
x = cantilever deflection

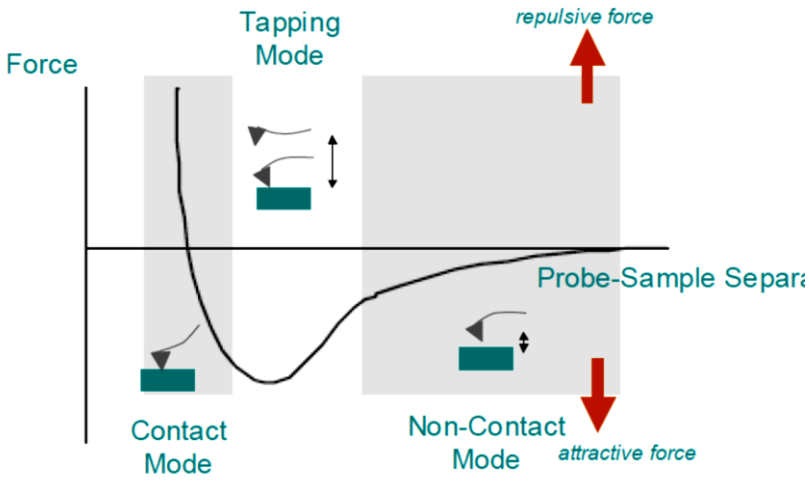

Figure 2.5: Graph shows the variation of force with probe sample separation

If the spring constant of cantilever (typically ~ 0.1-1 N/m) is less than the force exerted by the sample surface, the cantilever bends and the deflection is

monitored. The interaction between the cantilever and the sample surface, typically results in forces ranging from nN (10^{-9}) to μN (10^{-6}) in open air.

Figure 2.6: Atomic Force Microscope (Agilent 5500 series)

The dominant interactions at short probe-sample distances in the AFM are Van der Waals (VdW) interactions. However long-range interactions (i.e. capillary, electrostatic, and magnetic) are significant further away from the surface. These are important in other Scanning Probe Microscopy methods of analysis. During contact with the sample, the probe predominantly experiences repulsive Van der Waals forces (contact mode). This leads to the tip deflection described previously. As the tip moves further away from the surface, attractive Van der Waals forces are dominant (non-contact mode).[17-18]

2.2.6 Field Emission-Scanning Electron Microscopy

Field emission scanning electron microscopy is an imaging technique that works with electrons instead of light, which are liberated by a field emission source. The sample under study is scanned by electrons according to a zig-zag pattern. The FESEM is used to visualize very small topographic details on the sample surface. This technique can be applied to observe structures that may be as small as 1 nanometer and can be conveniently used to study organelles and DNA materials in cells, synthetic polymers and coatings on microchips.

Electrons are liberated from a field emission source and accelerated in a high electrical field gradient. Within the high vacuum column, these so-called primary electrons are focused and deflected by electronic lenses to produce a narrow scan beam that bombards the sample. As a result secondary electrons are emitted from each spot on the sample surface. The angle and velocity of these secondary electrons can be related to the surface features of the sample. A detector catches the secondary electrons and produces an electronic signal. This signal is amplified and transformed to a video scan-image that can be seen on a monitor or to a digital image that can be saved and processed further.[19-20]

Figure 2.7: Field Emission Scanning Electron Microscope
(FESEM-Carl Zeiss, Supra 40 VP)

2.2.7 DC Electrical Conductivity

The four- point probe technique is one of the most common methods for measuring electrical resistivity of solid samples. The classic arrangement is to have four needle-like electrodes in a linear arrangement with a current injected

into the material via the outer two electrodes. The resultant electric potential distribution is measured via the two inner electrodes as shown in figure 18. By using separate electrodes for the current injection and for the determination of the electric potential, the contact resistance between the metal electrodes and the material will not show up in the measured results. Because the contact resistance can be large and can strongly depend on the condition and materials of the electrodes, it is easier to interpret the data measured by the four-point probe technique than results gathered by two-point probe technique.

The four-point probe technique was originally developed by Wenner in 1916 to measure the earth's resistivity. In geophysics it is referred to as Wenner's method. In 1954 Valdes adopted the technique for semiconductor wafer resistivity measurements. The technique has also been applied to characterize electrolytes and to analyze gases.[21-22]

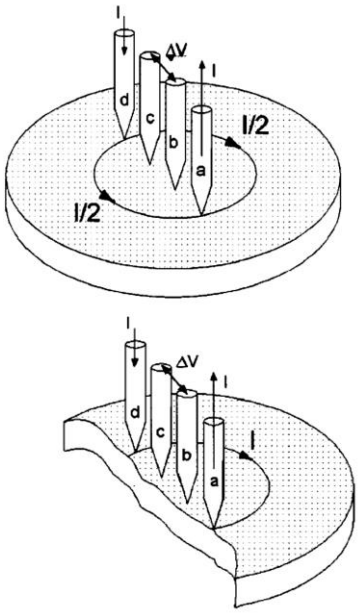

Figure 2.8: (a) Four-point probe measurement technique (b) Probe near the edge of the sample; the current has to go through the left half plane

In general, the material's sheet resistivity,ρ can be calculated using the relation

$$\rho = RCF\left(\frac{V_{measured}}{I_{measured}}\right) \quad (2.2)$$

The resistivity correction factor, RCF takes in to account the size of the test structure, the thickness of the material, the size of the electrodes, and the position of the electrodes with respect to the boundary of the test structure. The effect of the position of the electrodes with respect to the boundaries of the test structure is shown in figure 18 (b). By placing the electrodes at the edge rather than in the middle of the test structure, the measured voltage over the inner electrodes will be two times larger because all current has to take the right-half plane. Valdes had calculated the RCF for probes parallel and perpendicular to the boundary of a slab. Others have modified the linear arrangement of the electrodes and included different geometrical patterns.[23]

2.2.8 UV-Visible spectroscopy

Spectroscopy is based, principally, on the study of the interaction between electromagnetic radiation and matter. This interaction causes , electronic transitions from a lower energy level, say m, to a higher level, l , in the atom with the simultaneous absorption of energy equal to the energy difference between the levels, $E_1 - E_m$,

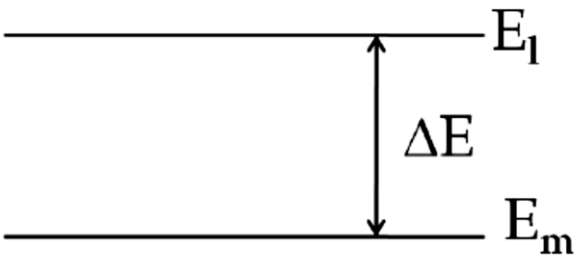

Figure 2.9: Transition of electrons from lower energy level to higher level

$$\Delta E = h\vartheta = \frac{hc}{\lambda} \qquad (2.3)$$

$$h = Plank's\ constant$$

$$\vartheta = Frequency$$

$$\lambda = Wavelength$$

A plot of these processes as a function of radiation wavelength is known as a spectrum that offers information about the difference of energy involved in

each electronic transition. Different types of spectroscopy can be found depending on the wavelength of the incident electromagnetic radiation as depicted below:

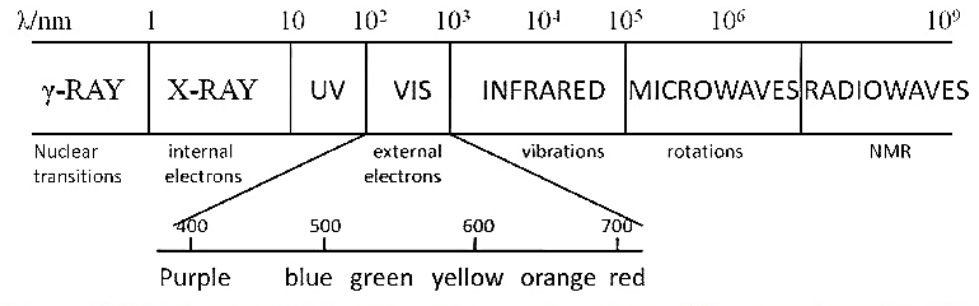

Figure 2.10: Electromagnetic spectrum as a function of the wavelength of the radiation

UV- Visible spectroscopy (radiations with wavelengths between 10 and 1000 nm) offers information about the transition of the most external electrons of the atoms (figure 19). Since atoms or molecules absorb UV - visible radiation at different wavelengths, spectroscopy/spectrometry is often used in physical and analytical chemistry for the identification of substances through the spectrum emitted from or absorbed by them. This technique is also used to assess the concentration or amount of a given species using the Beer-Lambert law.

Beer- Lambert law

This law relates the absorption of a radiation to the properties of the material through which it is passing. The law states that there is a logarithmic dependence between the transmission, T, of light through a substance and the product of the absorption coefficient of the substance,α, and the distance the beam travels through the material (i.e. the path length), l . The absorption coefficient can, in turn, be written as a product of the molar absorptivity of the absorber,ϵ, and the concentration c of absorbing species in the material. For liquids, these relations are usually written as,

$$\log T = \log \frac{I}{I_0} = \epsilon l c \qquad (2.4)$$

where I and I_0 are the intensities of the incident and the transmitted beams, respectively. The transmission can also be expressed in terms of absorbance (A):

$$A = -\log T \tag{2.5}$$

And so, Beer-Lambert equation can be written finally as

$$A = \epsilon l c \tag{2.6}$$

Either transmittance or absorbance can be measured experimentally with the spectrometer. Thus, if the path length and the molar absorptivity are known and the absorbance is measured, the concentration of the substance (or the number density of absorbers) can be deduced. Commonly, both parameters are constant for a given set of experiments. A plot of the sample absorbance against the concentration of the absorbing substance should be a straight line. In practice, a calibration curve is obtained by plotting the measured absorbance of a series of standard samples as a function of their concentration. If the absorbance of an unknown sample is then measured, the concentration of the absorbing component can be determined from this graph.

Figure 2.11: Jasco V 750 UV–VIS spectrophotometer

Spectrophotometry involves the use of a spectrophotometer, which is a device to measure light intensity as a function of the wavelength of light. A spectrophotometer can be either single beam or double beam. In a single beam instrument, all of the light passes through the same sample cell. First, the intensity of the reference material as a function of wavelength, I_o, (generally

the solvent) must be measured before measurements are carried out on the sample. This was the earliest design, but is still in common use in both teaching and industrial laboratories.

In a double-beam instrument, the light is split into two beams before it reaches the sample. One of the beams is used as reference and the other constitutes the sample beam. Some double beam instruments have two detectors (photodiodes), and the sample and reference beam intensities are measured at the same time.[24]

2.2.9 Z-Scan

The Z-scan is a versatile technique to investigate the nonlinear optical characteristics of materials using high intensity lasers as the excitation sources. In the Z-scan experiment, the sample is moved along the propagation direction (z) of a focused laser beam. The position of the focal point is taken as z = 0. The input intensity will be maximum at this point and will decrease symmetrically towards either side. For a spatially Gaussian laser beam, each z-position will correspond to an input laser energy density (fluence) of $4(\ln 2)^{1/2} E_{in}/(\pi^3/2\omega(z)^2)$, where E_{in} is the input laser pulse energy and $\omega(z)$ is the beam radius, which is given by $\omega(0)x[1+ (z/z_0)^2]^{1/2}$, where $\omega(0)$ is the beam radius at the focus and $z_0 = \pi\omega(0)^2/\lambda$ is the Rayleigh range (diffraction length) and λ is the excitation wavelength.

From the open aperture z-scan data it is possible to draw a graph between the input laser fluence and the sample transmission, which is known as the nonlinear transmission curve. In the curve, a peak signifies an increased transmission (Saturable absorption (SA)) while a valley represents a decreased transmission or reverse saturable absorption (RSA) or optical limiting.

Optical nonlinearity measurements in the samples can be carried out using the second harmonic output (532 nm) of a Q-switched Nd:YAG laser (Minilite, Continuum). The nominal pulse width of the laser is generally 5 ns. In the present experimental set up, a plano-convex lens of 10 cm focal length is used to focus the laser beam, and the focal spot radius is about 18 μm. The z-scans for all samples (PANI-Ag and PANI-Au) are carried out at laser pulse energies

of 50 µJ and 100 µJ. The samples are mounted on a programmable linear translation stage. The input energy reaching the samples and the energy transmitted by the sample are measured using two pyroelectric energy probes (RjP 735, Laser Probe Inc.). The time interval between each laser shot is generally kept sufficiently large (about 1 s) to allow complete thermal relaxation of the samples between successive laser pulses.[25]

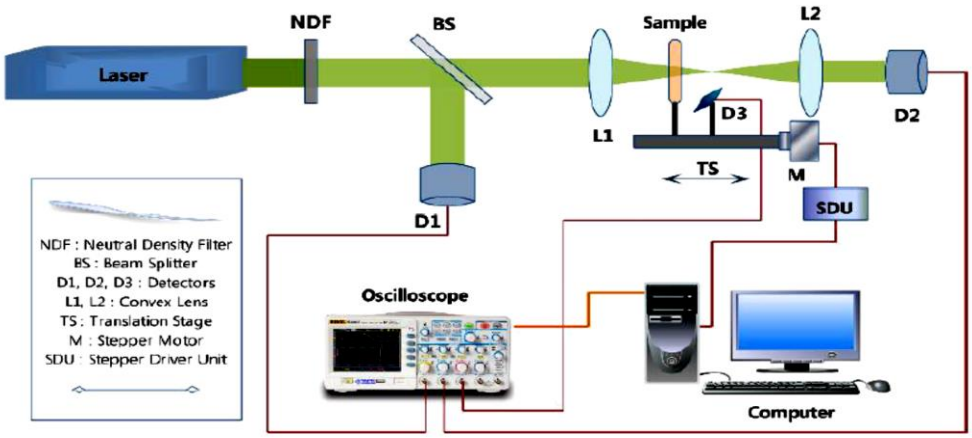

Figure 2.12: Z- Scan set up

2.2.10 Cyclic Voltammetry

Cyclic voltammetry (CV) is an extensively used method for studying electrode processes, especially for the purpose of understanding the thermodynamics and kinetics of electron transfer at the electrode-electrolyte interface. This technique is often employed as the first method to characterize new electrochemical systems. In this method the cell/system under test is cycled in a potential window, where the potential applied on the working electrode is continuously changed at a constant rate. In essence, the potential is swept through the potential range in which an electrode reaction occurs and the direction of scan is reversed, in order to define whether (a) the product of electron transfer is stable or (b) the reaction intermediates or the final products are electro-active. The change of potential as a function of time is called the scan rate. The potential sweep can be described by its initial (E_i) and switching (E_s) potentials, and also by the scan rate, ν. The potential as a function of time (t) is given by,

$$E = E_i + vt \ldots \text{(for forward voltage sweep)} \quad (2.7)$$

$$E = E_s - vt \ldots \text{(for reverse voltage sweep)} \quad (2.8)$$

with the scan rate (in mV/s) defined as

$$\nu = \frac{\Delta E}{\Delta t} \quad (2.9)$$

Figure 2.18: SP 300 Bio-Logic Unit

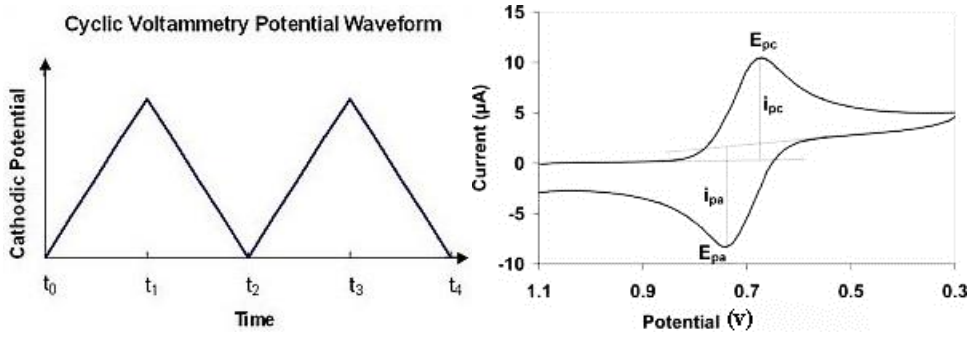

Figure 2.19: (a) Potential against time curve for cyclic voltammetry and (b) current against applied voltage curve

One of the most important criteria is the setting of the maximum and minimum potential ranges, which define the potential window. The cyclic voltammetry (CV) is performed by scanning the voltage between two chosen cut-off voltages at a given sweep rate, while simultaneously, measuring and recording the response current arising from the electron transfer. While choosing the cut-off voltages, the stability of the electrolyte must be taken into account in order to avoid its decomposition. In the present work, the SP 300

Bio-Logic Unit, shown in figure 2.18, is used for the CV characterization of the coin cells.[28]

Normally, this technique is applied in such a way that currents due to reduction processes are observed during the forward scan, and those due to oxidation on the reverse scan. A typical potential against time profile applied to the working electrode and the resulting cyclic voltammogram are shown in Figure 2.19.

2.2.11 Charge Discharge Cycling Test

In an effort to improve upon or replace existing battery technologies, researchers are trying to increase battery life and, at the same time, decrease the cost of rechargeable batteries. Common types of rechargeable batteries include Li-ion (Lithium Ion), Ni-MH (Nickel Metal Hydride), and NiCd (Nickel Cadmium). The characteristics of a rechargeable battery are commonly tested using charge-discharge and cycling. Cycle tests provide information about the battery parameters such as its internal capacity, number of usable cycles, and lifetime. In production testing, a discharge/charge cycle is often performed to verify battery specifications and to ensure that it is not defective.

In a galvanostatic charge/discharge cycling, a constant current is applied between the working and the counter electrodes. The current is applied until the set upper or lower potential limits are reached. For the working electrode a negative current would cause reduction and a positive current, oxidation. The investigation of the variation of potential with time of an electrochemical system is also called chronopotentiometry. The major advantage of this method is that, the electrode process can be investigated under actual battery working conditions, since the current or current density is kept constant.

For an insertion/extraction process into a compound *M*,

$$Li_xM + \Delta xLi^- + \Delta xe^- \leftrightarrow Li_{x-\Delta x}M \qquad (2.10)$$

The amount of inserted species Δx can be calculated as

$$\Delta x = \frac{I\,\Delta t M_r}{nFm} \qquad (2.11)$$

where I is the applied current in ampere, Δt is the time interval in seconds, M_r is the mass of the compound in gmol^{-1}, m is the active mass in grams, n is the number of electrons and F is Faraday's constant.

Figure2.20: 8 Channel Battery Analyzer (0.002-1mA, up to 5V) by MTI Corporation

The energy stored in a battery, called the battery capacity, is measured in either watt-hours (Wh), kilowatt-hours (kWh), or ampere-hours (Ahr). The battery cycle life is defined as the number of complete charge - discharge cycles a battery can perform before its nominal capacity falls below 80% of its initial rated capacity. The basic idea of charge discharge cycling is to study the capacity fading in rechargeable cells. The rate of charge and discharge is selected depending upon the theoretical capacity of the cathode material under investigation.

The 'C' rate is a method of expressing the constant current applied to an electrode in relation to its theoretical capacity. The specific capacity of the cells tested can be calculated by considering only the mass of the cathode active material in the electrode, and all electrochemical testing can be carried out at ambient temperatures (23 °C ± 5 °C).[29-30]

2.3 Glove Box

The glovebox is a rather sophisticated apparatus that has a large working area ("the box") which is kept under an inert atmosphere of Ar gas, generally. The

advantage is that one can perform air- and moisture-sensitive reactions using techniques one would use if the reactions were not sensitive to air or water. Conventional laboratory wares can be used in the box including: (i) a stirrer, (ii) a balance, and (iii) ring stands and clamps. One drawback is the lack of dexterity owing to the use of the large and thick glovebox gloves. However, with practice and patience, one can become very adept at performing a variety of tasks including weighing and transferring small amounts of materials. Furthermore, it is posssible to develop creative ways of accessing items beyond the reach of the gloves with the use of tongs and/or other items found in the glovebox.

Figure 2.13: Glove Box

Even though the box is sealed and the inert gas atmosphere is circulated over a catalyst to keep it inert, there are precautions that must be taken while working. Cross contamination of samples due to poor handling is problematic in particular when using volatile compounds and/or solvents. There are two common styles of use of glove boxes: (i) one where the box is used solely to store, weigh, and transfer air-sensitive reagents without using any solvents or volatile liquids, and (ii) one where the former operations are performed and solvents or volatile liquids are also handled and chemical reactions are also

carried out. The glovebox in the present work is used for the setup stage and product transfer stage of reactions. The operations that can be carried out include weighing compounds, transferring them to flasks or vials, dissolving them in solvents and reactions involving lithium substitution in polymers. In the present work, the assembling of coin type lithium ion cells using Li metal as the anode and air sensitive electrolytes is also carried out in the glove box under Ar atmosphere.

2.4 Coin Cell Assembly

The polymer-based Li ion cells, studied in the present work are assembled in the glove box as explained below.

Preparation of the Working Electrode (Cathode) - A Standard Methodology

1. Prepare a mixture of ~6 wt. % of polyvinylidene fluoride (PVDF) binder in N-methyl-2-pyrrolidone (NMP).
2. Weigh 80 wt. % of active material (Lithiated polyaniline and its composites in the present case) and 10 wt. % Carbon black (acetylene, 99.9+ %) and then mix them in a vortex for 1 minute.
3. Add NMP-binder mixture so that the binder constitutes 10 wt. % of the total weight of the mixture.
4. Transfer the above mixture into a small glass vial and mix in the vortex mixer at maximum rpm for about 30 minutes. Two zirconia balls of 5 mm diameter can be used as media for better mixing. If needed, add more NMP in order to obtain slurry of required consistency.
5. Spread a metal foil of the current collector (typically, aluminum for the cathode and copper for the anode) on to a glass plate. Use acetone and ensure that there are no air bubbles between the foil and the glass plate. Use two layers of masking tape to form a track and define the region to be coated.
6. Apply the slurry on to the metal foil using a stainless steel spatula and spread the slurry uniformly on to the track using a razor blade.
7. Dry the coating in air or vacuum at ~90-120 °C for about 2-8 hours (which should be adjusted depending on the material and binder used).

8. Place the coated metal foil between two steel plates (and two weighing papers to protect the coating) and press under a load of 10 tons using a hydraulic press.
9. Punch the dried coated metal foil into discs of 8 mm in diameter (preferably inside a glovebox). Weigh the cathode discs and wrap them before transferring into the glove box.
10. Punch the uncoated metal foil of the same material into discs of 8 mm in diameter and weigh these discs in order to estimate the actual weight of the cathode active material.

2. Preparation of Electrolyte

1. As the electrolyte is photosensitive, store the electrolyte which is 1M $LiPF_6$ dissolved in ethylene carbonate and dimethyl carbonate (EC: DMC, 1:1 ratio) in a Nalgene bottle wrapped by an aluminum foil.

3. Preparation of the Counter Electrode (Lithium foil in this case)

1. Clean the surface of the lithium foil using a nylon brush/stainless steel scalpel until a shiny silvery surface appears, inside the argon filled glovebox.
2. Punch the lithium foil into discs of ½ inch diameter inside the glovebox.

4. Coin Cell Assembling

1. Schematic diagram of the coin cell assembling procedure is shown in figure 30.
2. Punch Celgard C480 membranes into discs of 19 mm diameter and use them as separators.
3. Transfer coin cell cases (CR2032), springs and spacers (purchased from MTI Corp.), separators and working electrodes into the glove box (after flushing the exchanger five times with argon).
4. Add two drops of the electrolyte on to the cell cup and place the working electrode on it. Add another three drops of the electrolyte and place two separators with two drops of electrolyte between them. Add

two more drops of the electrolyte before placing the lithium counter electrode on it. Place two stainless steel spacers and a spring on the lithium disc.

5. Close the cell using the cell cap and crimp 3-4 times using the compact crimping machine (purchased from MTI Corp.).
6. After assembling the cells, handle the finished cells using plastic tweezers to avoid short circuiting.
7. Clean the excess electrolyte, leaking from the sides of the cell using a paper napkin.
8. The cells are ready for testing and can be taken out of the glovebox.

5. Coin Cell Testing

1. Keep the coin cell connected to the battery tester in the open circuit voltage (OCV) mode for one hour as soon as it is ready.
2. Define the voltage window for testing the cell based on the active material used in the working electrode.
3. Calculate the theoretical capacity of the electrode (the cathode) using the calculations shown below.

Weight of the electrode disc with the current collector = $\boldsymbol{W_{ED}}$
Weight of the uncoated current collector disc of the same diameter = $\boldsymbol{W_{CC}}$
Weight of electrode material,W_{EM}, is given by

$$W_{EM} = W_{ED} - W_{CC} \tag{2.12}$$

Weight of active material in the electrode, W_{AM}, is given by

$$W_{AM} = W_{EM} \times 0.8 \tag{2.13}$$

Theoretical capacity for the electrode disc, C_{ED}, is given by

$$C_{ED} = W_{AM} \times C \tag{2.14}$$

Where C is the theoretical specific capacity of the active material. The C-rate, which is the current rate at which charge discharge cycling is performed, can be deducted as follows,

$$C_{rate} = \frac{W_{AM} \times C}{n} \quad \text{Where n = 0.1- 10} \qquad (2.15)$$

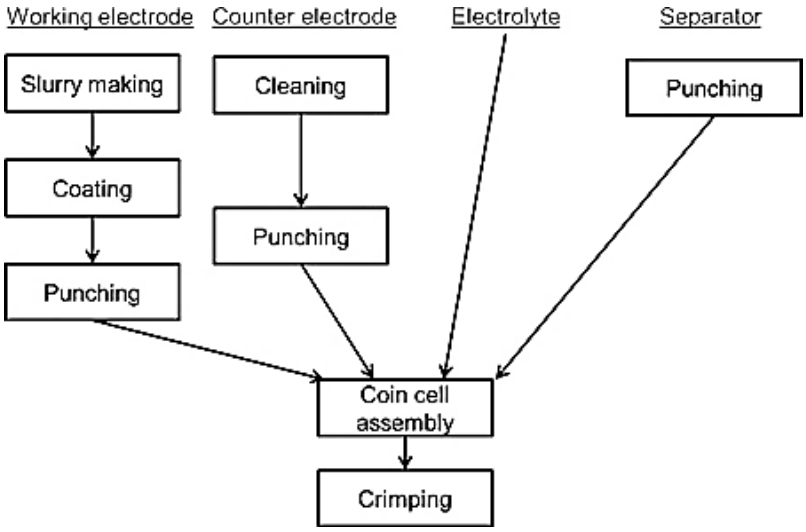

Figure 2.14: Flow chart of the coin cell construction procedure

First, a working electrode is prepared from the powder of the active material. Then, a counter electrode is prepared from a clean lithium foil and the separators are punched out. Finally, the cell is assembled inside an argon filled glovebox.[26-27]

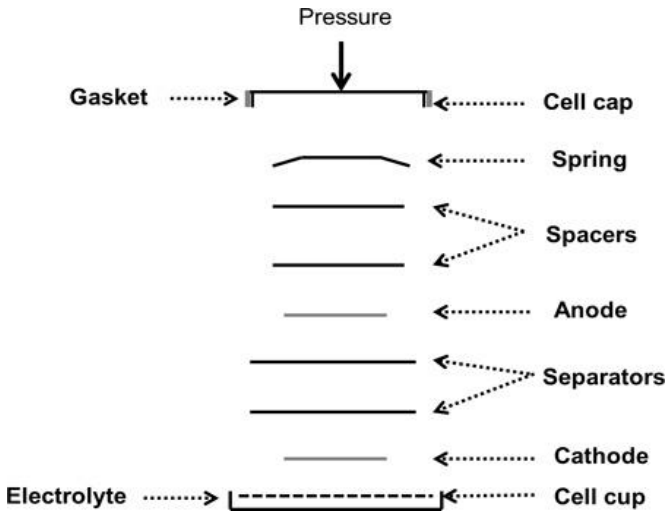

Figure 2.16: Schematic of a coin cell assembling process showing all the components in the order they are placed inside the coin cell case

Figure 2.15: Parts of coin cells

Figure 2.17: Coin Cell Crimper

References

1. Bish, DL and Post, JE, editors. Modern Powder Diffraction. *Reviews in Mineralogy*, v. 20. Mineralogical Society of America (1989).
2. Cullity, B. D. Elements of X-ray diffraction. *2nd ed. Addison-Wesley*, Reading, Mass. (1978).

3. Klug, H. P., and L. E. Alexander. X-ray diffraction procedures for polycrystalline and amorphous materials. *2nd ed. Wiley*, New York (1974).
4. Moore, D. M. and R. C. Reynolds, Jr. X-Ray diffraction and the identification and analysis of clay minerals. 2nd Ed. *Oxford University Press*, New York (1997).
5. Gerrard, D., .*Anal. Chem.* **66**, 547R-557R (1994).
6. Denton, M. B.Chem. *Eng. News*,**75(13)**, 42 (1997)
7. Nakamoto, K .Infrared and Raman Spectra of Inorganic and Coordinatio Compounds: Theory and Applications in Inorganic Chemistry, 5th ed.; *John Wiley & Sons*: New York (1997).
8. Nakamoto, K. Infrared and Raman Spectra of Inorganic and Coordination Compounds: Applications in Coordination, Organometallic, and Bioinorganic Chemistry, 5th ed.; *John Wiley & Sons*: New York (1997).
9. Introductory Raman Spectroscopy; *Academic Press*: New York (1995)
10. Laserna, J. Modern Techniques in Raman Spectroscopy; *J., Ed.; Wiley*: Chichester, U.K. (1996).
11. Raman Microscopy: Developments and Applications; Turrell, G., Corset, *J., Eds.; Academic Press*: New York (1996).
12. Wolverson, D. In Introduction Laser Spectroscopy; Andrews, D.L., Demidov, A. A., Eds.; *Plenum*: New York, pp 91-114 (1995)
13. Jean M. Bennett, Lars Mattsson, Introduction to Surface Roughness and Scattering, *Optical Society of America*, Washington, D.C. (1999).
14. W J Walecki, F Szondy and M M Hilali, "Fast in-line surface topography metrology enabling stress calculation for solar cell manufacturing for throughput in excess of 2000 wafers per hour" *Meas. Sci. Technol.,* **19**, 025302 (6pp) (2008)
15. Akamine, S., R. C. Barrett, and C. F. Quate, “Improved atomic force microscopy images using cantilevers with sharp tips,” *Appl. Phys. Lett.,* **57**, 316–318 (1990).
16. Albrecht, T. R., S. Akamine, T. E. Carver, and C. F. Quate “Microfabrication of cantilever styli for the atomic force microscope,” *J. Vac. Sci. Technol.,* **A 8**, 3386–3396 (1990).

17. Albrecht, T. R., P. Grutter, H. K. Horne, and D. Rugar, "Frequency modulation detection using high-Q cantilevers for enhanced force microscope sensitivity," *J. Appl. Phys.*, **69**, 668–673 (1991).
18. Allers, W., A. Schwarz, and U. D. Schwarz, in Noncontact Atomic Force Microscopy, edited by S. Morita, R. Wiesendanger, and E. Meyer, *Springer Berlin*, Chap. 14, pp. 233–256 (2002).
19. Goldstein, J. I. and Yakowitz, H. Practical Scanning Electron Microscopy, *Plenum*, New York (1975).
20. H Seiler, Secondary electron emission in the scanning electron microscope *J. Appl. Phys.,* **54**, R1 (1983).
21. I. Shiraki et al., *Surf. Rev. Lett*., **7**,533 (2000).
22. C.L. Petersen et al, *Appl. Phys. Lett*., **77**, 3782(2000).
23. I. Shiraki Et al., *Surf. Sci.*, **493**, 643 (2001).
24. W. Gottwald, K.H. Heinrich, UV/VIS-Spektroskopie für Anwender, *Wiley-VCH*, ISBN 3-527-28760-4 (1998).
25. Sheik-Bahae M, Said AA, Wei T-H, Hagan DJ and Van Stryland EW, *IEEE J Quantum Electr,* **26**:760–769 (1990).
26. Whittingham MS. Lithium batteries and cathode materials. *Chemical Reviews*. **104**:4271–4301 (2004).
27. Archana Kayyar et al. Construction and Testing of Coin Cells of Lithium Ion Batteries, *J Vis Exp*. **66**: 4104 (2012).
28. R. S. Nicholson, Theory and Application of Cyclic Voltammetry for Measurement of Electrode Reaction Kinetics. *Anal. Chem*., **37 (11)**, pp 1351–1355 (1965).
29. H. Kiehne, Battery technology handbook, *CRC*, 2 edition (2003).
30. M. R. Tomy, K.M. A. Kumar, S. Jayalekshmi, *Journal of Instrument Soc. of India,* **41**, 88 (2011).

Chapter 3

Studies on the Structural and Electrical Characteristics of Exceptionally Crystalline Polyaniline Films Doped with CSA, NSA, HCl and m-Cresol

Abstract: Emeraldine salt form of polyaniline (PANI) was synthesized by chemical oxidative polymerisation method using ammonium persulfate (APS) as oxidant. Resultant emeraldine salt form of PANI was dedoped using ammonia solution and then re-doped with camphor sulphonic acid (CSA), naphthaline sulphonic acid (NSA), hydrochloric acid (HCl) and m-cresol .Thin films of these doped PANI samples were deposited on glass substrates using solution casting method with m-cresol as solvent. A level surface was employed to get homogeneous thin films of uniform thickness. Detailed X-ray diffraction studies have shown that the films are exceptionally crystalline. The crystalline peaks observed in the XRD spectra can be indexed to simple monoclinic structure. FTIR and Raman spectroscopy studies provide convincing explanation for the exceptional crystallinity observed in these polymer films. FESEM and AFM images give better details of surface morphology of doped PANI films. The dc electrical conductivity of the samples was measured using four point probe technique. It is seen that, the samples also exhibit quite high dc electrical conductivity, about 287 S/cm for CSA doped PANI, 67 S/cm for NSA doped PANI 65 S/cm for HCl doped PANI and just below 1S/cm for m-cresol doped PANI. Effect of using the level surface for solution casting is studied and correlated with the observed crystallinity. It is also observed that this

technique of film deposition can be conveniently employed to grow thicker films of PANI which can be peeled off the substrates with the addition of small amounts of binding materials like polyvinyl dine fluoride (PVDF) . Such free standing films can be rolled in the form of wires to be used as connectors in electrical circuits.

3.1 Introduction

Conducting polymers, also termed as synthetic metals, have been the subject of extensive theoretical and experimental studies for the past four decades. Conducting polymers are interesting materials in modern technology since they find potential applications in the areas of electromagnetic radiation shielding, antistatic coatings, sensors, rechargeable batteries, polymer LEDs etc. Among them, polyaniline (PANI) has received much attention because of its tunable electrical and optical properties, and excellent environmental stability. [1-4]

Polyaniline is conventionally synthesized using chemical or electrochemical techniques. The effects of dopants and oxidants on the crystallinity of polyaniline samples have already been studied. Recently, some researchers have studied the relationship between the crystallinity of PANI and its charge transport properties and have found that the electrical conductivity of PANI samples strongly depends on the degree of crystallinity. [5-8]

The synthesis of highly crystalline PANI films with ordered structure and high electrical conductivity has not been pursued in depth. In present work, PANI samples, with high crystallinity and electrical conductivity were synthesized, by chemical oxidative polymerization followed by de-doping and re-doping processes, using m-cresol as solvent [9-12]. As a new approach, a level surface was employed to grow homogenous films with uniform thickness on glass substrates using solution casting. The effect of using the level surface on the structural, microstructural and electrical transport properties of PANI films was investigated in detail. The technique is novel as far as the growth of highly crystalline PANI films on various substrates is concerned. The films were characterized structurally, and electrically to establish the exceptionally

good crystallinity and also to highlight the benefits of using the level surface for the growth of highly crysatalline and ordered polymer films.

3.2 Materials and Methods

3.2.1 Synthesis

Polyaniline in powder form was synthesized by chemical oxidative polymerization of aniline in 1 molar HCl using 1 molar ammonium peroxydisulphate as initiator. The reaction was carried out for 5 hrs in an ice bath. The resultant sample was thoroughly washed and filtered using acetone and water to remove oligomers and excess acid. The filtered product was dried under dynamic vacuum for 24 hrs and then ground using a mortar to yield PANI in the form of fine powder.[11] The sample was de-doped using 1 molar ammonia solution and then re-doped using 1 molar camphor sulfonic acid (CSA), naphthalene sulfonic acid (NSA) and hydrochloric acid (HCl) using m-cresol as the solvent.[12] In order to study the doping effect of m-cresol, the ammonia de-doped PANI was dissolved in m-cresol without adding any acid dopants. The solutions were stirred well for about 24 hours to achieve maximum homogeneity. The solutions were filtered using a 0.45 μm polytetrafluoroethylene filter. In the previous studies on crystalline PANI films, the use of ultra-sonication or self-stabilized dispersion polymerisation technique followed by spin coating has been cited as a prerequisite for achieving crystallinity in PANI films.[11] However in the present work, without using any of the above techniques, good extent of crystallinity has been achieved in PANI films by using a level surface, by allowing the films to grow on glass substrates by solution casting. Homogenous PANI films having uniform thickness in the range 0.5-1.5 μm could be grown on glass substrates. Sample films were named as PANI-CSA, PANI-NSA, PANI-HCl and PANI-m-cresol for various characterisations.

3.2.2 Characterisations

X-ray diffraction technique employing the PAN-analytical's X'Pert Pro high resolution diffractometer with Cu Kα radiation of 1.542 Å was used for structural characterisation of doped PANI films. Raman spectra of the film

samples were recorded using high resolution Raman spectrometer (Horiba JY). The Thermo Nicolete Avatar 370 DTGS model FTIR spectrophotometer was used to record the IR spectra of the samples in the range 400–4000 cm^{-1}. Microstructure imaging was done by Field Emission Scanning Electron Microscope (FESEM-Carl Zeiss, Supra 40 VP). Surface topography of the film samples was analysed using Atomic Force Microscope(Agilent 5500 series) .The dc electrical conductivity of the samples was measured using the standard four-probe technique employing a Keithley 2400 source meter and Keithley 2001 multimeter interfaced to a PC with a program developed in LabVIEW.

3.3 Results and Discussions

3.3.1 X-Ray Diffraction studies

X-ray diffraction patterns of the samples are shown in figures 3.1A and 1B. Since majority of the peaks lie in the range 10^0 to 25^0, the portion covering 10^0-25^0 is expanded and shown in figure 1B. The observed diffraction peaks match quite well with the already reported data in literature. [11, 13] The sharp peaks observed around 4.6^0 for CSA and NSA redoped PANI are signature peaks specific to CSA and NSA doping, arising as a result of the ordered arrangement of the sulphonic groups. Attempts have been made to model the crystal structure using the observed diffraction data, employing the Fullprof-Suite (2.05 version July 2011). It is found that PANI-CSA and PANI-NSA samples have mono clinic like crystal structure. In the case of PANI-HCl and PANI-m-cresol, amorphous nature dominates and hence the number of peaks is inadequate to achieve a good fitting. The details of analysis and the results are shown in Table 3.1.

Percentage of crystallinity is calculated from the diffraction pattern of each sample which corresponds to, the ratio of the total area under the crystalline peaks to the total area under the crystalline and amorphous peaks. Origin 8 software has been used for peak fitting (Gaussian) to estimate the area under the crystalline peaks and amorphous peaks. It is seen that PANI-CSA film has got the highest percentage of crystallinity among the samples followed by PANI-NSA and PANI-HCl.

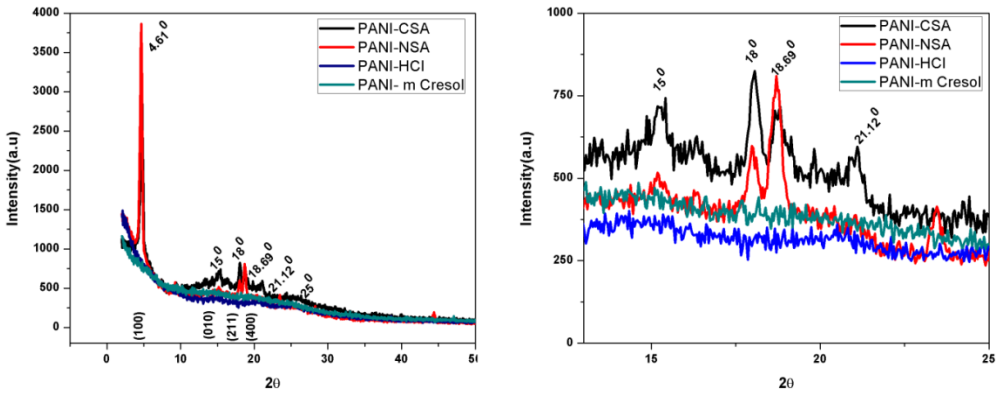

Figures 3.1A and 1B: X-Ray Diffraction patterns of doped PANI films

Table 3.1: Fullprof fitting data

Sample	a(Å)	b(Å)	c(Å)	β(degree)	Volume (Å^3)
PANI-CSA	19.03	5.82	22.42	96.34	2470.03
PANI-NSA	5.4385	2.5455	19.01	95.77	95.77

Percentage of crystallinity could not be estimated for PANI-m-cresol due to the lack of identifiable crystalline peaks. The results are shown in table 3.2.

Table 3.2: Percentage of crystallinity analysis data

Sample Name	**Total Area under the peaks (a.u)**	**Area under the Crystalline Area (a.u)**	**% of Crystalinity**
PANI-CSA	23954.85	18878.82	78.81 %
PANI-NSA	20903.43	14403.51	68.90 %
PANI-HCl	45068.64	30045.76	66.67 %
PANI-m-Cresol	-	-	-

3.3.2 FTIR Analysis

The FTIR spectra of the samples are shown in figure 3.2. In the case of CSA and NSA doped PANI samples, the peak at 1040 cm^{-1} is due to the vibration modes of HSO_4/SO_3 groups on sulphonated aromatic ring. The shoulder

observed at 1045 cm^{-1} is attributable to the symmetric SO_3 stretching in the hydrogen sulphate counter-ion. Peak observed at 1184 cm-1 is of in-plane deformation of N=quinoid ring=N vibration mode which coincides with that of in-plane deformation of C–H vibration mode. The peak at 1408 cm^{-1} is of phenazine ring stretching and that at 1632 cm^{-1} is of N–H scissoring vibration mode of primary aromatic amine.[13, 14, 17] It is observed that absorption peaks are narrow and sharp, which indicates that, the vibration modes are rigid and perfect without any overlapping. Absorption peaks of PANI-CSA and PANI-NSA are sharper than those of PANI-HCl and PANI-m-cresol. These observations support the X-ray Diffraction data and the analysis of percentage of crystallinity shown by the film samples.

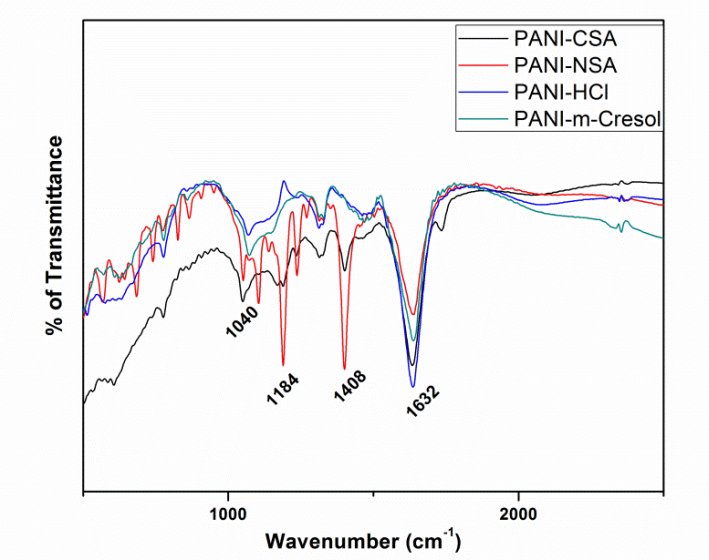

Figure 3.2: FTIR spectra of doped PANI samples

3.3.3 Raman Studies

Raman spectra of the doped PANI films are shown in figure 3.3. The bands from 1324 cm^{-1} to 1375 cm^{-1} in the Raman spectra of the sample films can be related to the vibrational modes νC-N of polarons with different conjugation lengths and those from 1450 cm-1 to 1520 cm^{-1}, to the νC=N stretching of the quinoid units with different conjugation lengths. The 1594 cm^{-1} band is of the C=C stretching of the quinoid ring. The observed Raman peak positions match well with the reported values.[15, 16]

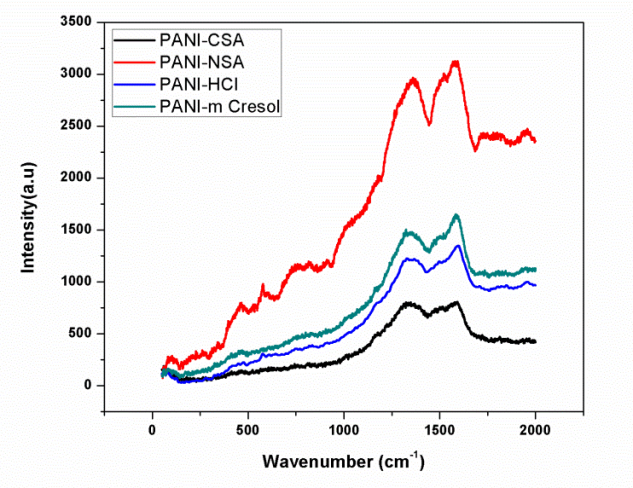

Figure 3.3: Raman spectra of doped PANI films

For PANI-CSA and PANI-NSA film samples, the peaks are found to be broader compared to the other two samples. This broadening is attributed to the confinement of phonons to the smaller crystalline particles in these samples. It is seen from the X-ray peak fitting analysis that, the cell volume of PANI-NSA is much smaller compared to that of PANI-CSA. This may be the reason for the highest Raman peak intensity shown by PANI-NSA film sample. The intensity of Raman peaks for PANI-HCl and PANI-m-cresol films is intermediate between that of PANI-NSA and PANI-CSA.

3.3.4 Microstructure Analysis- FESEM

FESEM images of doped PANI films are shown in figure 3.4. PANI-CSA, PANI-NSA and PANI-HCl, which constitute the re-doped film samples, show flake/plate like structures while PANI-m-Cresol films show uniformly sized globules like morphology.[17-20] Conducting form of PANI consists of islands of crystalline regions over a pool of amorphous region. The presence of more crystalline regions gives rise to higher electrical conductivity in PANI. Conduction can occur due to inter-chain hopping, intra-chain hopping and tunnelling of charge carriers from one crystalline region to another through the amorphous regions of PANI. From microstructure analysis it is clear that PANI-CSA, PANI-NSA and PANI-HCl films show more ordered structures while PANI-m-Cresol shows a less ordered structure which will be reflected on its dc-electrical conductivity values.

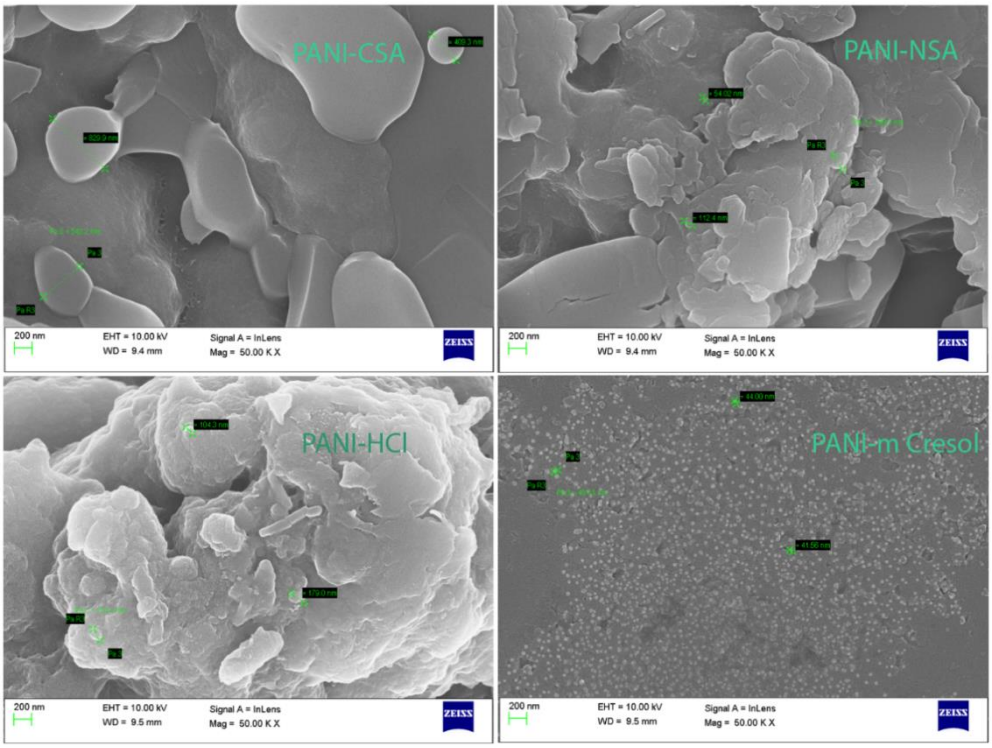

Figure 3.4: FESEM images of doped PANI films

3.3.5 Atomic Force Microscopic Studies (AFM)

Atomic Force Microscopy is a standard technique for analysing the surface morphology of films at high resolution. The AFM images of doped PANI films are shown in figure 3.5. It is clear from the AFM characteristic images that doped PANI films deposited using the level surface have higher extent of homogeneity than the normally cast film samples.[21,22] The surface roughness of the films has been calculated and tabulated in table 3.3.

Table 3.3: Roughness data of Doped Film Samples

Sample	Roughness (nm)
PANI-CSA	3.46
PANI-NSA	8. 65
PANI-HCl	9.978
PANI-m-Cresol	10.9

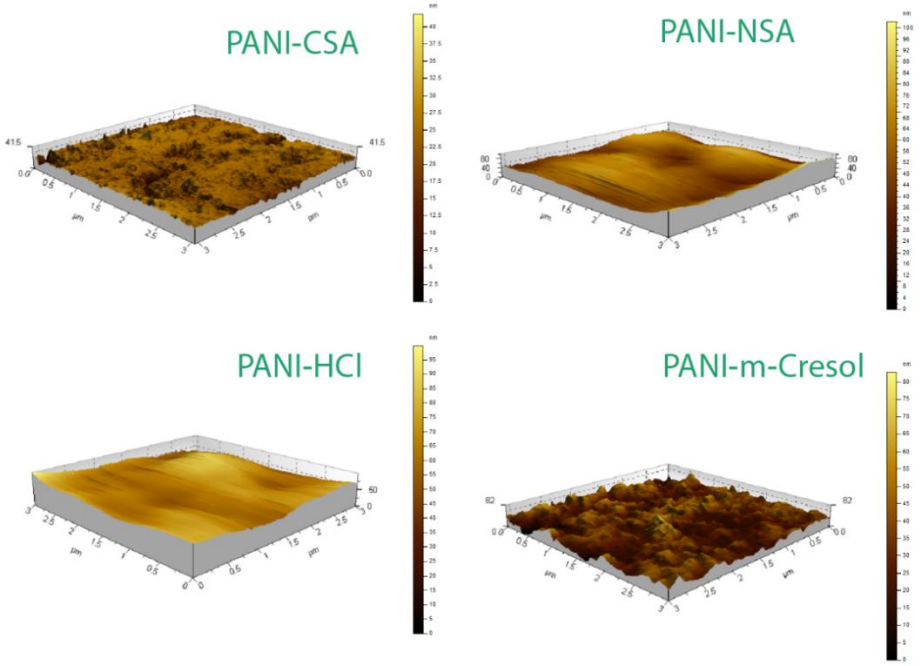

Figure 3.5: AFM images of doped PANI films

Surface roughness is lowest for PANI-CSA followed by PANI-NSA and PANI-HCl and it is highest for PANI-m-cresol. During the four probe dc conductivity measurement, the surface current and voltage are being sampled. Hence the roughness and uniform ordering at the surfaces of the film samples have definite role in determining the electrical conductivity of the samples.

3.3.6 DC Electrical Conductivity Studies

The electrical conductivity of the film samples was measured using the four point probe technique. The current voltage (I-V) characteristics for the various doped PANI film samples are shown in figure 3.6, from which the electrical conductivity for each sample has been evaluated. The conductivity values shown by the doped film samples are much higher compared to the previous literature reports.[23-27] The maximum electrical conductivity is exhibited by PANI-CSA film, which is around 281 S/cm. PANI-NSA and PANI-HCl samples have got comparable electrical conductivity around 65 S/cm. The electrical conductivity of PANI-m-cresol is comparatively quite low and is below 1 S/cm. The results are tabulated in table 3.4.

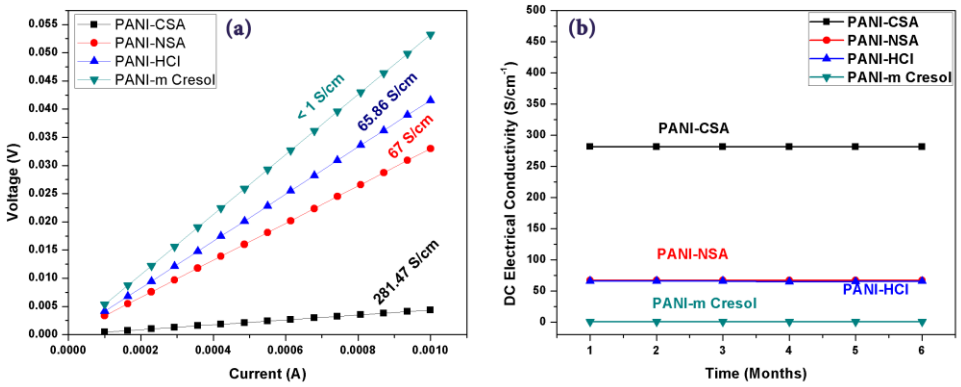

Figure 3.6: (a) IV Curves of doped PANI films (b) Variation of DC electrical conductivity of doped PANI films with aging

From the dc electrical conductivity studies it can be inferred conclusively that the dc electrical conductivity and crystallinity as well as homogeneity in polymer films are closely related to each other. When the crystallinity of the polymer sample increases the dc electrical conductivity also increases. For the film samples, surface homogeneity also has a crucial role to determine the electrical conductivity of the samples.

Table 3.4: Four point probe dc electrical conductivity measurement data

Sample	DC Electrical Conductivity(S/cm)	Previous Reported Values Conductivity(S/cm)
PANI- CSA	281.47	$\leq$ 10
PANI-NSA	67.00	$\leq 10^{-2}$
PANI-HCl	65.86	$\leq$ 1
PANI-m-cresol	<1	---

3.4 Conclusions

Polyaniline films doped with various dopants like CSA, NSA, HCl and m-Cresol were grown on glass substrates using solution casting technique with the aid of a level surface. In the light of the structural, microstructural and electrical characterisation studies it can be concluded that with the help of the

level surface, doped films of PANI with remarkable homogeneity can be grown on glass substrates using solution casting. Good extent of crystallinity as well as appreciably high dc electrical conductivity have been observed in CSA, NSA and HCl doped films grown by solution casting with m-cresol as solvent. Solution casting of polymer films with the help of a level surface offers a novel and cost effective approach compared to the more expensive spin coating technique, for realising polymer films with high extent of crystallinity, homogeneity and high electrical conductivity. It has also been observed that the films grown on glass substrate using this technique are quite stable in air without any structural degradation or change in the electrical properties even after six months of exposure to atmosphere. One of the highlights of the present work is the observation that using the level surface assisted film casting technique, thicker films can be grown on glass substrates which can be peeled off the substrates to get free standing films, with the addition of a small amount of binding materials such as PVDF. These films can be rolled to make wires to be used as connectors in electrical circuits.

References

1. Wu-Song Huang, Brian D. Humphrey and Alan G. MacDiarmid, *J. Chem. Soc., Faraday Trans.* **1, 82**, 2385-2400 (1986).
2. A.G. Macdiarmid, J.C. Chiang, A.F. Richter, *Synthetic Met.*, **18**, 1–3, 285–290 (1987).
3. Alan G. MacDiarmid and Arthur J. Epstein, Faraday Discuss, *Chem. Soc.*, **88**, 317-332 (1989).
4. Manju Gerard, Asha Chaubey, B.D. Malhotra, *Biosens Bioelectron.*, **17**, 5, 345–359 (2002).
5. J. Stejskal, R. G. Gilbert, *Pure Appl. Chem*., **74**, 5,857–867 (2002).
6. G. Tourillon, F. Garnier, *J. Electroanal. Chem. Interfac*., **135, 1,173**–178 (1982).
7. Xinyu Zhang , Warren J. Goux , and Sanjeev K. Manohar, *J. Am. Chem. Soc*., **126 (14)**,4502–4503 (2004).
8. S.-H. Lee, D.-H. Lee, K. Lee and C.-W. Lee, *Adv. Funct. Mater.* **15**, 9, 1495–1500 (2005).

9. Biscaro RS, Rezende MC and Faez R, *Polym Adv Technol*., **20**, 28–34 (2009).
10. Bhadra and Khastgir, *Polym Test*., **27**, 851–857 (2008).
11. Sreekanth J Varma, Francis Xavier, Soney Varghese and Sankaran Jayalekshmi, *Polym Int*., **61**,743–748(2012).
12. Yunze Long, Zhaojia Chen, Nanlin Wang, Zhiming Zhang, Meixiang Wan, *Physica B.*, **325**, 208–213 (2003).
13. J. P. Pouget, M. E. Jdzefowiczt ,A. J. Epstein, X. Tang and A. G. MacDiarmid, *Macromolecules*., **24**, 779-789 (1991).
14. Miroslava Trchová, Ivana Šeděnková, Eva Tobolková, Jaroslav Stejskal, *Polym Degrad Stabil*. 86, 1, 179–185 (2004).
15. Miroslav Trchova and Jaroslav Stejskal, *Pure Appl. Chem*., **83**, 10, 1803–1817 (2011).
16. Gustavo M. do Nascimento and Marcia L. A. Temperini, *J. Raman Spectrosc*., **39**: 772–778(2008).
17. Chuanqiang Zhou, Jie Han and Rong Guo, *Macromolecules*, **41**, 17, 6473–6479 (2008).
18. Jiang, L. P. Xu, S.Zhu, J. M. Zhang, J. R. Zhu, J. J. Chen, H. Y, *Inorg. Chem*., 43, 5877–5883(2004).
19. Han, J.; Song, G.; Guo, R. *Adv. Mater*., **19**, 2993–2999 (2007).
20. Zhou, C.; Han, J.; Song, G.; Guo, R. *Macromolecules*, **40**, 7075– 7078 (2007).
21. Jamshid K. Avlyanova, Jack Y. Josefowiczb, Alan G. MacDiarmid, *Synthetic Metals*. 73, 3, 15, 205–208 (1995).
22. E.C. Venancio, C.A.R. Costa, S.A.S. Machado, A.J. Motheo, *Electrochem Commun*., **3, I5**, 229–233 (2001).
23. Elizabeth W. Paul, Antonio J. Ricco, and Mark S. Wrighton, *J. Phys. Chem*., **89**, 1441–1447(1985).
24. Hu Yan, Norina Sada, Naoki Toshima, *J Therm Anal Calorim*., **69**, 3, 881-887(2002).
25. Zhiming Zhang, Meixiang Wan, *Synthetic Metals*. **128**, 1, 83–89 (2002).

26. J. Haberko et.al, *Mol. Cryst. Liq. Cryst*., **485**, 48 (2008).
27. D.Geethalakshmi, N. Muthukumarasamy, R. Balasundaraprabhu, *Optik.* **125**, 1307–1310 (2014).

Chapter 4

A novel method of synthesizing gold nanoparticles embedded polyaniline and its structural and optical characterization in the linear and nonlinear regimes

Abstract: Gold nanoparticles embedded polyaniline (PANI) was synthesized by an insitu oxidative polymerization of monomer aniline. X-ray diffraction and FTIR techniques were used to establish the structure of the gold-PANI composite. UV Visible absorption studies show that, along with the normal absorption peak of polyaniline, the composite shows the absorption peak characterized by surface plasmon resonance. The presence of surface plasmon resonance is a signature of the nano size of the gold particles embedded in PANI. EDS reveals the elemental composition of the composite sample quantitatively. Raman spectroscopic study strengthens the presence of plasmon resonance. Single-beam Z-scan results confirm the third order optical nonlinearity associated with the nanocomposite. The present investigations show that gold nanoparticle embedded PANI composite can be of potential applications in the fields of both linear and nonlinear optics.

4.1 Introduction

From the early stages of the twentieth century onwards, Polyaniline (PANI), a well-known and extensively studied conducting polymer has captured the

attention of scientific community owing to its interesting electrical and optical properties.[1] Starting from its fundamental properties, to the currently pursued applications in optoelectronics, energy storage and photonics, investigations on pure PANI and its composites are still much relevant to explore its potentialities to the maximum extent.

Presently a host of information is available related to the versatile applications of conducting polymers in the technological field, especially PANI. Chemical oxidative polymerization is the easiest and the most convenient method of preparing emeraldine salt of PANI which can be reduced to emeraldine base form by treating with suitable alkaline materials.[2] A variety of synthesis methods is available and by changing synthesis conditions, PANI with different morphology can be obtained.[3-7] Using proper solvents and dopants, very thin and homogeneous nanostructured polyaniline films on glass, quartz and flexible substrates can be obtained using spin coating technique,[8] showing quite interesting properties such as quantum confinement effects.[9-12]

Recently, the structural and optoelectronic properties of nanostructured PANI and its nanocomposites are being subjected to vigorous investigation. Among them, metal nanoparticle embedded polyaniline finds special attention due to the application prospects as imaging probes in bio-Nano photonics. [13- 16]

Present scientific community is in need of potential materials with environmental friendliness and long term stability for designing and realizing highly efficient devices. In this respect, PANI is one of the highly pursued candidates.[17] Gold nanoparticle embedded composite systems are extensively studied for various optical applications both in the linear and nonlinear regimes.[18, 19] In the present work, attempts have been made to synthesize a highly stable PANI-gold nanocomposite using a modified oxidative polymerization method with monomer aniline and bulk gold as precursors. The synthesized PANI-gold nanocomposite in powder form has been characterized structurally and optically to check its prospects of application in linear and nonlinear optics.

4.2 Materials and Methods

4.2.1 Synthesis

To start with, 0.2 g of bulk gold was dissolved in aqua-regia (1:3 mixtures of HNO_3 and HCl) and the resultant solution was made up in to 1M, 100ml solution. Weighed quantity of ammonium-peroxy-sulphate (11.4 g) was dissolved in 50 ml of the above solution .The remaining 50 ml of aqua-regia solution was used to dissolve 4.5 ml of distilled aniline. Then ammonium-peroxy-sulphate dissolved in aqua-regia was added drop wise to the aniline in aqua-regia solution in an ice bath with constant stirring. Stirring was continued for about 24 hours to get the maximum polymerization yield. The resultant solution was filtered and washed several times with distilled water and acetone to remove oligomers. The filtrate was dried at a temperature of 50^0C under dynamic vacuum conditions to get PANI-gold nano composite in powder form.

4.2.2 Characterizations

X-ray diffraction technique employing the Rigaku Dmax C diffractometer with Cu Kα radiation of 1.54 Å was used for structural characterization of PANI-gold nanocomposite. The Thermo Nicolete Avatar 370 DTGS model FTIR spectrophotometer was used to get the IR spectrum of the sample in the range 400–4000 cm^{-1}.A thin film of the PANI-gold nanocomposite was obtained on glass substrate using m-cresol as solvent and the optical absorption spectrum of the film sample was recorded using a Jasco V 570 UV–vis spectrophotometer in the wavelength range 330– 2500 nm.Raman spectra of the nanocomposite sample was recorded using high resolution Raman spectrometer (Horiba JY).The elemental composition of the composite was confirmed using EDS analysis(JEOL Model JED –2300).The nonlinear optical properties of the PANI-gold nano composite sample were investigated using Z Scan technique employing the second harmonic output (532 nm) of a Q-switched Nd:YAG laser (Minilite, Continuum).

4.3 Results and discussions

4.3.1 X-ray Diffraction Studies

Figure 4.1 represents the X-ray diffraction spectrum of PANI-gold nanocomposite sample. In semi crystalline polymers, two kinds of diffraction peaks are generally observed. The crystalline peaks arising due to Bragg type reflections of X-rays from structurally ordered regions of the polymer and broad and low intensity peaks characterizing the amorphous regions of the polymer. In the spectrum, the relatively sharp peak centred at $2\theta=26^{o}$ can be ascribed to the periodicity of planes parallel to the polymer chain. The peak at $2\theta=20.5^{o}$ corresponds to the periodic nature of planes perpendicular to the polymer back bone, which is of amorphous nature. It is already reported that

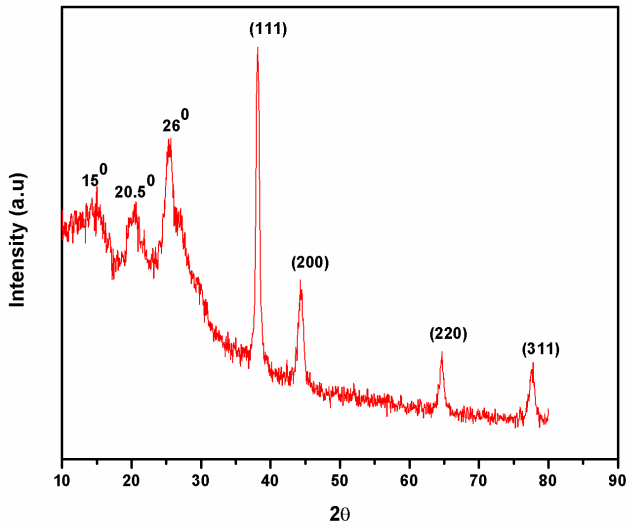

Figure 4.1: X- Ray Diffraction spectrum of PANI-gold nanocomposite

inter-chain distance perpendicular to the polymer chain direction is affected by dopants and their size. Presence of a few numbers of peaks which are broad and less intense can be ascribed to the various planes with different inter-chain length which are formed due to the presence of O, Cl, and Au like atoms in the system matrix. [20, 21, and 22] The present spectrum also exhibits characteristic reflections of fcc gold (JCPDS No.04-0784). The diffraction features appearing at 2θ = 38.20°, 44.41°, 64.54° and 77.8° correspond respectively to the (111), (200),(220) and (311) planes of the standard cubic phase of Au.

4.3.2 Composition Analysis

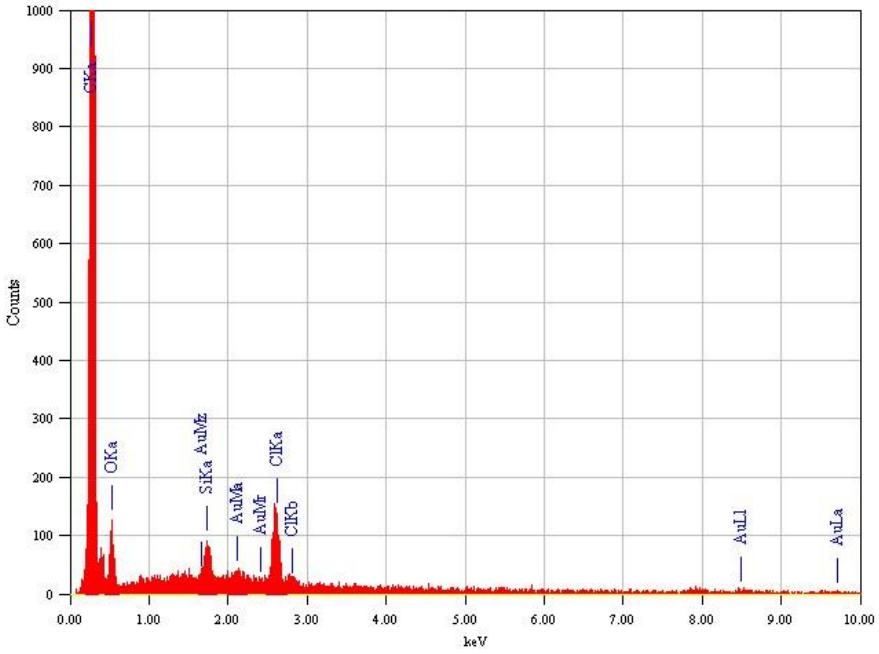

Figure 4.2: EDS spectrum of PANI-gold nanocomposite

Figure 4.2 shows an EDS spectrum collected from the PANI–gold nanocomposite. Table 4.1 depicts the composition of the composite sample obtained from EDS analysis. By atomic percentage, carbon is the most abundant element and then S, O, Cl and N in descending order. The atomic percentage of gold is 0.52. The presence of gold in the PANI–gold nanocomposite is thus further confirmed from the EDS spectrum.

Table 4.1: Composition of PANI-gold nano composite from EDS analysis

Element	Atom%
C	89.03
S	4.79
O	2.5
Cl	2.35
N	0.81
Au	0.52

4.3.3 Fourier Transform Infrared Spectroscopic Study

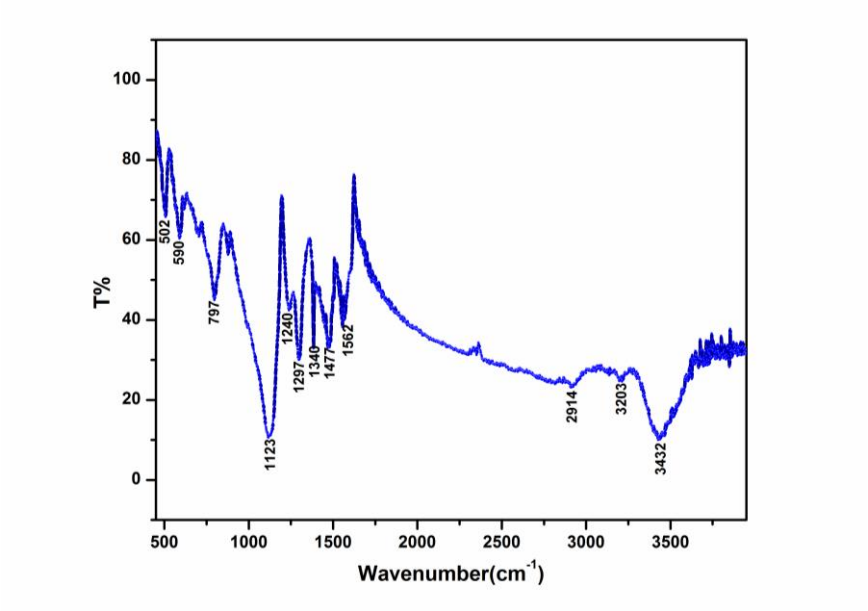

Figure 4.3: FTIR Spectrum of PANI-Gold Composite

FTIR spectrum of PANI-gold nanocomposites is shown in figure 4.3. The peak at 590 cm^{-1} corresponds to C-Cl stretching and that at 797 cm^{-1} is of N-H out of plane bending vibration of PANI. The C-C stretching and C-C twisting frequencies can be ascribed to the peaks at 1123 cm^{-1} and 1240 cm^{-1} respectively. C-N stretching mode can be observed at 1297 cm^{-1}. The benzenoid and quinoid vibrations of PANI are characterized by the peaks at 1477 cm^{-1}, 1562cm^{-1} respectively.The C-H and N-H stretching vibration modes are observed respectively at 2914 cm^{-1} and 3432 cm^{1}.[23-26] The observed FTIR data of the PANI-gold nanocomposite sample agrees quite well with the already reported FTIR data of the emeraldine salt form of PANI. Hence it can be inferred that, the presence of gold nanoparticles in the PANI matrix does not have any noticeable effects on the vibrational modes of PANI.

4.3.4 Raman Spectroscopic Study

The Raman spectrum of PANI-gold nanocomposite sample is depicted in figure 4.4.The presence of the bands from 1324 cm^{-1} to 1375 cm^{-1} in the Raman spectrum of the PANI-gold composite is related to the vibrational modes ν*C*-N of polarons with different conjugation lengths. The bands from

1450 cm^{-1} to 1520 cm^{-1} are assigned to the νC=N stretching of the quinoid units with different conjugation lengths. The 1587 cm^{-1} band is of the C=C stretching of the quinoid ring.[27, 28]

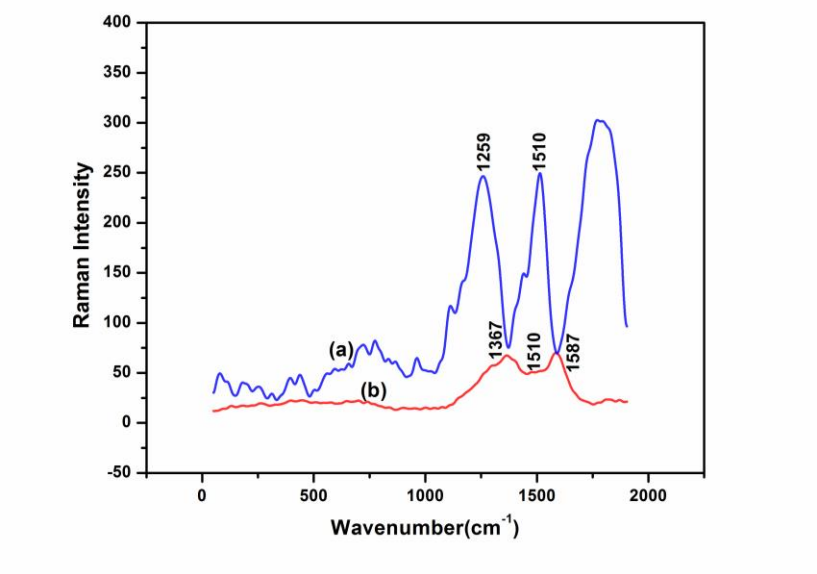

Figure 4.4: Raman Spectrum of (a) PANI-gold nanocomposite and (b) PANI

These results show that the PANI-gold composite's response to Raman scattering matches with that of PANI. But it can be seen that the Raman spectrum of PANI-gold composite has much higher intensity than that of PANI. This result can be attributed to the presence of Surface-Enhanced Raman scattering (SERS) phenomenon in the composite. This phenomenon is of electromagnetic origin, and happens when a molecule lies close to a roughened metal surface. The enhancement in intensity comes from the increase of the local optical field intensity in the proximity of sharp points of textured metals such as Au, Ag, Cu, or in the nano-scale gaps.[29] In the PANI-gold composite the proximity of the PANI molecules to the embedded gold nanoparticles brings about the enhancement in Raman intensity.

4.3.5 Linear Optical Absorption Studies

The UV-Visible absorption spectrum of PANI-gold nanocomposite is shown in figure 4.5. Normally in the spectrum of PANI, along with two absorption

peaks, an absorption tail extending to the NIR region can be seen and this tail is a signature of the free carrier absorption in the PANI-gold composite.

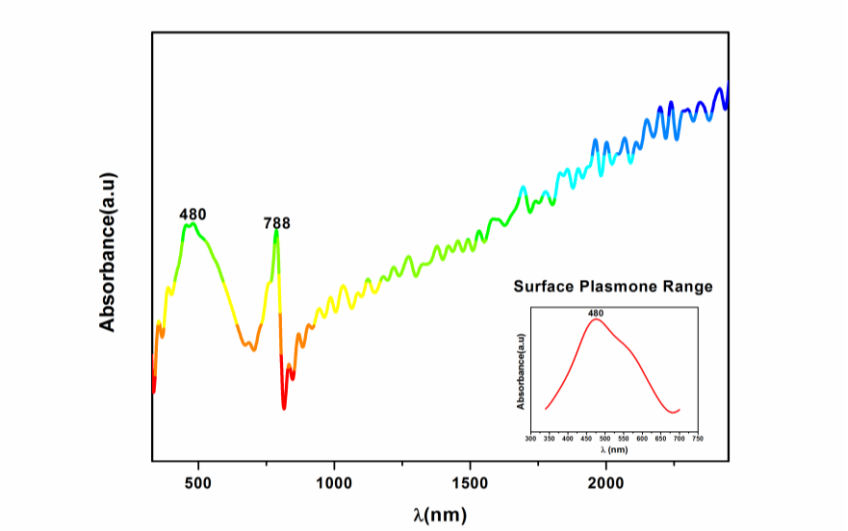

Figure 4.5: UV-Visible Absorption Spectrum of PANI-Gold Composite

The absorption peak around 420 nm corresponds to the π-π* transition of the benzenoid ring and that at 780 nm is of transitions in polaron bands. However, in the spectrum of PANI-Gold composite, instead of an absorption peak at 420 nm, a broad peak centred at 480 nm can be observed. Presence of this broad peak is assigned to the surface plasmon resonance of gold in nano dimensions inside the polymer matrix.[30] It is clear that this broad and intense peak suppresses the normal absorption peak at 420 nm. The presence of the narrow peak with sufficient intensity at 788 nm indicates that the environments of the quinoid and benzenoid rings are apparently not changed in the gold-PANI composite, and the polarons are more delocalized. [31, 32]

4.3.6 Nonlinear Optical studies

Nonlinear Optical measurements of the sample were carried out using the second harmonic output (532 nm) of a Q-switched Nd:YAG laser (Minilite, Continuum) with pulse width of 5 ns. In a Z-scan experiment, the sample is moved along the propagation direction (z) of a focused laser beam. The position of the focal point is taken as z = 0. The input intensity will be

maximum at this point and will decrease symmetrically towards either side. For a spatially Gaussian laser beam, each *z*-position will correspond to an input laser energy density (fluence) of $4(\ln 2)^{1/2}E_{in}/\pi^{3/2}\omega(z)^2$, where E_{in} is the input laser pulse energy and $\omega(z)$ is the beam radius. $\omega(z)$ is given by $\omega(0)*[1+(z/z_0)^2]^{1/2}$, where $\omega(0)$ is the beam radius at the focus and $z_0 = \pi\omega(0)^2/\lambda$ is the Rayleigh range (diffraction length) and λ is the excitation wavelength. From the open aperture z-scan data, it is possible to draw a graph between the input laser fluence and the sample transmission, which is known as the nonlinear transmission curve. In the curve, a peak signifies an increased transmission termed as saturable absorption (SA) while a valley represents a decreased transmission termed as reversible saturable absorption (RSA), alternatively referred to as optical limiting. [33]

In the present experiment, a plano-convex lens of 10 cm focal length was used to focus the laser, and the focal spot radius was about 21 μm. The z-scan for the composite sample was carried out at two different laser pulse energies of 50 μJ and 100 μJ respectively. The samples were dissolved in m-cresol and were taken in a 1 mm glass cuvette (Hellma GmBH) for the measurements. The cuvette was mounted on a programmable linear translation stage. The input energy reaching the sample and the energy transmitted by the sample were measured using two pyroelectric energy probes (RjP 735, Laser Probe Inc.). The time interval between each laser shot was kept sufficiently large (about 1 s) to allow complete thermal relaxation of the sample between successive laser pulses.

The Z- scan plot of the solvent (m-cresol) used is shown in figure 4.6. It is clear that the solvent is completely inefficient as an optical limiter.

From the Z scan plot of PANI alone (Figure 4.7(a)), it is seen that PANI, here the host material of gold nano particles, shows reasonable nonlinear optical limiting behavior. Using the best curve fit possible, the mechanism behind this optical nonlinearity has been found to be two-photon absorption (TPA). The propagation equation can be written as,

$$\frac{dI}{dz} = -\alpha I - \beta I^2 \qquad (4.1)$$

Here, I is the input laser intensity, α is the linear absorption coefficient (which can be very small) and β is the two-photon absorption coefficient.[34]

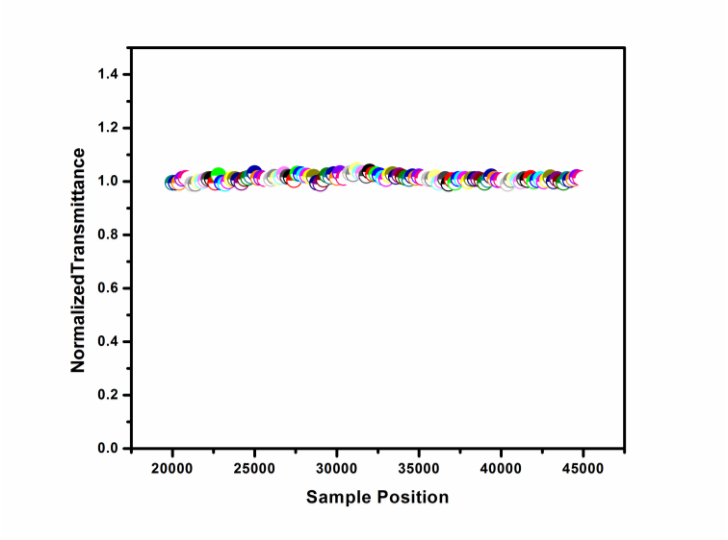

Figure 4.6: Open Aperture Z-Scan plot of m-Cresol (Solvent)

The normalized transmittance vs input fluence plots of gold-PANI show that the sample exhibits good optical limiting (OL) behavior (Figure 4.7 (b)). This arises from free carrier absorption (FCA) phenomenon. A signature of saturable absorption (SA) is found, which results in a slightly decreased absorption at moderate laser intensities. This happens when atoms or molecules are excited under laser irradiation, at such a rate that the ground state gets depleted before the excited species get de-excited back to the ground state. But this intensity is not sufficient to induce FCA.[35] At sufficiently higher intensities, FCA will completely overrule SA, resulting in an overall optical limiting behaviour. By considering the simultaneous occurrence of FCA and SA, an effective nonlinear absorption coefficient α (I) with an expression

$$\boldsymbol{\alpha(I) = \frac{\alpha_0}{1+\left(\frac{I}{I_s}\right)} + \beta_{eff} I} \qquad (4.2)$$

can be considered. Here α_0 is the unsaturated linear absorption coefficient at the wavelength of excitation, I is the input laser intensity, and I_s is the saturation intensity (intensity at which the linear absorption drops to half of its

original value). β_{eff} is the effective two photon absorption coefficient, a number, which represents the two-photon like absorption happening in the system (ground state excitation followed by FCA). For a given input intensity, the transmitted intensity can be calculated by solving the propagation equation given by

$$\frac{dI}{dz'} = \left[\left(\frac{\alpha_0}{1+\frac{I}{I_s}}\right) + \beta_{eff} I\right] I \qquad (4.3)$$

Here z' indicates the propagation distance within the sample.

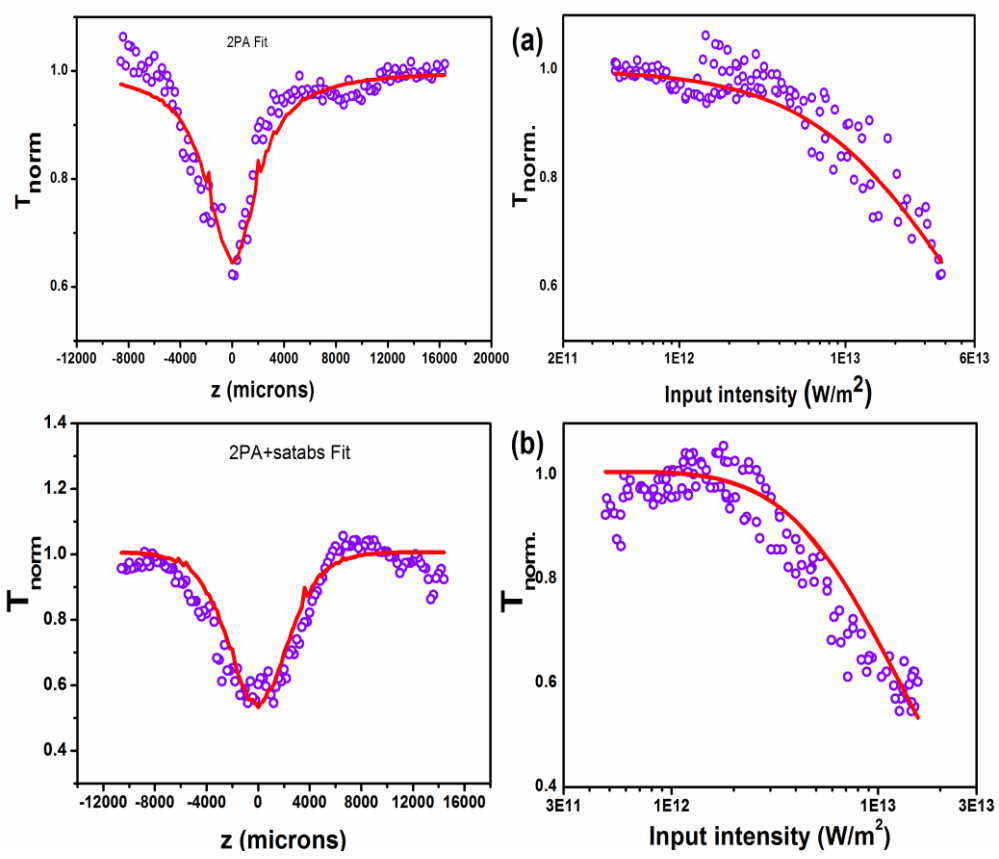

Figure 4.7: Open Aperture Z-Scan curves and Nonlinear Transmission curves of (a) PANI alone and (b) PANI-gold nano-composite

From the best-fit curves (Figure 4.7) to the experimental data, the nonlinear parameters I_s and β_{eff} are calculated for the samples, which are given in Table 2.On comparison, it is clear that saturable absorption is absent in pure PANI

sample and two photon absorption has the sole role for nonlinear optical activity. However in the PANI-gold composite sample both SA and TPA are observed. Even in the absence of SA, optical limiting behavior of PANI sample is not as efficient as PANI-gold composite, as evident from table 4.2.

Table 4.2: Nonlinear transmission parameters calculated from the Z-Scan Measurement

Sample	Excitation Energy (μJ)	Linear Transmission (%)	Saturation Intensity(I_s) ($x10^{12}W/m^2$)	Effective two photon absorption coefficient (β_{eff}) ($x10^{-10}$ m/W)
Au-PANI	50	60	4.99	1.8
PANI	50	60	NA	0.97

4.4 Conclusions

The present work highlights the development of a novel, simple and cost effective method to synthesize PANI, embedded with gold nanoparticles. The formation of PANI-gold nanocomposite has been confirmed based on FTIR, Raman and UV- visible absorption spectroscopic techniques. It is observed that even in the presence of SA, the PANI-Gold nanocomposite sample shows about 50% optical limiting behaviour, compared to the 37% of pure PANI in which SA is absent. Though the percentage of gold in the composite is quite low (atomic percentage: 0.52) the Surface Plasmon Resonance due to gold nano particles is clearly observed in the UV-visible absorption spectrum. Surface Enhanced Raman Scattering effect is also dominant in the composite sample as seen from the Raman studies. These composite samples are also found to be quite stable, since the structural and optical properties are found to remain the same over a period of more than six months. The present work extends ample scope of further investigations by changing the atomic percentage of gold in the composite and the synthesis conditions of PANI. By optimizing these parameters it may be possible to get optical limiting efficiency close to 80%.

References

1) H. Letheby, On the production of a blue substance by the electrolysis of sulphate of aniline, *j. Chem. Soc.*, **15**, 161-163 (1862).
2) N. Gospodinova, L. Terlemezyan, Conducting polymers prepared by oxidative polymerization: polyaniline, *Prog. Polym. Sci.*, **23,** Issue 8, 1443-1484(1998).
3) Akheel A. Syed, Maravattickal K. Dinesan, Review: Polyaniline,A novel polymeric material, *Talanta*,**38,** Issue 8, 815-837 (1991).
4) Zhiming Zhang, Zhixiang Wei, and, and Meixiang Wan, Nanostructures of Polyaniline Doped with Inorganic Acid**s**, *Macromolecules*, ***35*** **(15)**, 5937-5942(2002).
5) Yong Wang, Zhimin Liu, Buxing Han, Zhenyu Sun, Ying Huang, and Guanying Yang Facile, Synthesis of Polyaniline Nanofibers Using Chloroaurate Acid as the Oxidant, *langmuir*, **21 (3)**, 833–836 (**2005**).
6) Q.M. Jia, J.B. Li, L.F. Wang, J.W. Zhu, M. Zheng, Electrically conductive epoxy resin composites containing polyaniline with different morphologies, *Mater. Sci. Eng., A*, **448,** Issues 1-2,356-360 (2007).
7) Kh. Ghanbari, M.F. Mousavi, M. Shamsipur, M.S. Rahmanifar, H. Heli, Change in morphology of polyaniline/graphite composite: A fractal dimension approach, *Synth. Met.*, **156**, Issues 14-15,911-916 (2006).
8) S.J. Varma, Jerin George, P.P. Jeeju, S. Jayalekshmi, Quantum confinement effects in highly conducting, ultrathin Polyaniline films pursued through spectroscopic investigations**,** *J. Lumin.*, Available online 21 July (*2011*).
9) Iva Turyan and Daniel Mandler, Two-Dimensional Polyaniline Thin Film Electrodeposited on a Self-Assembled Monolayer, *J. Am. Chem. Soc.* ***120*** **(41),** 10733-10742 (1998).
10) Dan Xie, Yadong Jiang, Wei Pan, Dan Li, Zhiming Wu, Yanrong Li, Fabrication and characterization of polyaniline-based gas sensor by

ultra-thin film technology, *Sens. Actuators, B: Chemical,* **81**, 2-3,158-164 (2002) .

11) Deepak Verma and V Dutta, Novel microstructure in spin coated polyaniline thin films *J. Phys.: Condens. Matter* **19** 186212 (2007).
12) Anurag lodha, s. Michael kilbey , praveen c. Ramamurthy, Richard v. Gregory**,** Effect of Annealing on Electrical Conductivity and Morphology of Polyaniline Film**s,** *J. Appl. Polym. Sci.*, **82**, 3602–3610 (2001).
13) Pilli Satyananda Kishore ,Balasubramanian Viswanathan,Thirukkallam Kanthadai Varadarajan, Synthesis and Characterization of Metal Nanoparticle Embedded Conducting Polymer–Polyoxometalate Composites, *Nanoscale Res Lett* **3**:14–20 (2008).
14) Convertino, A., Capobianchi, A., Valentini, A. and Cirillo, E., A New Approach to Organic Solvent Detection: High-Reflectivity Bragg Reflectors Based on a Gold Nanoparticle/Teflon-like Composite Material., *Adv. Mater.*, **15**: 1103–1105 (2003).
15) Pulickel M. Ajayan, Linda S. Schadler, Paul V. Braun, Nanocomposite Science and Technology, *wiley-vch*, weinheim (2003).
16) Jianyong Ouyang, Chih-Wei Chu, Charles R. Szmanda, Liping Ma, Yang Yang, Programmable polymer thin film and non-volatile memory device, *Nat. Mater.* **3**, 918 - 922 **(**2004).
17) H. V. Rasika Dias, R. M. Gamini Rajapakse, D. M. Milan Krishantha, Mauro Fianchini, Xiaoyu Wang and Ronald L. Elsenbaumer, Eco-friendly synthesis of high-quality polyaniline using a copper scorpionate catalyst, *J. Mater. Chem.*, **17**, 1762-1768 (2007).
18) Kenneth E. Gonsalves, G. Carlson, , J. Kumar, , F. Aranda, and , M. Jose-Yacaman, Polymer Composites of Nanostructured Gold and Their Third-Order Nonlinear Optical Properties, *Nanotechnology***.** , 151-161 (1996).
19) Shinya Abe and Kotaro Kajikawa , Linear and nonlinear optical properties of gold nanospheres immobilized on a metallic surface, *Phys. Rev. **B*** **74,** 035416 (2006).
20) Jadwiga Laska, David Djurado, Wojciech Łużny, X-ray study of plasticized polyaniline, *Eur. Polym. J.*, **38,** Issue 5, 947-951 (2002)

21) H. Liu, X. B. Hu, J. Y. Wang, and R. I. Boughton , Structure, Conductivity, and Thermopower of Crystalline Polyaniline Synthesized by the Ultrasonic Irradiation Polymerization Method**,** *macromolecules**, 35,*** 9414-9419 **(**2002)

22) Asma B Afzal, M J Akhtar, M Nadeem, M Ahmad, M M Hassan, T Yasin and M Mehmood, Structural and electrical properties of polyaniline/silver nanocomposites**,** *J. Phys. D: Appl. Phys.* **42** 015411 (2009)

23) Asma B. Afzal, M. Javed Akhtar, Muhammad Nadeem and M. M. Hassan, Investigation of Structural and Electrical Properties of Polyaniline/Gold Nanocomposites, *J. Phys. Chem. C*, ***113***, 17560–17565 (2009)

24) A M Pharhad Hussain and A Kumar, Electrochemical synthesis and characterization of chloride doped polyaniline, *Bullettin Of Material Scince* **26**, N0. 3 , Page 329-3349 (2003)

25) James Y Shimano, Alan G MacDiarmid, Polyaniline, a dynamic block copolymer: key to attaining its intrinsic conductivity, *Synth. Met.*, **123**, Issue 2, 51-262 (2001)

26) S. Quillard, G. Louarn, S. Lefrant and A. G. Macdiarmid, , Vibrational analysis of polyaniline: A comparative study of leucoemeraldine, emeraldine, and pernigraniline bases, *Phys. Rev*. B **50**, 12496–12508 (1994**).**

27) Gustavo M. do Nascimento and Marcia L.A. Temperinil, Studies on the resonance Raman spectra of polyaniline obtained with near-IR excitation, *J. Raman Spectrosc.* ***39***: 772–778 (2008).

28) M. Baibarac, M. Cochet, M. Łapkowski, L. Mihut, S. Lefrant, I. Baltog, , SERS spectra of polyaniline thin films deposited on rough Ag, Au and Cu. Polymer film thickness and roughness parameter dependence of SERS spectra, *Synthetic Metals*, **96**, Issue 1, 63-70 (1998).

29) F. J. Garcia-vidal and J. B. Pendry, Collective Theory for Surface Enhanced Raman Scattering, *Physical review letters* **77,** 6 (1996**).**

30) Hsiang-Yang Wu, Wan-Ling Huang, and Michael H. Huang, Direct High-Yield Synthesis of High Aspect Ratio Gold Nanorods, *Crystal Growth & Design*, ***7*** **(4)**, 831–835 (2007).

31) Yong Yan, Zai Yu, Yongwei Huang, Wenxia Yuan, and Zhixiang Wei , Helical Polyaniline Nanofibers Induced by Chiral Dopants by a Polymerization Process, *adv. Mater.*, ***19***, 3353–3357 (*2007*).

32) Yen-Yu Ou and Michael H. Huang, High-Density Assembly of Gold Nanoparticles on Multiwalled Carbon Nanotubes Using 1-Pyrenemethylamine as Interlinke , J. Phys. Chem. B, ***110***, 2031-2036 (2006).

33) Mansoor Sheik-Bahae, Ali A. Said, Tai-Hue1 Wei, David J. Hagan and E. W. Van Stryland, Sensitive Measurement of Optical Nonlinearities Using a Single Beam, *ieee journal of quantum electronics.* , **26**. No. 4 (1990)

34) Bing Gu, Wei Ji, P. S. Patil, S. M. Dharmaprakash, and Hui-Tian Wang, Two-photon-induced excited-state absorption: Theory and experiment, *Applied physics letters* **92**, 091118 (2008).

35) Yachen Gao, Xueru Zhang, Yuliang Li, Hanfan Liu, Yuxiao Wang, Qing Chang, Weiyan Jiao, Yinglin Song, Saturable absorption and reverse saturable absorption in platinum nanoparticles, *Optics Communications*, **251,** Issues 4-6, s 429-433 (2005).

Chapter 5

Observation of switching between SA and RSA in silver/gold-polyaniline nanocomposite films

Abstract: In the present work, attempts have been made to embed Silver (Ag) /Gold (Au) - nanoparticles into polyaniline (PANI) matrix using an easy wet chemical route. It is expected that the resulting nanocomposite films will show the interesting third order nonlinear optical characteristics of Ag/Au-nanoparicles modified by the advantageous properties of the conducting polymer PANI. Structural characterisation of Ag/Au-PANI nanocomposite samples was done using X-ray diffraction and Raman studies. UV-visible absorption spectra show the presence of surface plasmon resonance (SPR) peaks centred at 410 nm and 520 nm for Ag-PANI and Au-PANI nanocomposite films respectively, which is a signature of nano dimensionality of the composite samples. Third order nonlinear behaviour of the nanocomposite films was analysed using Z Scan technique employing the second harmonic output (532 nm) of a Q-switched Nd:YAG laser (Minilite, Continuum). It is seen that Ag/Au-PANI nanocomposite film samples show simultaneous presence of saturable absorption (SA) and reverse saturable absorption (RSA) behaviour at 50 μJ laser excitation. This switching between SA and RSA has been reported in many metal nanocomposite systems. However similar behavior in nanocomposite film samples has not been pursued much. The highlight of the present work is the observation of the switching between SA and RSA in Ag/Au polyaniline nanocomposite films which can be of application in optical switching devices. This

phenomenon can be ascribed to the interplay between ground state plasmon band bleaching and excited state absorption. Two photon assisted absorption has been identified as the prime factor contributing towards the observed RSA in these nanocomposite films.

5.1 Introduction

Investigations on noble metal nanoparticles have received considerable attention, due to their large nonlinear susceptibilities and fast response time, which make them promising materials for applications in photonic devices. Among the nanoparticles of noble metals, silver (Ag) and gold (Au) nanoparticles have received immense interest since they exhibit Surface Plasmon Resonance (SPR) band in the visible region of the electromagnetic spectrum. The SPR is attributed to the collective oscillations of the free electrons near the Fermi level, by absorbing electromagnetic fields of suitable wavelength. By varying the size and shape of the nanoparticles, the SPR absorption band can be tuned across the entire visible spectrum. The SPR of metal nanoparticles is effective in local field enhancement which leads to many interesting optical properties. As a consequence, metal nanoparticles find applications in optical limiting and sensor protection, in the design of plasmon waveguides and as nanoprobes in the medical field.[1] Recently the structural, electrical and optical properties of nanostructured PANI and its nanocomposites are being subjected to vigorous investigations. Among them, metal nanoparticles embedded PANI finds special attention owing to its quite interesting non-linear optical properties. [2]

In the present work, highly stable PANI-silver and PANI-gold nanocomposites were synthesized using oxidative polymerization method with monomer aniline and silver/gold colloidal solutions as precursors. The thin films of these nanocomposite samples were deposited on glass substrates using spin casting. The synthesized PANI-silver and PANI-gold nanocomposite films were characterized structurally and optically, to assess the prospects of applications in linear and nonlinear optics.

5.2 Materials and Methods

5.2.1 Synthesis

To synthesize the PANI- Ag nanocomposite, the colloidal suspension of Ag-nanoparticles in water was prepared by the chemical reduction method described by Lee and Meisel.[3] This was added directly to aniline monomer just before chemical oxidative polymerisation. The resultant product after polymerisation, using the oxidant ammonium persulfate $(NH_4)_2S_2O_8$, was filtered and dried in a hot air oven under dynamic vacuum. Thin films of the nanocomposite samples were coated on glass substrates using spin coating method with m-cresol as solvent. For the synthesis of PANI-Au nanocomposite, gold nanoparticles were obtained in a colloidal form by the reduction of chloroauric acid (H $[AuCl_4]$). The previous procedure was followed to get the PANI-Au nanocomposite sample in thin film form. The spin speed was optimized to get good quality thin films of both the nanocomposite samples with uniform thickness of about 1.5μm. They were named as PANI-Ag and PANI-Au films respectively for further investigations.

5.2.2 Characterizations

X-ray diffraction technique employing the Rigaku Dmax C diffractometer with Cu Kα radiation of 1.54 Å was used for structural characterization of PANI-Ag and PANI-Au nanocomposite samples. The optical absorption spectra of the film samples were recorded using a Jasco V 570 UV–VIS spectrophotometer in the wavelength range 330–1300 nm. Raman spectra of the nanocomposite samples were recorded using high resolution Raman spectrometer (Horiba JY).The elemental composition of the samples was confirmed using EDS analysis (JEOL Model JED – 2300). A Q-switched Nd:YAG laser (Spectra Physics LAB-1760, 532 nm, 7 ns, 10Hz) was used as the light source to carry out the non-linear optical studies, using the Z-scan technique.

5.3. Results and Discussions

5.3.1 X-Ray Diffraction Studies

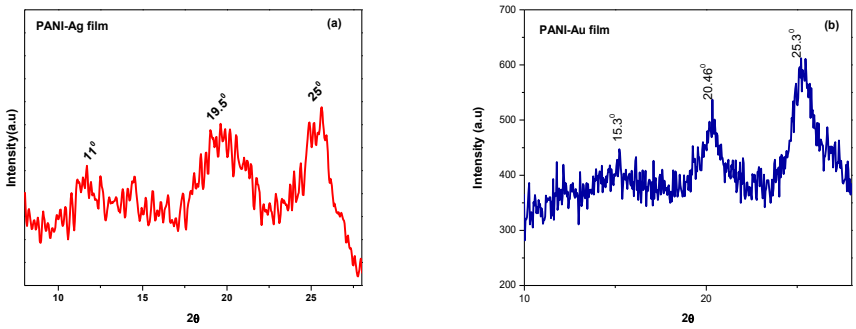

Figure 5.1: X-ray diffraction spectrum of (a) PANI-Ag and (b) PANI-Au

The crystallinity and chain packing of the synthesized composite samples were examined by XRD analysis. The XRD patterns are shown in figures 5.1(a) and 5.1 (b). For the film samples, a broad peak is observed at 25^0. This is the characteristic peak of PANI, which is ascribed to the periodicity in parallel and perpendicular directions of the polymer chain**.** A broad peak centred around 19. 5^0 is present in both the nanocompisite samples, which is characteristic of diffraction by an amorphous polymer and is often observed for PANI**.**[4] The peaks corresponding to silver/gold are not observed because their atomic concentration is only around 1% in the composite. It is further confirmed from the EDAX analysis that the atomic percentage of silver in the PANI-Ag nanocomposite is 0.91 and that of gold in the PANI-Au nanocomposite is 0.42 respectively.

5.3.2 Raman Studies

The Raman spectra of PANI-Ag and PANI-Au nanocomposite films are shown in figures 5.2 (a) and 5.2 (b) respectively. The bands appearing in the 1200 cm^{-1} to 1375 cm^{-1} range in the Raman spectra of both PANI-Ag and PANI-Au composite samples can be related to the vibrational modes C-N of polarons with different conjugation lengths. The bands in the range 1410 cm^{-1} to 1520 cm^{-1} are assigned to the C=N stretching of the quinoid units with different conjugation lengths.[5] The Raman response of both of these nanocomposite films matches with that of PANI with enhancement in the

intensity of the peaks. The observed intensity enhancement is a signature of Surface-Enhanced Raman scattering (SERS) phenomenon in the nanocomposites which also gives confirmation for the formation of the nanocomposites.

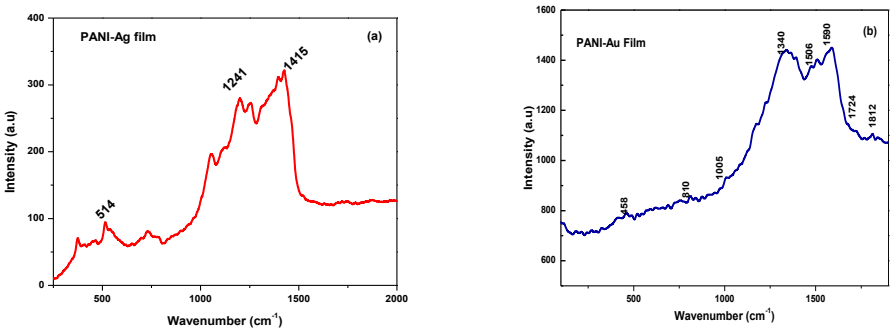

Figure 5.2: Raman spectrum of (a) PANI-Ag and (b) PANI-Au

5.3.3 Optical Absorption Studies

The optical absorption spectra of PANI-Ag and PANI-Au nanocomposite films were recorded in the wavelength range of 300-800nm and the absorption spectra are shown in figure 5.3.The peak at 421 nm in figure 5.3(a) corresponds to the surface plasmon resonance of the silver nanoparticles [1] and the peak at 480 nm in figure 5.3(b) corresponds to that of the gold nanoparticles.

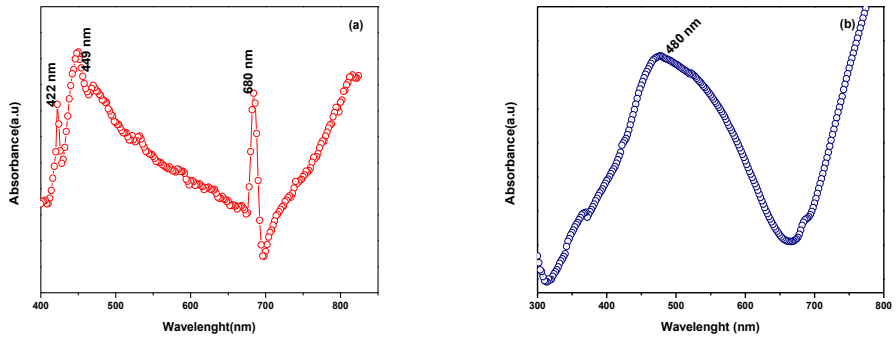

Figure 5. 3: Absorption spectrum of (a) PANI-Ag and (b) PANI-Au

The light absorption of metallic nanoparticles is described in terms of coherent oscillation of the electrons, which is induced by the interaction with the

electromagnetic field. When nanoparticles are incorporated in PANI matrix, the observed plasmon band in both the nanocomposite samples is found to be broad and less prominent because of the polydispersity present in the samples. Still, the presence of silver/gold nanoparticles in the composite samples is quite evident. In the absorption spectrum of PANI-Ag nanocomposite film, two humps are seen within the broad peak centred at 420 nm. This may be due to surface plasmon resonance of the silver nanoparticles of different sizes, embeded in the polymer matrix, due to the agglomeration of the nanoparticles.

5.3.4 Z-Scan Studies

Nonlinear optical studies were carried out on both the nanocomposite films as explained in chapter 4 . The Z-scans for each film sample (PANI-Ag and PANI-Au) were obtained at laser pulse energy of 50 μJ. The films were mounted on a programmable linear translation stage. The input energy reaching the sample and the energy transmitted by the sample were measured using two pyroelectric energy probes (RjP 735, Laser Probe Inc.). The time interval between each laser shot was kept sufficiently large (about 1 s) to allow complete thermal relaxation of the samples between successive laser pulses.

The nonlinear coefficients for 50 μJ excitation energy were calculated for the nanocomposite film samples. The normalized transmittance plots of PANI-Ag and PANI-Au film samples show SA dominated nonlinearity (Figures 5.4 (a) and 5.4(b)) which is different from the behavior shown by the PANI-Au nanocomposite sample in powder form.

On comparison, it is clear that saturable absorption (SA) dominates over reverse saturable absorption (RSA) in film samples for 50 μJ excitation energy. The highlight of the present work is the observation of switching between SA and RSA in polyaniline-Ag/Au nanocomposite films which offers the prospects of applications of these nanocomposite films in optical switching devices. The switching behavior can be ascribed to the interplay between ground state plasmon band bleaching and excited state absorption (ESA). Two photon assisted absorption (TPA) has been identified as the prime factor

contributing towards the observed RSA in these nanocomposite films as the laser fluence is increased. From the best-fit curve (Figure 5.4(a)) to the experimental data for PANI-Ag film, the nonlinear parameters I_s and β_{eff} are calculated for the sample and are given in Table 5.1. The Z-scan data obtained for PANI-Au film was not good enough to do the theoretical fitting. Nevertheless, the Z-scan curve of PANI-Au film has the same nature as that of PANI-Ag film.

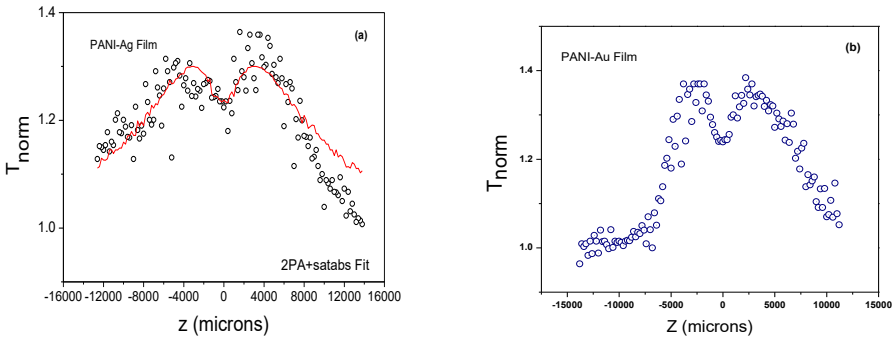

Figure 5.4. Open aperture Z-scan curves of (a) PANI-Ag and (b) PANI-Au films

Table 5.1: Nonlinear transmission parameters calculated from the Z-Scan Measurement

Sample	Excitation Energy (μJ)	Saturation Intensity (I_s) (x10^{10} W/m^2)	Effective two photon absorption coefficient (β_{eff}) (x10^{-10} m/W)
PANI-Ag film	50	10	0.72
PANI-Au film	50	--	--

5.4. Conclusions

PANI-Ag and PANI-Au nanocomposites were synthesized via modified oxidative polymerisation method. Thin films of the composites were grown on glass substrates by spin coating technique. Spin speed was optimized to get films of uniform thicknesses of the order of 1.5 μm. Structural and optical properties (in the linear and nonlinear regimes) were investigated for both PANI-Ag and PANI-Au film samples. Samples show plasmonic properties

such as surface plasmon resonance (SPR) and surface enhanced Raman scattering (SERS). The highlight of the present work is the observation of the switching behavior from SA to RSA in PANI-Ag and PANI-Au films as the laser fluence is increased. The SA phenomenon is characteristic of ground state plasmon band bleaching and RSA is due to the cumulative effects of TPA, ESA, and nonlinear scattering. The observed switching from SA to RSA in these nanocomposite films of PANI extends ample scope for applications in optical switching devices. It is generally difficult to obtain nanocomposite film samples with sufficient transparency to carry out similar nonlinear studies and observe such switching behavior. The observed switching behavior, specifically in the nanocomposite film samples is of high technological relevance, since it offers the possibility of direct application of these films as optical switches.

References

1) M. Anija et al, "Nonlinear light transmission through oxide-protected Au and Ag nanoparticles: an investigation in the nanosecond domain," *Chem. Phys. Lett*. **380**, 223–229 (2003).
2) Jianyong Ouyang et al, "Programmable polymer thin film and non-volatile memory device" *Nat. Mater*. **3**, 918 - 922 (2004).
3) P. C. Lee and D. Meisel, "Adsorption and Surface-Enhanced Raman of Dyes on Silver and Gold Sols" *J. Phys. Chem*., **86**, 3391-3395(1982).
4) Asma B Afzal et al, "Structural and electrical properties of polyaniline/silver nanocomposites," *J. Phys. D: Appl. Phys*. **42**, 015411(2009).
5) Gustavo M. do Nascimento and Marcia L.A. Temperinil, "Studies on the resonance Raman spectra of polyaniline obtained with near-IR excitation," *J. Raman Spectrosc*. **39**, 772–778 (2008).
6) F. J. Garcia-vidal and J. B. Pendry, "Collective Theory for Surface Enhanced Raman Scattering," *Phys Rev Lett* **77**, 6(1996).

7) Bing Gu et all, "Two-photon-induced excited-state absorption: Theory and experiment," *Applied physics letters* **92**, 091118 (2008).
8) Yachen Gao et al., "Saturable absorption and reverse saturable absorption in platinum nanoparticles," *Opt Commun* **251**, 429-433 (2005).
9) Misha Hari et al., "Saturable and reverse saturable absorption in aqueous silver nanoparticles at off-resonant wavelength," *Opt Quant Electron* **43**, 49–58(2012).
10) P.B. Anand et al., "On the structural and optical properties of gold–polyaniline nanocomposite synthesized via a novel route", *Polym. Int.*, **61**, 1733-1738(2012)

Chapter 6

On the structural and electrochemical properties of lithium doped Polyaniline - A prospective cathode active material for environment friendly and flexible Li-ion battery applications

Abstract: The present work is aimed at investigating the structural and electrochemical properties of Li-ion cells, assembled using Li-substituted polyaniline (PANI) as the cathode active material. Emeraldine salt form of PANI was synthesized via oxidative polymerization method. It was de-doped to get emeraldine base form of PANI and then treated with "*n*-Butyllithium in hexanes (*n*-BuLi)" to get the Li-substituted form of PANI, since *n*-BuLi partially disaggregates the polyaniline clusters by binding the amines to its lithium centers. The lithiation was carried out in an argon (99.999% purity) filled glove box. Concentration of the *n*-BuLi was varied and the level of lithiation was analyzed using atomic emission spectroscopy. X-ray diffraction, FTIR and SEM techniques were used to get the structural and surface morphological details of the Li-substituted PANI (LIPO) sample. Coin cells were assembled in the glove box using LIPO as cathode and lithium metal foil as anode with 1 M $LiPF_6$ in EC: DMC (1:1) as electrolyte. Voltage sweep cyclic voltammetry and charge-discharge cycling were employed to characterize the electrochemical capabilities of the assembled cells. The cells are found to show a maximum discharge capacity of 25.04 mAh/g with 99.99 % columbic efficiency and have got tremendous cycling stability over 50 cycles. The dopant, n-Butyllithium is a

cheaper alternative to other expensive, generally used dopants like $LiPF_6$ and $LiBF_4$. By suitably optimizing the Li- doping conditions, it is expected that the specific capacity of these cells can be still further enhanced. Pouch cells were assembled using LIPO sample as cathode, graphite as anode and gel polymer (Poly (ethylene oxide)) as electrolyte. The pouch cells are found to hold the open circuit voltage of 0.6 V (OCV) even when bent up to 90^0 from the initial state.

6.1 Introduction

The development of conducting polymer-based rechargeable Li-ion cells with high specific capacity and excellent cycling characteristics is a highly competitive area among research and development groups, worldwide. Polymer-based rechargeable batteries are specifically attractive due to the environmentally benign nature and the possible constructional flexibility they offer. Another particular feature of conducting polymer-based Li-ion cells is that the electrode kinetics is generally controlled by the diffusion of the dopant anions throughout the polymer structure. As expected, the charge-discharge rate of polymer electrodes greatly depends upon the nature (size and charge density) of the dopant anion and the electrode morphology. Therefore, the synthesis conditions of conducting polymers become very important for assuring their capability as electrodes in battery applications. Among polymers having electrical transport properties suitable for rechargeable battery applications, polyaniline is the most favoured one due to its excellent environmental stability, tunable electrical conducting properties and the availability of cost effective precursor materials for its synthesis.[1-4] The polymer electrode configuration retains specific advantages such as flexibility in geometry and design, compatibility with the environment and projected low cost which are factors that make them competitive for small sized, low rate, button prototypes for the microelectronics consumer market

Secondary battery systems have become an inevitable part of daily life. They can be found in most of the portable electronic gadgets and recently they have

started powering automobiles, although the power generated is low. The efficient storage of electrical energy generated from solar cells is achieved by using suitable secondary battery systems. The development of rechargeable battery systems having excellent charge storage capacity, cyclability, environmental friendliness and flexibility has yet to be realized in practice. Rechargeable Li-ion cells employing cathode active materials like $LiCoO_2$, $LiMn_2O_4$ and $LiFePO_4$ have got remarkable charge storage capacity with least charge leakage when not in use. However, material toxicity, chance of cell explosion and lack of effective cell recycling mechanism pose significant risk factors which are to be addressed seriously. These cells also lack flexibility in their design due to the structural characteristics of the electrode materials.[5, 6]

Global research is directed towards identifying new class of electrode materials with less risk factors and better structural stability and flexibility. Polymer-based electrode materials with inherent flexibility, stability and eco-friendliness can be a suitable choice. [7-10] One of the prime drawbacks of polymer-based cathode materials is the low electronic conductivity. Hence the real task with this class of materials is to get better electronic conductivity with good electrical storage capability. Electronic conductivity can be enhanced by using proper dopants. In the designing of rechargeable Li ion cells with polymer-based cathode active materials, the key issue is to identify the optimum lithiation of the polymer cathode which can ensure the highest electronic conductivity and specific charge capacity possible.[11, 12]

In the present work, attempts have been made to assemble rechargeable Li ion cells employing Li substituted polyaniline as the cathode active material, lithium foil as anode and lithium hexafluorophosphate ($LiPF_6$) in ethylene carbonate(EC) : dimethyl carbonate (DMC) (1:1) as electrolyte. In earlier reports, using lithium substituted (lithiated) PANI as cathode, the lithiation has been achieved by treating PANI with $LiPF_6$ or $LiBF_4$.[13-17] In the present work lithiation has been effected by treating PANI with *n*-Butyllithium(*n*-BuLi) in hexanes which is a novel approach to achieve lithium substitution in PANI. The prime advantage of this technique is the much reduced material cost involved in the synthesis. The cost of *n*-BuLi is about 1/10 th of that of $LiPF_6$ and $LiBF_4$. Structural and morphological studies on Li-substituted PANI,

along with the electrochemical characterization have not been carried out extensively. In the present work, rechargeable Li-ion cells with lithiated PANI as cathode active material, have been assembled and thoroughly characterized.

6.2 Materials and Methods

6.2.1 Synthesis

To start with, the emeraldine salt (ES) form of HCl doped PANI was synthesized via chemical oxidative polymerization method [18]. It was de-doped using NH_4OH solution to get the emeraldine base (EB) form of PANI. The resultant product was treated with "*n*-Butyllithium in hexanes (*n*-BuLi)" in an argon filled glove box (99.999% purity) with moisture content less than 5ppm, to get the lithiated form of PANI. The *n*-BuLi is expected to disaggregate the polyaniline clusters by binding the amines to its lithium centers and this process is referred to as metalation. Concentration of the *n*-BuLi was varied in three steps to achieve improved metalation[19]. The reaction mechanism is illustrated in figure 6.1. Resultant products are named as LIPO 1, LIPO 2 and LIPO 3 respectively. These samples were subjected to detailed structural characterization. Coin cells were assembled in the argon filled glove box using LIPO 1, LIPO 2 and LIPO 3 as cathode active materials and lithium metal foil as anode with 1 M $LiPF_6$ in EC: DMC (1:1) as electrolyte, as explained in detail in chapter 2. The assembled coin cells were characterized to assess the electrochemical capabilities.

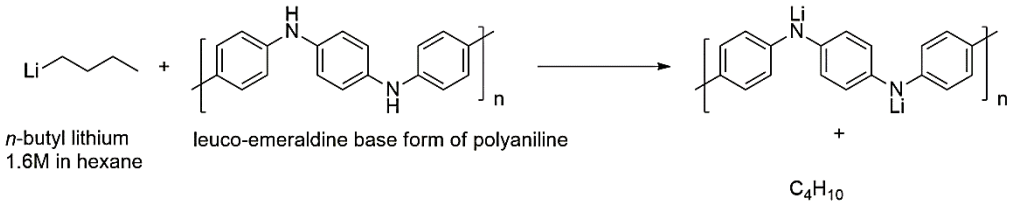

Figure 6.1: Possible mechanism of partial metalation process

6.2.2 Characterisations

Thermo Electron IRIS INTREPID II XSP DUO model ICP-AES system was used for the qualitative and quantitative determination of the presence of lithium in the samples. X-ray diffraction (XRD) employing Rigaku Dmax C

diffractometer (USA) with Cu Kα radiation of 1.54 Å was used for the structural characterization of the samples. A Thermo Nicolete Avatar 370 DTGS model Fourier Transform IR (FTIR) (USA) spectrophotometer was used to obtain the IR spectrum of the samples in the range 400–4000 cm^{-1}. JEOL Model JSM - 6390LV Scanning Electron Microscope (SEM) was used to generate surface morphological images of the samples with the resolution of a micrometre. Cyclic Voltammetry experiment was carried out employing the Biologic SP300 research grade potentiostat / galvanostat (Scan rate: 0.1 mV/s). Charge discharge test was carried out between 2V and 4 V using 8 channel battery analyser (5V, 1 mA-MTI Corporation USA) at C/10 current rate.

6.3 Results and Discussions

6.3.1 Inductively Coupled Plasma Atomic Emission (ICP-AES) Analysis

The atomic spectrum emitted by a sample is used to determine its elemental composition in this instrument. The wavelength at which emission occurs is used to identify the element, and the intensity of the emitted radiation quantifies its concentration [20]. LIPO 1, LIPO 2 and LIPO 3 samples were digested using 5ml HNO_3 and made up into 100ml using HPLC grade water and were analysed using ICP-AES system. Results of the analysis are tabulated in Table 6.1.

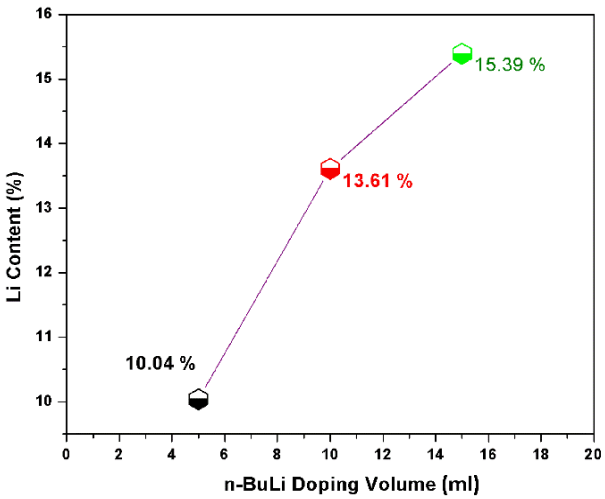

Figure 6.2: Variation of Lithiation with respect to *n*-Buli doping concentration

Table 6.1: ICP-AES Measurement Data

Sample Name	Lithium Content (%)
LIPO 1	10.04
LIPO 2	13.61
LIPO 3	15.39

It can be seen that on increasing the *n*-BuLi concentration, the lithium content in the sample is getting increased (figure 6.2). However the metalation is partial and the maximum metalation achieved is only 15.39%.

6.3.2 X-Ray Diffraction studies

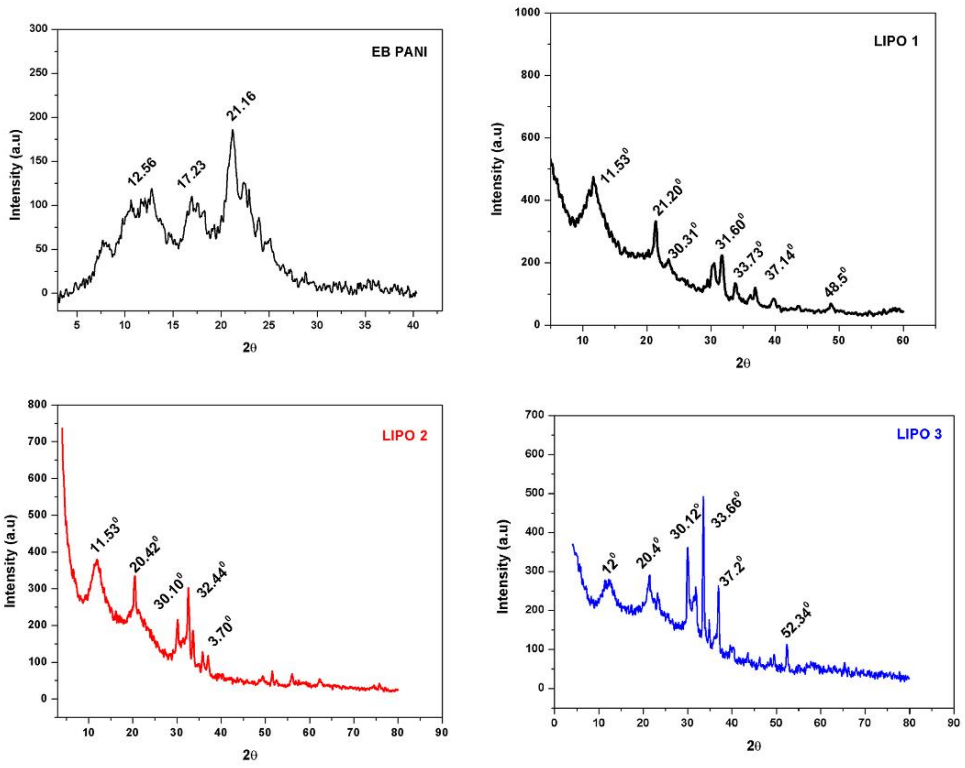

Figure 6.3: X- ray diffraction patterns of EB PANI and lithiated PANI Sample

On studying the powder diffraction data shown in figure 6.3, it is clear that emeraldine base form of PANI shows broad peaks around 2θ values of 11^0,17^0

and 21^{0} [21] which agree with the already reported data. For lithiated samples, instead of broad peaks indicating amorphous structure, intense and narrow peaks are seen around 11^{0} and 21^{0} with additional diffraction peaks at 30^{0},33^{0},37^{0},50^{0}. The presence of these peaks indicates a semi crystalline nature for all the lithiated samples. Better crystalline nature of these lithiated PANI samples compared to normal PANI is a good sign of better structural order, which in turn is helpful to sustain the structural integrity during Li ion exchange.

6.3.3 FTIR Analysis

The IR response of the emeraldine base form of PANI and the lithiated samples is illustrated in figure 6.4.

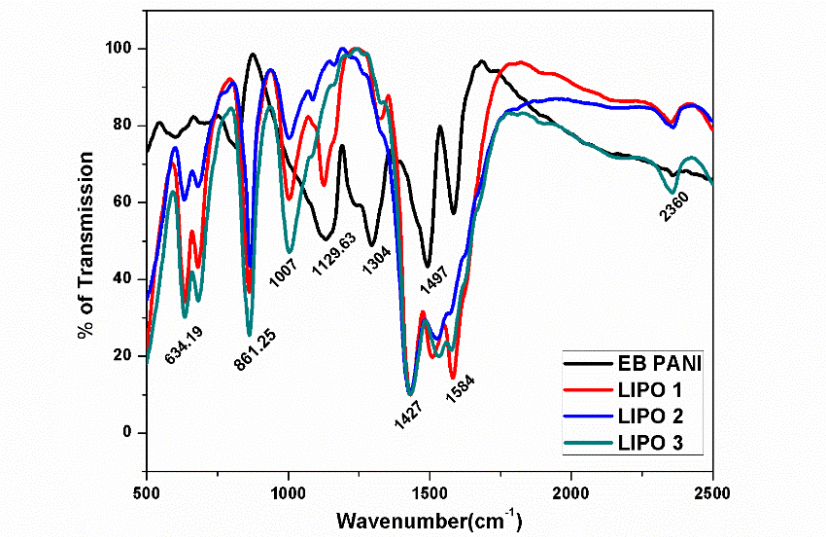

Figure 6.4: IR transmission curves of EB PANI and lithiated PANI samples

In PANI, the characteristic peaks at 1584cm^{-1} and 1497cm^{-1}correspond to the quinoid ring (Q) and the benzenenoid ring stretching modes respectively. It can be seen that for the lithiated samples, the peak at 1584 cm^{-1} is broadened enough to be hardly considered as the signature of quinoid stretching. The characteristic peak of polyaniline base is the N=Q=N stretching band at 1129cm^{-1}.[22] The bands in the range 1200–1400cm^{-1} represent the C–N stretching modes of the aromatic ring. For the lithiated samples, vibration modes at 1304 cm^{-1} and 1497 cm^{-1} are absent which are of secondary aromatic

amine stretching and benzenoid ring stretching respectively. These modes are signatures of the presence of amine and imine groups in the sample. It is seen that on lithiation, these modes rather disappear or become very feeble to be detected by the sensor. This is a strong evidence for lithium substitution of PANI, although it is partial.

6.3.4 Microstructure Analysis-SEM

The scanning electron microscope images of EB PANI and the three lithiated PANI samples are shown in figures 6.5 and 6.6 respectively. It is seen that surface morphology is considerably modified at the submicron level on increasing the *n*-BuLi concentration. For the lowest *n*-BuLi concentration, rod like structures are formed. For the medium *n*-BuLi concentration flake like structures are observed and for the highest *n*-BuLi concentration, the result is the formation of bigger flake like structures. Unlike the random distribution of polymer chains in EB PANI, on treating with *n*-BuLi, more ordered structures are formed in LIPO1, LIPO 2 and LIPO 3 samples, complementing the presence of crystalline peaks in the X-ray diffraction patterns of these samples. These ordered structures can comfortably sustain this morphology during Li ion exchange process with a healthy Li ion transport.

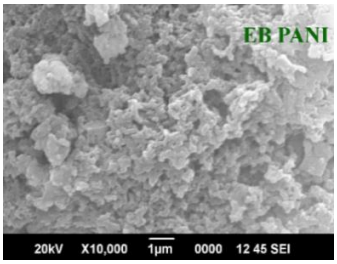

Figure 6.5: SEM image of EB PANI

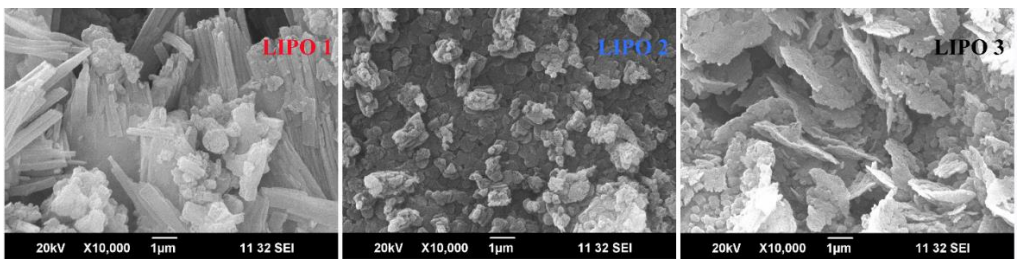

Figure 6.6: SEM images of LIPO 1, LIPO 2 and LIPO 3

6.3.5 Electronic Conductivity Studies

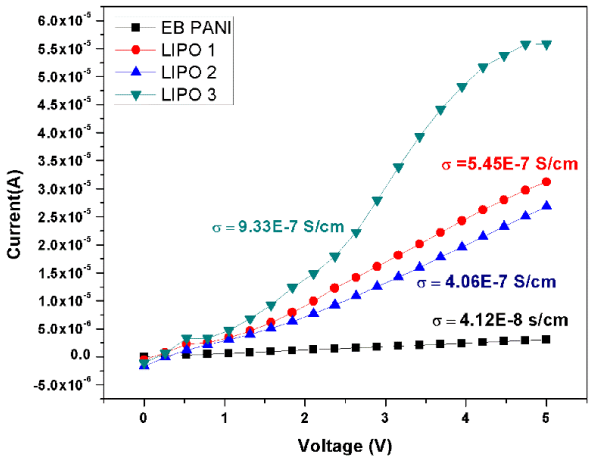

Figure 6.7: I-V curves of the samples for different *n*-BuLi concentration along with the calculated conductivity values

The DC electrical conductivity of the samples was measured using two probe technique, employing Keithley source meter, interfaced to a computer using Lab-View program. The current-voltage (I-V) curves for different concentrations of *n*-BuLi, with the calculated conductivity values, are shown in Figure 6.7. Conductivity of the samples shows only a marginal increase on treating with *n*-BuLi. However the conductivity values obtained are in the expected range for cathode active materials.

6.3.6 Cyclic Voltammetry Analysis

The cyclic voltammetry studies were carried out on coin cells assembled in the glove box using lithiated PANI as cathode and Li metal as anode. The cyclic voltammetry curves of the LIPO 1, LIPO 2 and LIPO 3 samples are shown in figure 6.8. The response curves for voltage scan between 2V to 4V show reversible characteristics with broad peaks corresponding to cathodic and anodic scans. The cathodic peak corresponds to one step Li oxidation process to form Li deficient PANI with the release of an electron from the cathode. The anodic peak corresponds to the reduction of Li ion and the insertion of Li back into cathode. It is seen that, the oxidation potential is in the range 3.5V-4 V and the reduction potential falls between 2.6 V to 3.5 V. The cathodic

and anodic peaks become more prominent and resolved as the percentage of lithiation increases. The area of the CV curve also increases with increase in the percentage of lithiation. The open circuit voltage of the assembled coin cells is around 3.5 V.

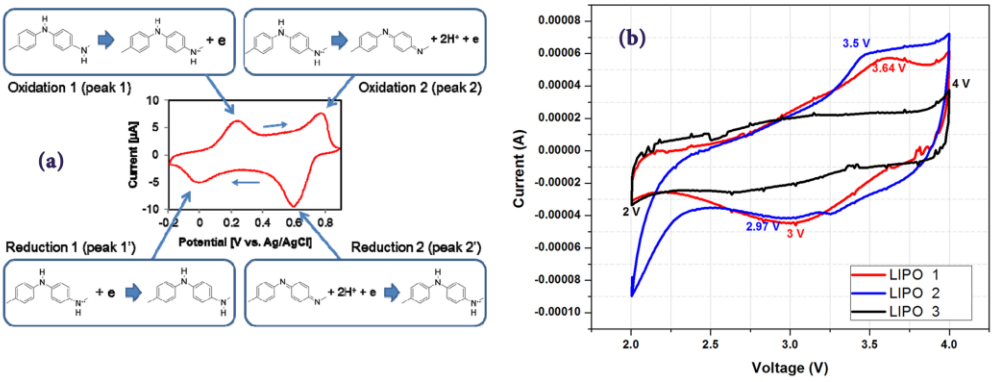

Figure 6.8: (a) A typical cyclic voltammetry curve of polyaniline in HCl (*Nanomaterials* **2013**, *3*(3), 498-523) (b) Voltage sweep cyclic voltammetry response of LIPO 1, LIPO 2 and LIPO 3

6.3.7. Charge Discharge Cycle Analysis

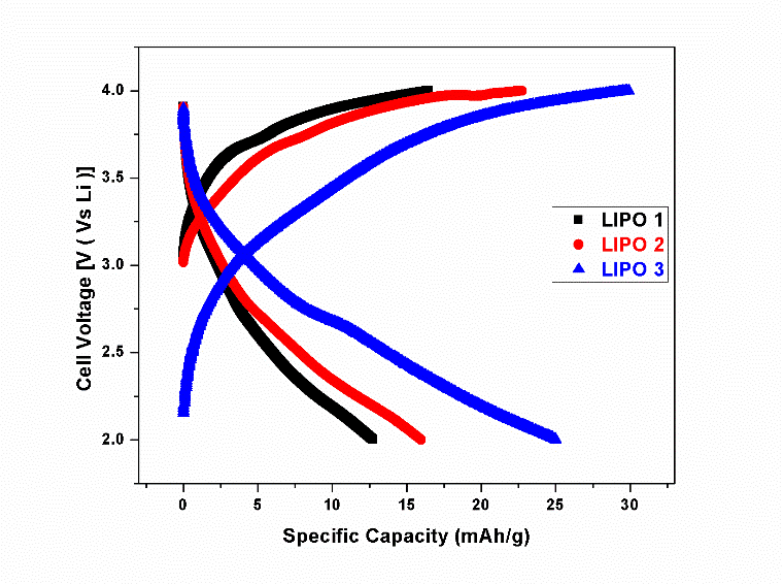

Figure 6.9: Charge-discharge curves of LIPO 1, LIPO 2 and LIPO 3

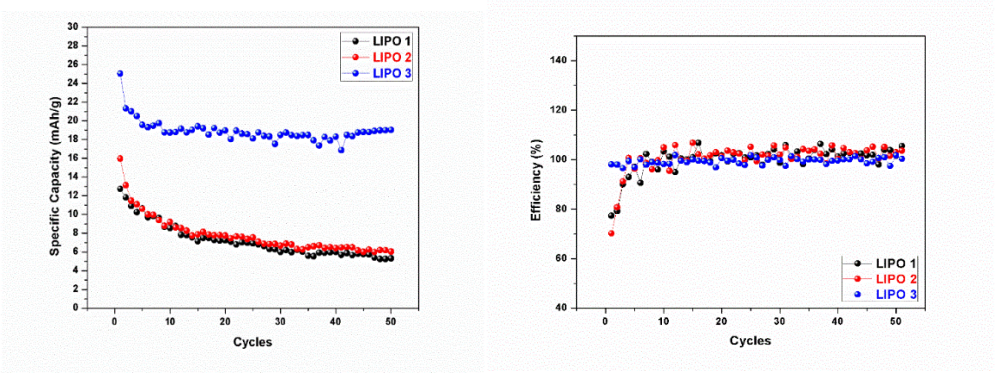

Figure 6.10: Specific capacity versus charge discharge cycle number and % of efficiency versus cycles for LIPO 1, LIPO 2 and LIPO 3

The theoretical capacity of lithiated polyaniline is 142 mAh/g which corresponds to 100 % lithiation. [23] In the present work, maximum lithiation achieved is only 15 %. Hence the theoretical capacity expected is around 25 mAh/g. The maximum specific capacity of 25.04 mAh/g is obtained for LIPO 3 sample with the maximum Li substitution around 15 %. Lithiated PANI based Li-ion cells with fairly good specific capacity close to theoretical capacity, columbic efficiency close to 100 % and excellent cycling stability have not been reported earlier. In the present case, LIPO 3 sample shows the maximum capacity of 25.04 mAh/g for the first cycle and then shows a decreasing nature for a few following cycles. After the fifth cycle onwards, the capacity remains the same at 20 mAh/g up to the 50th cycle. In the case of the other two samples, for the first few cycles, a capacity in the range 13 mAh/g – 16.5 mAh/g is observed and thereafter there is a fall in capacity till the 10th cycle. Then the capacity shows no fading for the rest of the cycles until the 50th one. The charge-discharge curves of the three cells are shown in figure 6.9 and the specific capacities against the number of cycles and efficiency of cycling are plotted in figure 6.10.

After the 5th and 10th charge discharge cycles, all the three samples show a stable cycling behaviour up to the 50th cycle. All the three samples show columbic efficiency close to 99 % for all the charge discharge cycles.

Pouch cells were assembled using LIPO samples as cathode, graphite as anode[24] and gel polymer (Poly(ethylene oxide)) as electrolyte.[25,26] Schematic

diagrams of the assembled cells are shown in figure 6.11 and the realised pouch cell is picturised in figure 6.12.

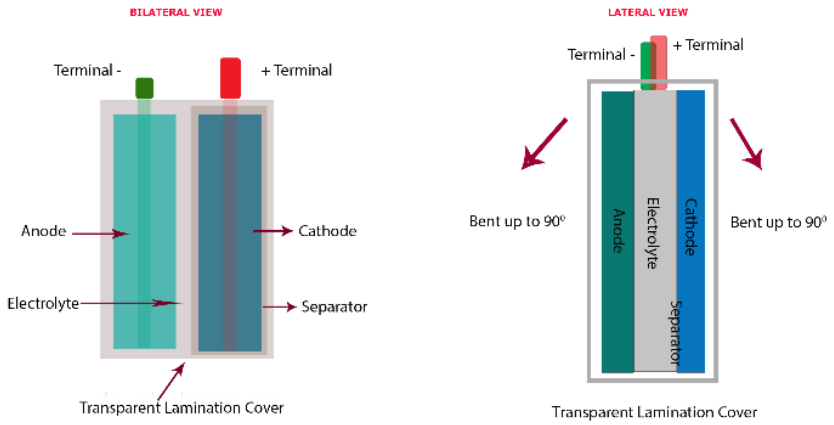

Figure 6.11: Schematic representation of pouch cells assembled with LIPO 1, LIPO 2 and LIPO 3

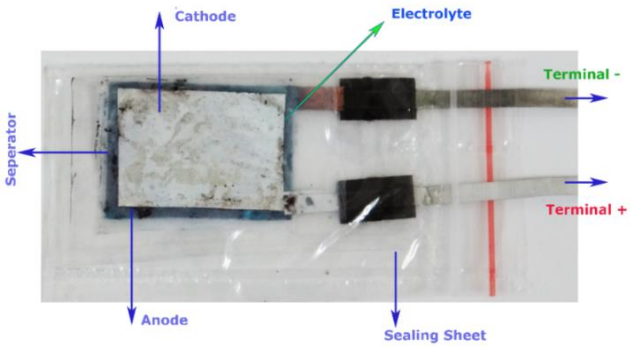

Figure 6.12: Pouch cells assembled with LIPO 1, LIPO 2 and LIPO 3

The pouch cells are found to hold the open circuit voltage of 0.6 V (OCV) even when they are bent up to 900 from the initial state. This gives the first signature of flexibility associated with polymer-based Li-ion cells.

6.4 Conclusions

The present work highlights the suitability of using n-butyllithium, a cost effective substitute for expensive counterparts like $LiPF_6$ and $LiBF_4$, for synthesizing Li substituted polyaniline to be used as the cathode active material in rechargeable Li ion cells. Lithium substituted PANI samples were

synthesized for three different concentrations of *n*-BuLi and were subjected to detailed structural characterization using XRD, FTIR and SEM techniques. The structural analysis confirms the enhanced crystallinity/order in Li substituted samples compared to pure PANI. The coin cells assembled using Li substituted PANI as cathode show quite good electrochemical behaviour. Specific capacity close to the expected theoretical capacity has been obtained for the cells with 15% lithium substitution. All the three assembled cells show excellent columbic efficiency above 99% and stable charge discharge cycling behaviour up to 50 cycles. The cells are found to be capable of showing stable cycling behaviour above 100 cycles and it may not be surprising if these cells are found to withstand 1000-2000 charge discharge cycles without significant capacity loss. The pouch cells assembled hold the open circuit voltage even when they are bent up to 90^0 from the initial state. This opens up a new methodology to fabricate all solid state, flexible and environmentally friendly lithium ion cells.

References

1) De Surville, R.; Josefowicz, M.; Yu, L. T.; Perichon, J.; Buvet, R. *Electrochim. Acta*, **13**:1451 (1968).
2) Osaka, T.; Nakajima, T.; Naoi, T.; Owens, B. B. *J. Electrochem. Soc.*, **135**:2139 (1990).
3) Murray, D. P.; Kispert, L. D.; Petrovic, S. *Syn. Met.*, **28**:C269 (1989).
4) S. Neves, C. Polo Fonseca, *J.Power Sources.*,; **107**:13 (2002).
5) Masaki Yoshio, Ralph J. Brodd, Akiya Kozawa, Lithium-Ion Batteries, Science and Technologies, *Springer **XXVI**.*,; 452:279 (2009).
6) Bo Xu, Danna Qian, Ziying Wang, Ying Shirley Meng, *Materials Science and Engineering.*,**73**:51–65 (2012).
7) D.A. Notter, M. Gauch, R. Widmer, P. Wager, A. Stamp, R. Zah, H.J. Althaus *Environ. Sci. Technol.*, **44**: 6550–6556 (2010).
8) E. Karden, S. Ploumen, B. Fricke, T. Miller, K. Snyder *J. Power Sources.*, **168** : 2–11(2007).
9) H. Li, Z. Wang, L. Chen, X. Huang, *Adv. Mater.*; **21**: 4593–4607(2009).

10) J.W. Fergus ,J. Power Sources., **195**: 939–954 (2010).
11) K. Ghanbari, M. F. Mousavi, M. Shamsipur, H. Karami, *J. Power Sources.*, **170**:513 (2007).
12) W.-M. Chen, L. Qie, L.-X. Yuan, S.-A. Xia, X.-L. Hu, W.-X. Zhang, Y.-H. Huang, *Electrochim. Acta.*, **56**: 2689 (2011).
13) Nigrey, P. J.; Maclnnes, D. Jr.; Nairns, D. P.; MacDiarmid, A. J. *J. Electrochem. Soc.*, 128(8):1651 (**1981**).
14) Panero, S.; Prosperi, P.; Bonino, F.; Scrosati, B.; Corradini, A.; Mastragostino, M. *Electrochim. Acta.*, **32**(7): 1007(1987).
15) Nishio, K.; Fujimoto, M.; Yoshinaga, N.; Furukawa, N.; Ando, O.; Ono, H.; Suzuki, T. *J. Power Sources.*, **34**: 153 (1991).
16) Kwang Sun Ryu et al. *Syn. Met.*, **110**: 213–217(2000).
17) Kwang Sun Ryu et al. *Bull. Korean Chem. Soc.*, **23**: 8(2008).
18) Irina Sapurina and Jaroslav Stejskal, Review, *Polym Int.*, **57**: 1295–1325 (2008).
19) Miah, M. A.; Snieckus, V. *J. Org. Chem.*, **50**: 5436 (1985).
20) Thomas J. Manning and William R. Grow, The chemical educator, *Springer-Verlag S.*, 1430-4171 (1997).
21) A. Mani, K. Athinarayanasamy, P. Kamaraj, S.Tamil Selvan, S. Ravichandran, K. L. N. Phani, S. Pitchumani, *J Mater Sci Lett.*, **14(22):** 1594-1596 (1995).
22) Miroslava Trchova and Jaroslav Stejskal, *Pure Appl. Chem.*, **83:** 1803–1817 (2011).
23) Rajive Tomy M, Anil Kumar K M and S Jayalekshmi, *Journal of Instrument Society of India.*,; **41**: 2 (2011).
24) K.S. Ryu, K.M. Kim , *J.Power Sources.* **165**: 420–426 (2007).
25) C. P. Sandhya, Bibin John, C. Gouri, *Ionics* 20:601 –620 (2014).
26) J.Y. Song, Y.Y. Wang, C.C. Wan, Journal of Power Sources, 77, 183–197 (1999).

Chapter 7

Organic In-organic hybrid cathode materials for Li-ion Cells with improved performance and structural flexibility

Abstract: The investigations on the electrochemical properties of Li-ion cells, assembled using the mixture of Li-substituted polyaniline (PANI) and Lithium iron phosphate ($LiFePO_4$) as the cathode active material are addressed in this chapter. Polyaniline was doped with *n*-Butyllithium in hexanes (*n*-BuLi) to get Li-enrichment in the host. This sample is labeled as Lithiated PANI (LIPO). The *n*-BuLi doping concentration was varied from 5 ml to 15 ml in three steps. These samples are named respectively as LIPO 1, LIPO 2 and LIPO 3. Among the conventional Li-ion battery cathodes, including Lithium Cobalt Oxide ($LiCoO_2$), Lithium Manganese Oxide ($LiMn_2O_4$), Lithium Iron Phosphate ($LiFePO_4$), and Lithium Nickel Manganese Cobalt Oxide, $LiFePO_4$ is a highly preferred one, due to its higher charge density and environmental friendliness. The main drawback of this material is regarding its poor electrical conductivity. Keeping these things in mind, LIPO (1-3)-$LiFePO_4$ composite based cathode materials were synthesized by mixing LIPO (1- 3) and $LiFePO_4$ in 9:1 ratio by weight, with the following combinations, 9(LIPO1):1($LiFePO_4$), 9(LIPO2):1($LiFePO_4$), 9(LIPO3):1($LiFePO_4$). These samples as cathode materials were used to assemble coin cells in an argon filled glove box using lithium metal foil as the anode and 1 M $LiPF_6$ in EC: DMC (1:1) as the electrolyte. Voltage sweep cyclic

voltammetry and charge-discharge cycling tests were employed to characterize the electrochemical potentiality of the assembled cells. The cells are found to show a maximum discharge capacity of 37 mAh/g with 99.99 % columbic efficiency and have got tremendous cycling stability over 50 cycles. There are no reports on the electrochemical characteristics of Li-ion cells using *n*-BuLi treated PANI and $LiFePO_4$ composite as cathode material. By suitably optimizing the mixing ratios, it is expected that the specific capacity of these cells can be considerably enhanced.

7.1 Introduction

In the present work, with the objective of increasing the charge storage capacity of lithiated PANI based cells, LIPO- $LiFePO_4$ composite cathodes were synthesizes by mixing LIPO (1-3) and $LiFePO_4$ in 9:1 ratio by weight. The resultant products were used as the active material in cathode preparation. The cyclic voltammograms and charge-discharge characteristics of LiPO-$LiFePO_4$ composite cathode based coin cells were investigated and their capabilities compared.[1-11]

7.2 Materials and Methods

7.2.1 Synthesis

Lithium enriched PANI samples (LIPO 1, LIPO 2 and LIPO 3) for different concentrations of the dopant, n-butyl lithium in hexane (*n*-BuLi) were synthesized as explained in the previous chapter. The resultant samples were mixed with $LiFePO_4$ in 9:1 proportion by weight. They are named as LiFe 1, LiFe 2 and LiFe 3. These composites with 10 % conductive additives were coated on battery grade aluminum foils and dried for 3 hours at 60 ^oC under dynamic vacuum. [11-12] Coin cells were assembled using the coated aluminum foil as cathode, porous polyethylene film as separator, lithium metal as anode, and 1 M $LiPF_6$ dissolved in 1: 1 (volume ratio) mixture of EC and DMC as the electrolyte in an argon filled glove box.

7.2.2 Characterizations

X-ray diffraction (XRD) employing Rigaku Dmax C diffractometer (USA) with Cu Kα radiation of 1.54 Å was used for the structural characterization of the composite samples. The cells were tested by using a galvanostatic charge-discharge cycler (MTI Corporation, USA) in the voltage range of 2.0-4.0 V and C/10 current rate with resting at open circuit voltage condition for 1 min after every charging. Cyclic voltammograms were obtained using a Bio-Logic SP300 Unit at a constant scan rate of 1 mV/sec in the range of 2.0 to 4V.

7.3 Results and Discussions

7.3.1 X-ray Diffraction Study

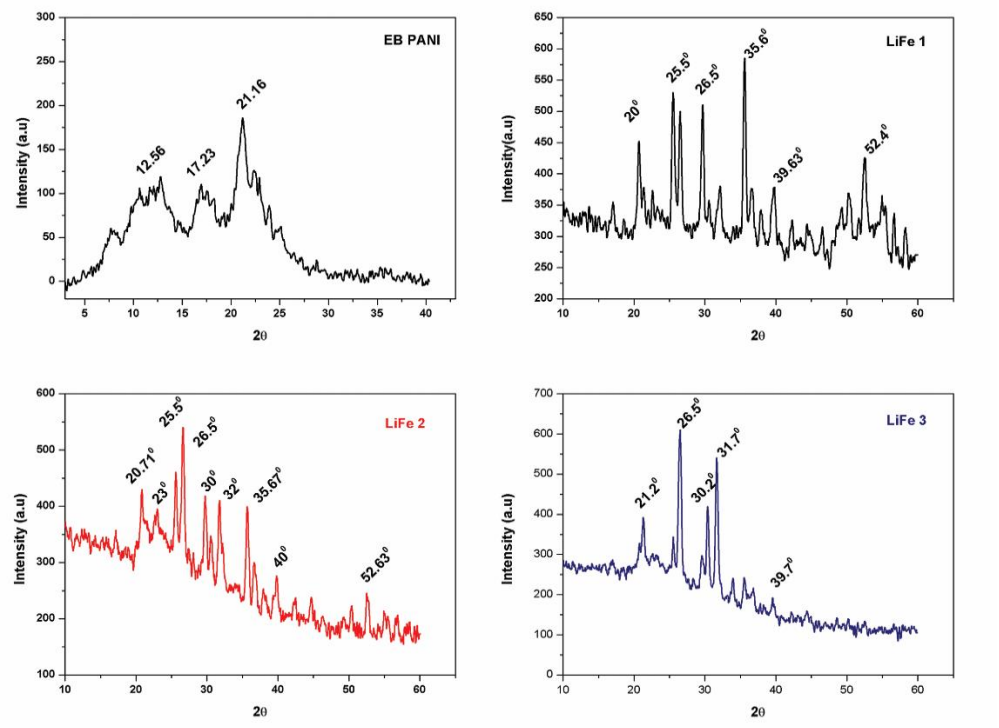

Figure 7.1.The XRD patterns of EB PANI, LiFe1, LiFe 2 and LiFe 3

X-ray diffraction patterns of LiFe composite samples are shown in figure 7.1. The patterns consist of the characteristics peaks of both lithiated PANI and $LiFePO_4$. Characteristic peaks of LIPO are well evident from the XRD patterns. There are also peaks at 20^0 (101), 25^0(201, 111), 30^0(211, 020) and

35^0 (311) which correspond to the signature peaks of $LiFePO_4$ in the composite system.[13]

7.3.2 Cyclic Voltammetry studies

In order to identify oxidation/reduction potentials and study the electrochemical capability of the cells assembled using LiFe composite cathodes, cyclic voltammetry test was performed (Scan rate: 0.1 mV/s). The oxidation and reduction peaks of these systems occur within 2 to 4 V and show good reversibility. For these LiFe cells, the upper two broad peaks (~3.32 and ~3.7 V) correspond to the oxidation and the lower two broad peaks (~2.82, and ~2.41 V) to the reduction as shown in figure 7.2. The upper peak at 3.32 V corresponds to the oxidation of Li in lithiated PANI and that at 3.7 V to the oxidation (de-intercalation of Li+ ion) of Li in $LiFePO_4$ and the lower peaks at ~2.82 and ~2.18 V correspond to the reduction of LIPO and that (intercalation of Li+ ion) of $LiFePO_4$ respectively.[12]

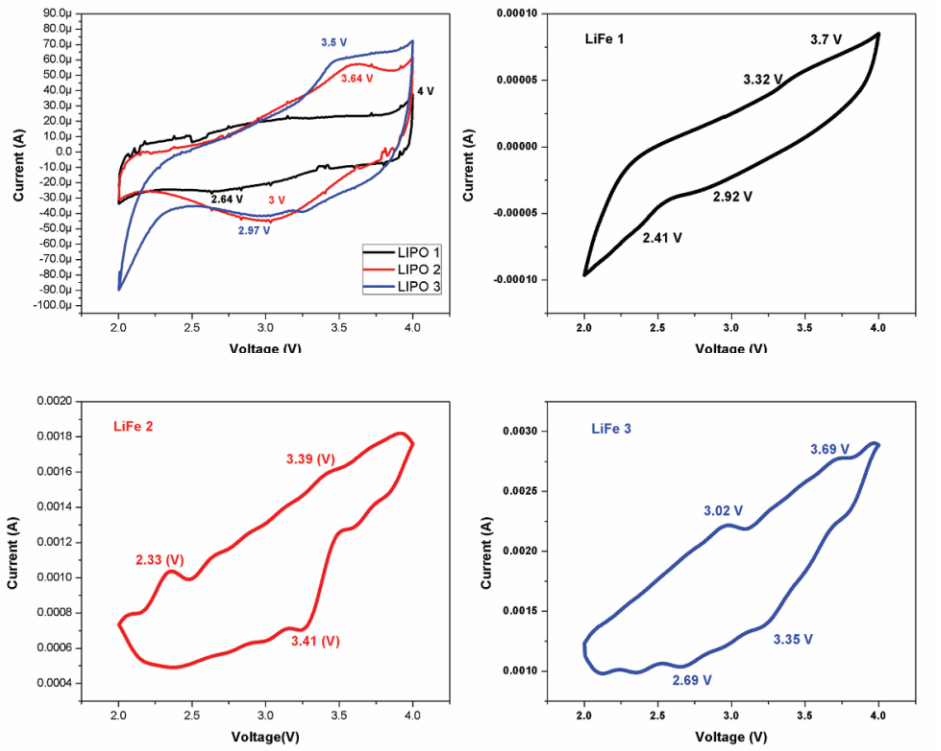

Figure. 7.2: Cyclic voltommograms of LiPO, LiFe 1, LiFe 2 and LiFe 3

7.3.3 Charge Discharge Analysis

The discharge characteristics of LiFe 1, LiFe 2 and LiFe 3 cells are shown in figure 7.3. These discharge curves resemble those of transition metal oxide electrodes in conventional rechargeable lithium ion cells. The average operating voltage of these cells may be approximated to 3.3 V in spite of different LIPOs used. The plots showing the variation of discharge capacity with number of cycles are shown in figure 7.4. The highest discharge capacity obatined is around 40 mAh/g for LiFe 3 followed by 25 mAh/g for LiFe 2 and 21 mAh/g for LiFe 1. The variation of charge efficiency with cycle number of the assembled coin cells is shown in figure 7.5. All the cells show an average efficiency around 98%. The observed cell performance is very impressive and can be compared with that of the conventional Li-ion secondary battery systems.

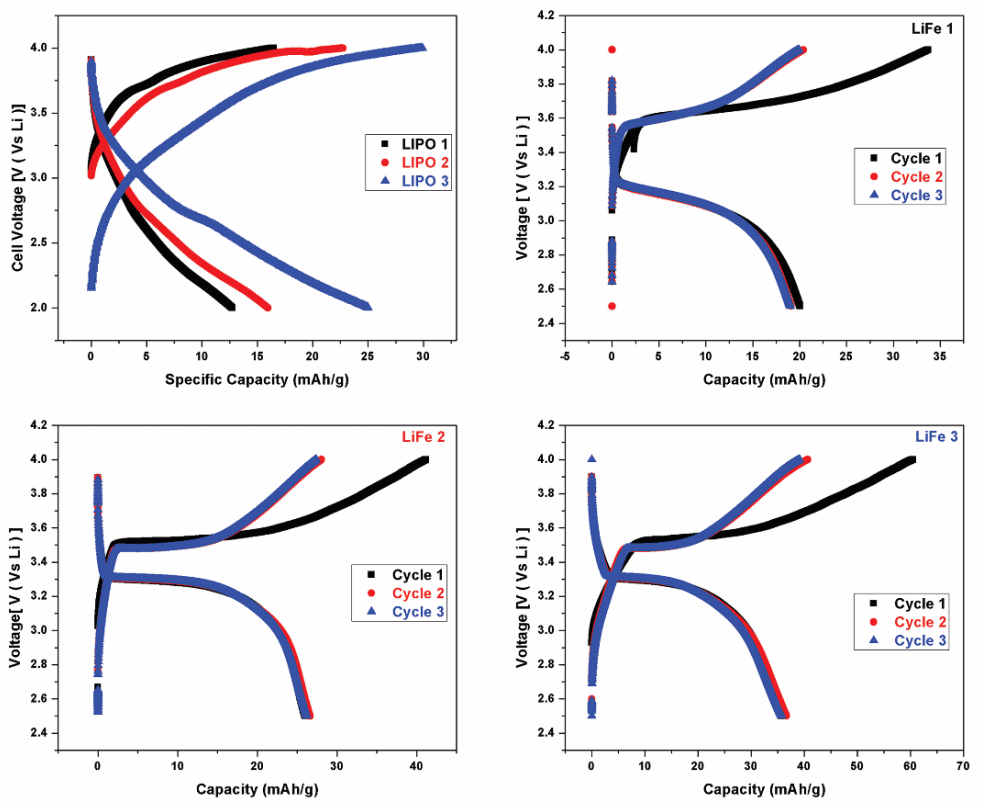

Figure 7.3: Charge-discharge curves of LIPO, LiFe 1, LiFe 2 and LiFe 3 cells

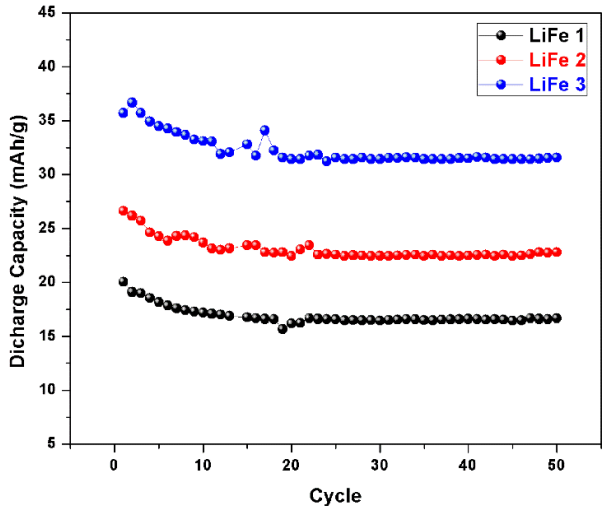

Figure 7.4: Discharge Capacity against Cycle number curves for LiFe 1, LiFe 2 and LiFe 3 cells

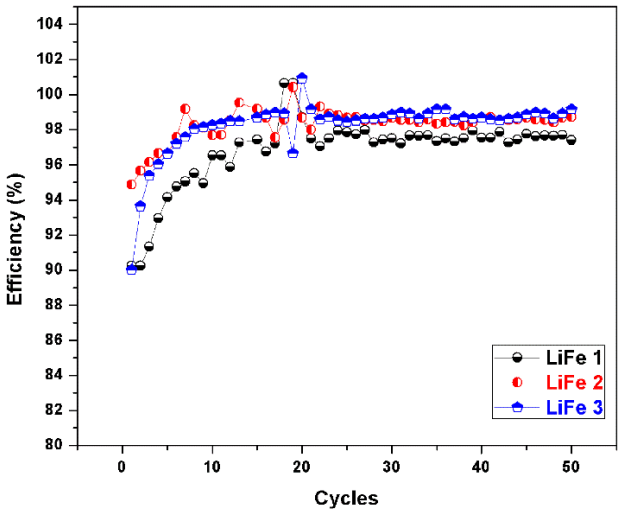

Figure 7.5: Charge Efficiency against Cycle number curves for LiFe 1, LiFe 2 and LiFe 3 cells

7.4 Conclusions

Lithiated PANI (LIPO 1, LIPO 2 and LIPO 3) - $LIFePO_4$ (9:1 ratio) composite electrode based Li-ion cells were assembled and detailed electrochemical characterization was carried out. The cells assembled with LIPO 3- $LiFePO_4$ composite as active electrode show dominant electrochemical characteristics

over LIPO1-$LiFePO_4$ and LIPO 2-$LiFePO_4$ based cells. The average voltage of these cells is around 3.3 V. The highest discharge capacity obtained is close to 40 mAh/g. All the three cells have an average coloumbic efficiency of 98 % and have got tremendous capacity retention over 50 cycles. The average power densities of the cells are not promising but moderate, with the capability of delivering a maximum power of 4 mWh/g. One of the highlights of the present work is the observation that with 10% addition of $LiFePO_4$ to lithiated PANI, it is possible to obtain impressive charge discharge curves resembling those of the cells based on transition metal oxide cathodes. The presence of higher concentration of lithiated PANI in LiFe composite cathode guarantees the possibility of constructional flexibility in the cell design. Both the components of the LiFe composite cathodes are eco-friendly materials. These aspects offer ample scope for realizing polymer-based Li-ion cells having promising performance characteristics with the added advantages of structural flexibility and environmental friendliness.

References

1. Ito, T.; Shirakawa, H.; Ikeda, S. *J. Polym. Sci. Polym. Chem.* **12**, 11 (1974).
2. Nigrey, P. J.; Maclnnes, D. Jr.; Nairns, D. P.; MacDiarmid, A. J. *J. Electrochem. Soc.* , **128(8)**, 1651 (1981).
3. Panero, S.; Prosperi, P.; Bonino, F.; Scrosati, B.; Corradini, A.; Mastragostino, M. *Electrochim. Acta*, **32(7)**, 1007 (1987).
4. Nishio, K.; Fujimoto, M.; Yoshinaga, N.; Furukawa, N.; Ando, O.; Ono, H.; Suzuki, T. *J. Power Sources*, **34**, 153 (1991).
5. Loufty, R. D.; Sharp, J. H. *J. Chem. Phys*. **71(3)**, 1211 (1979).
6. Jelle, B. P.; Hagen, G.; Nodland, S. *Electrochim. Acta*, **38(11)**, 1497 (1993).
7. Bao, Z.; Feng, Y.; Dodabalpu, A.; Raju, V. R.; Lovinger, A. *J. Chem. Mater*. **9(6)**, 1299 (1997).
8. Arbizzani, C.; Mastragostino, M.; Scrosati, B. Handbook of Organic Conductive Molecules and Polymers; Nalwa, H. S., Ed.;*John Wiley & Sons Ltd.,* Ch. 11 (1997).

9. Osaka, T.; Naoi, K.; Ogano, S. *J. Electrochem. Soc*., **135(5)**,1071 (1988)
10. Kwang Sun Ryu et all, *Bull. Korean Chem. Soc*., **23**, 8 (2002)
11. Genies, E. M.; Hany, P.; Santier, C. *J. Appl. Electrochem*.,**18(5)**, 751 (1988).
12. MacDiarmid, A. G.; Chiang, J. C.; Richter, A. R.; Epstein, A. *J.Syn. Met*.,**18(1-3)**, 285 (1987).
13. L. Lin, Y. Wen, O. Junke, Y. Guo and D. Xiao, *RSC Adv*., **3**, 14652–14660 (2013).

Chapter 8

Can Jahn -Teller effect be diluted by making composites of $LiMn_2O_4$ with Lithiated PANI? An Investigation

Abstract: Among the electrode materials with spinel structure, the lithium manganese oxide $LiMn_2O_4$ is the most attractive one due to its environmental safety and cost-effective nature. However, $LiMn_2O_4$ based materials suffer from a limited cycling stability. On cycling, the cubic spinel $LiMn_2O_4$ structure gets transformed slowly into a tetragonal spinel compound, leading to poor cyclability of the electrode. This drawback, its inability to sustain the charge capacity over the charge discharge cycles due to Jahn–Teller effect may be overcome by mixing with suitable Li-containing conducting polymer-based materials. Lithiated Polyaniline, a conducting polymer having outstanding structural and electrical properties with excellent stability can hence be considered as one of the promising materials to be used with $LiMn_2O_4$ for cathode preparation. Composites of lithiated PANI (LiPO) samples, synthesized as mentioned earlier with $LiMn_2O_4$ were prepared for different weight proportions of the component materials. The investigations carried out to analyze the effect of LIPO in the composite in reducing the inherent drawback of $LiMn_2O_4$ due to Jahn Teller effect are addressed in this chapter. By mixing LIPO (1- 3) and $LiMn_2O_4$ in 9:1 ratio by weight, composite samples with the following combinations, 9(LIPO1):1($LiMn_2O_4$), 9(LIPO2):1($LiMn_2O_4$), 9(LIPO3):1($LiMn_2O_4$) were synthesized. These samples as cathode

materials were used to assemble coin cells in an argon filled glove box using lithium metal foil as the anode and 1 M $LiPF_6$ in EC: DMC (1:1) as the electrolyte. Voltage sweep cyclic voltammetry and charge-discharge cycling tests were employed to characterize the electrochemical potentiality of the assembled cells. The cells are found to show a maximum discharge capacity of 52 mAh/g with 98 % columbic efficiency and have got tremendous cycling stability over 50 cycles. One of the highlights of these studies is the observation that the inherent Jahn Teller effect associated with $LiMn_2O_4$ cathode material can be eliminated to a great extent by making composites with LIPO samples.

8.1 Introduction

In the present work, with the objective of increasing the charge storage capacity of lithiated PANI based cells, and overcoming the Jahn–Teller effect in $LiMn_2O_4$ based cells LIPO- $LiMn_2O_4$ composite cathodes were synthesizes by mixing LIPO (1-3) and $LiMn_2O_4$ in 9:1 ratio by weight. The resultant products were used as the active material in cathode preparation. The cyclic voltammograms and charge-discharge characteristics of LiPO- $LiMn_2O_4$ composite cathode based coin cells were investigated and their capabilities compared.[1-11]

8.2 Materials and Methods

8.2.1 Synthesis

Lithium enriched PANI samples (LIPO 1, LIPO 2 and LIPO 3) for different concentrations of the dopant, *n*-Butyl lithium in hexanes (*n*-BuLi) were synthesized as explained in chapter 6. The resultant samples were mixed with $LiMn_2O_4$ in 9:1 proportion by weight. They were named respectively as LiMO 1, LiMO 2 and LiMO 3. LiPO- $LiMn_2O_4$ composites with 10 % conductive additives were coated on battery grade aluminum foils and dried for 3 hrs at 60 ^oC under dynamic vacuum. The electrochemical cells were assembled using LiMO powder as cathode, porous polyethylene film as separator, lithium metal as anode, and 1 M $LiPF_6$ dissolved in 1: 1 (volume ratio) mixture of EC and

DMC as electrolyte solution. Coin cells were assembled as described earlier in an argon filled glove box. To test the efficiency of LiPO in the LiMO samples, in reducing the adverse effects of Jahn Teller phenomenon, the LiMO composite samples were also synthesized in 8:2 ratio of LiPO and $LiMn_2O_4$ respectively.

8.2.2 Characterizations

X-ray diffraction (XRD) employing Rigaku Dmax C diffractometer (USA) with Cu Kα radiation of 1.54 Å was used for the structural characterization of the composite samples. The assembled cells were subjected to detailed electrochemical characterization using galvanostatic charge-discharge test and cyclic voltammetry as explained earlier.

8.3. Results and Discussions

8.3.1 X-Ray Diffraction Study

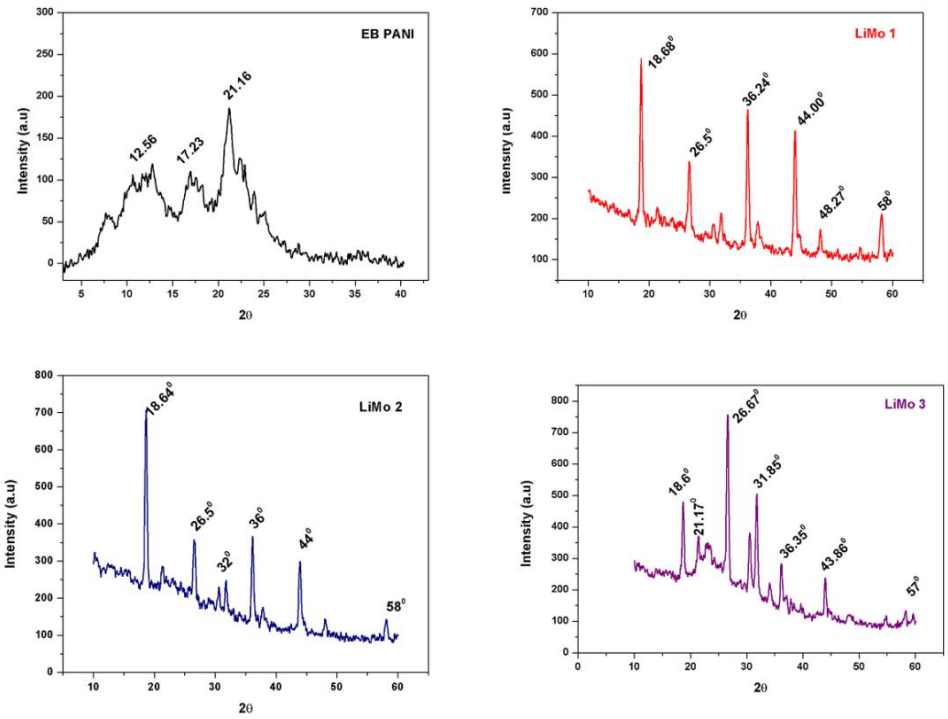

Figure 8.1: X-ray diffraction patterns of EB PANI, LiMO 1, LiMO 2 and LiMO 3

X-ray diffraction patterns of LIPO-$LiMn_2O_4$ composite samples are depicted in figure 8.1 and they consist of the characteristic peaks of both Lithiated PANI and $LiMn_2O_4$. Major peaks of $LiMn_2O_4$ are present at 20^0 (111), 36^0 (311), 45^0 (400) and 59^0 (511) in the XRD patterns. The presence of LiPO in the composite can also be confirmed from the XRD patterns.[12]

8.3.2 Cyclic voltammetry

The cyclic voltammograms of the cells in the range 2- 4 V are shown in figure 8.2 (Scan rate: 0.1 mV/s). The oxidation and reduction peaks of these cells occur within 2 to 4 V and show good reversibility. The upper broad peak at ~3.5 V is common to both LIPO and $LiMn_2O_4$ which corresponds to the oxidation of Li in lithiated PANI and that (de-intercalation of Li+ ion) of Li in $LiMn_2O_4$. The lower broad peak at ~2.32 V is also common to both LIPO and $LiMn_2O_4$ and corresponds to the reduction of Li^+ in these components of the composite systems.

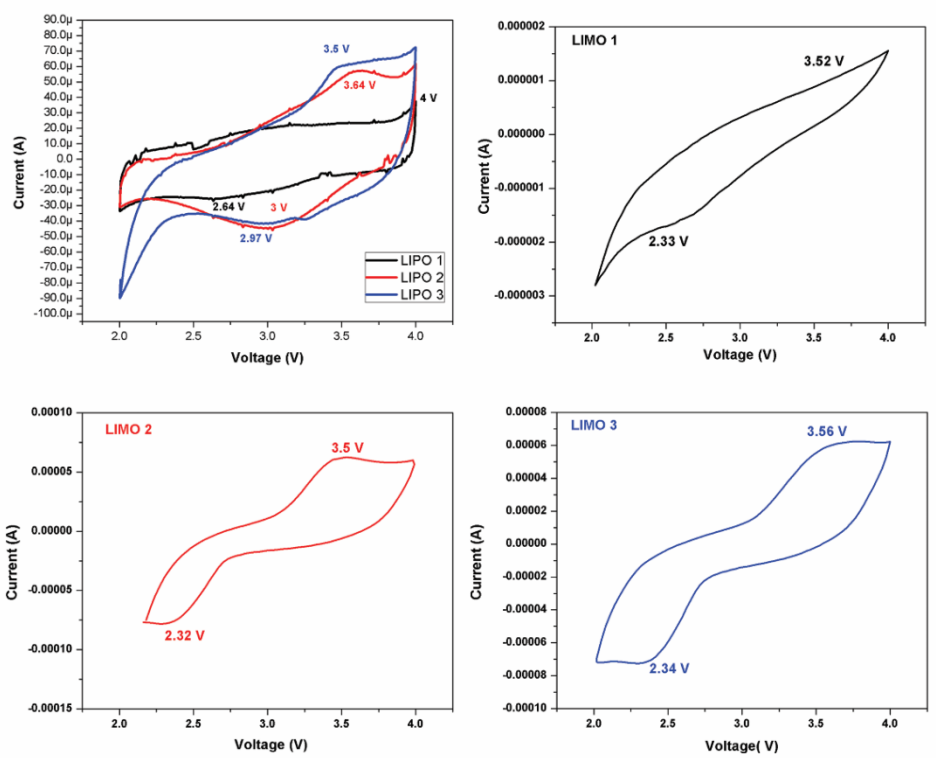

Figure 8.2: Cyclic voltommograms of LiPO, LiMO 1 , LiMO 2 and LiMO 3

8.3.3 Charge Discharge Characteristics

The discharge characteristics of LiMO 1, LiMO 2 and LiMO 3 based cells are shown in figure 8.3. These discharge curves also resemble those of transition metal oxide electrodes in conventional rechargeable lithium ion cells.

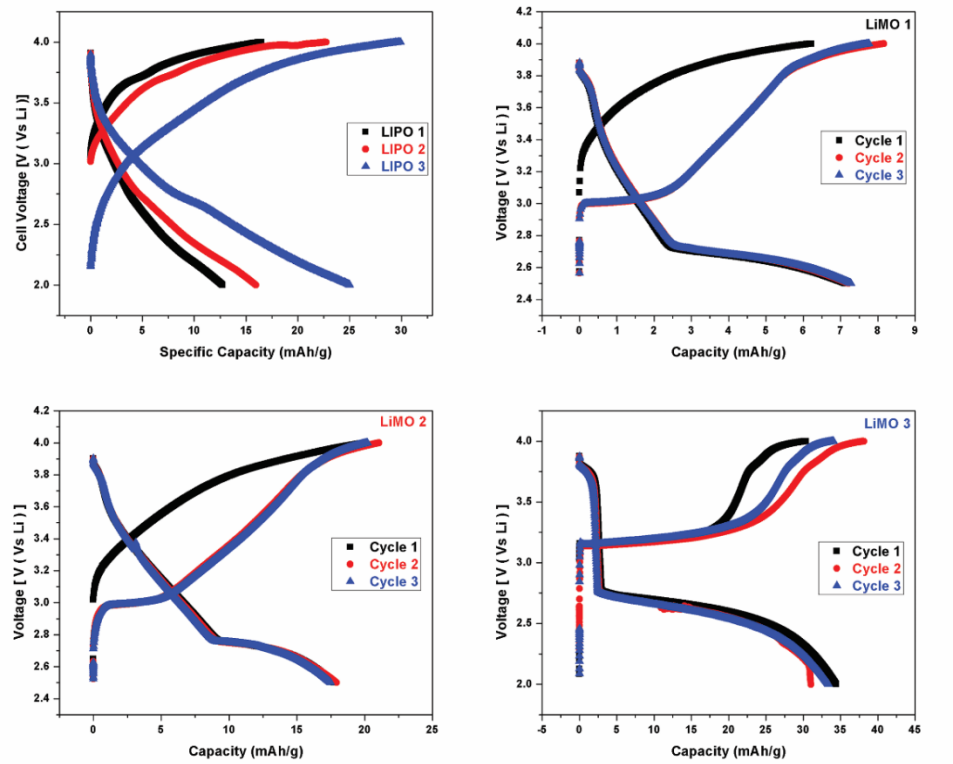

Figure 8.3: Charge-discharge curves of LiMO 1, LiMO 2 and LiMO 3 cells

The operating voltages of these cells can be approximated to 3.0 V in spite of the differences in the LIPO samples used. The plots of discharge capacity against number of cycles of LiMO (1-3) cells are shown in Figure 8.4. The highest discharge capacity is around 37 mAh/g for LiMO 3 based cell, followed by 20 mAh/g for LiMO 2 and 10 mAh/g for LiMO 1 based cells respectively. For all the cells assembled, the cycling stability over the first fifty cycles is quite remarkable and there is hardly any capacity loss (figure 8.5). This could be the result of the nullifying of the Jahn–Teller distortion in $LiMn_2O_4$ due to the presence of lithiated PANI in the cathode material. To confirm this further, LiMO composite was synthesized in the 8:2 ratio of LiPO and $LiMn_2O_4$ respectively. The cells assembled using this composite as the

cathode active material were subjected to detailed electrochemical evaluation. The charge discharge plot of this cell is shown in figure 8.6 and the efficiency plot is shown in figure 8.7. It is observed that, for this cell, the capacity obtained is around 52 mAh/g. This increase in specific capacity is definitely due the increase in concentration of $LiMn_2O_4$ in the LiMO composite.

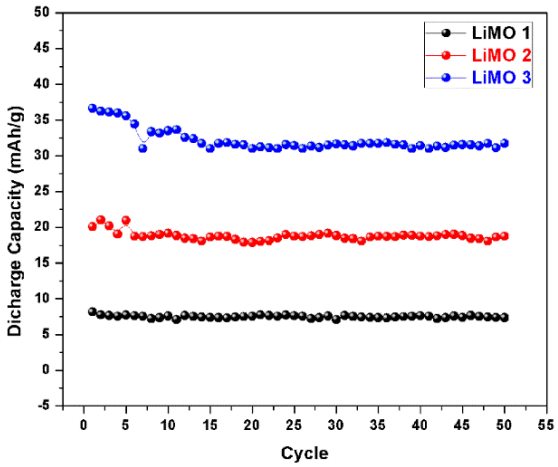

Figure 8.4: Discharge Capacity against Cycle number curves of LiMO 1, LiMO 2 and LiMO 3 cells

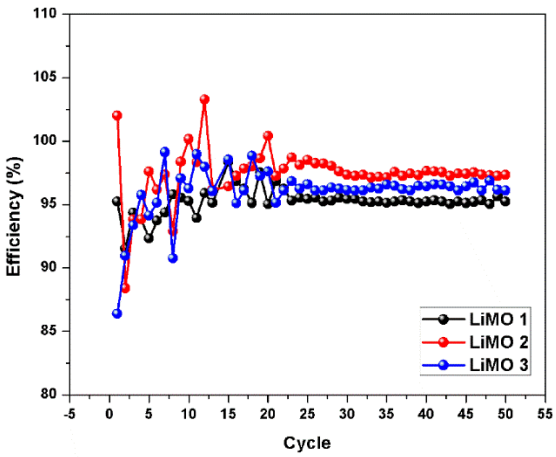

Figure 8.5: Charge Efficiency against Cycle number curves of LiMO 1, LiMO 2 and LiMO 3 cells

The specific capacity of lithiated-PANI based cells, observed in the present work is of the order of 25 mAh/g. On making the composite with $LiMn_2O_4$

(9:1 ratio) the specific capacity of the cells gets increased by 12 mAh/g to reach 37 mAh/g which is sustained during the 50 charge discharge cycles. The contribution of $LiMn_2O_4$ towards enhancing the specific capacity is well evident. To confirm this further, higher $LiMn_2O_4$ loading percentage was attempted (8:2 ratio) and the outcome is supporting the previous data. The specific capacity gets further enhanced to 52 mAh/g initially which stabilizes at 48mAh/g up to the 50^{th} cycle. The cell efficiency is found to stabilize at 98 %.

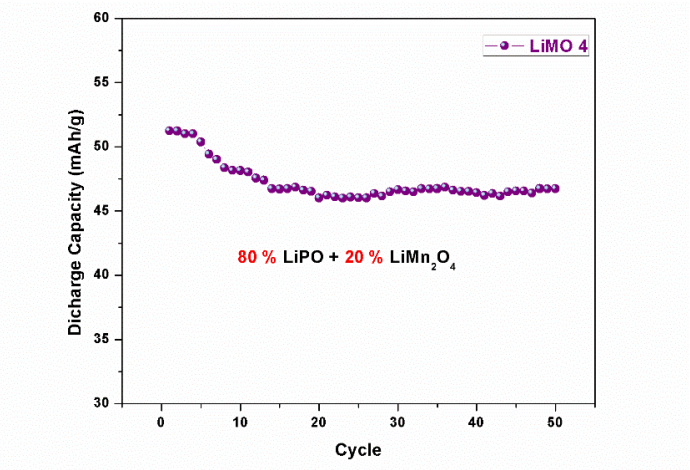

Figure 8.6: Graph showing the Discharge Capacity against Cycle number for the cells having higher $LiMn_2O_4$ loading

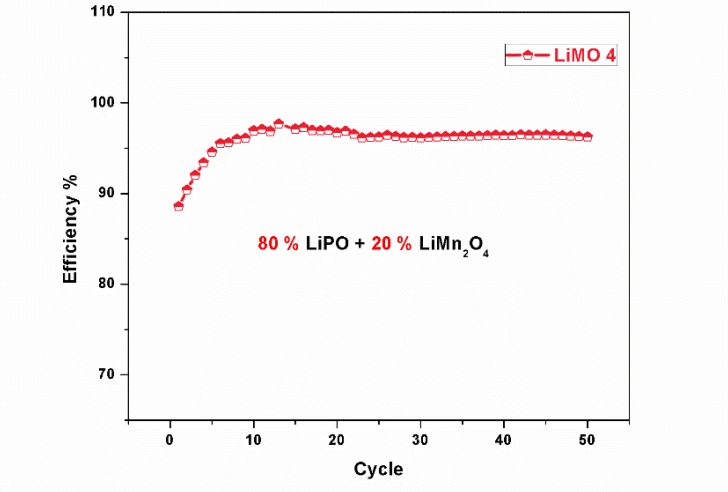

Figure 8.7: Graph showing the charge efficiency against cycle number for the cells having higher $LIMn_2O_4$ loading

8.4 Conclusions

Lithiated PANI (LIPO 1, LIPO 2 and LIPO 3)-$LiMn_2O_4$ (9:1 ratio) composite electrodes based Li-ion cells were assembled and detailed electrochemical characterization was carried out. The cells assembled with LIPO 3- $LiMn_2O_4$ composite as active electrode show dominant electrochemical characteristics over LIPO 2-$LiMn_2O_4$ and LIPO 1-$LiMn_2O_4$ based cells. The average voltage of these cells is almost 3.0 V. The highest discharge capacity is around 37 mAh/g. LiMO 1, LiMO 2 and LiMO 3 based cells have an average columbic efficiency of 98 % and have got tremendous capacity retention over 50 cycles. Unlike pure $LiMn_2O_4$ based cells with poor cyclability due to Jahn–Teller distortion, LiMO cells have been found to overcome this distortion effect and show healthy cycling stability, due to the presence of lithiated PANI in the cathode active material. To confirm this further, LiMO composite was synthesized in the 8:2 ratio of LiPO and $LiMn_2O_4$ respectively. The electrochemical performance of the cells assembled using this composite as the cathode active material was analysed. It is observed that, for this cell, the capacity gets enhanced to 52 mAh/g and this capacity enhancement is a consequence of the increase in the concentration of $LiMn_2O_4$ in the LiMO composite. The capacity is observed to stabilize at 48 mAh/g from the 10^{th} to the 50^{th} cycle. The present work highlights a novel but simple approach to nullify the Jahn-Teller distortion in $LiMn_2O_4$ by properly mixing it with Lithiated PANI to function as the cathode. Even though the maximum concentration of $LiMn_2O_4$ in the LiMO composite samples is 20% the results of the present investigation suggest that with increase in $LiMn_2O_4$ concentration, the capacity will further be enhanced and will be stabilized at an appropriate value and retained up to longer charge-discharge cycles.

References

1. Ito, T.; Shirakawa, H.; Ikeda, S. *J. Polym. Sci. Polym. Chem.* **12**, 11 (1974).
2. Lilong Xiong et al, *J. Mater. Chem.*, **22**, 24563-24568 (2012).
3. A. Blyr et al, *J. Electrochem. Soc*. **145**, 1, 194-209 (1998).

4. R.J. Gummow, D.C. Liles, M.M. Thackeray, *Mater. Res. Bull*. **28**, 1249 (1993).
5. R.J. Gummow, M.M. Thackeray, *J. Electrochem. Soc.* **141**, 1178 (1994).
6. Bao, Z.; Feng, Y.; Dodabalpu, A.; Raju, V. R.; Lovinger, A., *J. Chem. Mater*, **9(6)**, 1299 (1997).
7. Arbizzani, C.; Mastragostino, M.; Scrosati, B. Handbook of Organic Conductive Molecules and Polymers; Nalwa, H. S., *Ed*.;*John Wiley & Sons Ltd*. Ch. 11 (1997).
8. Osaka, T.; Naoi, K.; Ogano, S., *J. Electrochem. Soc*., **135(5)**, 1071 (1988).
9. Kwang Sun Ryu et. all, *Bull. Korean Chem. Soc*. **23**, 8 (2002).
10. Genies, E. M.; Hany, P.; Santier, C. J. Appl. *Electrochem*, **18(5)**, 751(1988).
11. MacDiarmid, A. G.; Chiang, J. C.; Richter, A. R.; Epstein, A. *J.Syn. Met.* **18(1-3),** 285 (1987).
12. R. M. Tomy, K. M. A. Kumar, P. B. Anand and S. Jayalekshmi, *J. Phys. Chem. Solids*, **72**, 1251–1255 (2011).

Chapter 9

Lithium doped PEO-a prospective solid electrolyte with high ionic conductivity, developed using *n*-Butyl lithium in hexanes as dopant

Abstract: The present work is an effort to study the effects of Li doping on the structural and transport properties of the solid polymer electrolyte, poly-ethelene oxide (PEO) (Molecular weight: 200,000). Li doped PEO was synthesized by treating PEO with *n*-Butyllithium in hexane for different doping concentrations. It is seen that, the crystallinity of the doped PEO decreases on increasing the Li doping concentration and XRD and FTIR studies support this observation. FESEM images give better details of surface morphology of doped PEO samples. The TGA curves of PEO and Li doped PEO samples reveal the weight loss region and it is observed that the weight loss process of the solid polymer electrolyte is gradual rather than abrupt, contrary to the case of liquid electrolytes. The purity and the electrochemical stability of the samples were established by cyclic voltammetry studies. Impedance measurements were carried out to estimate the ionic conductivity of Li doped PEO samples. The present value of ionic conductivity observed at room temperature in Li-doped PEO is about five orders higher than that of pure PEO and is quite close to that of liquid electrolytes. It is inferred that, ionic conductivity of the sample is increasing on increasing the Li doping concentration due to enhanced charge carrier density and flexibility of the doped sample structure. The ionic mobility and ionic transport are significantly improved by the less crystallinity and higher

flexibility of the Li doped PEO samples which in turn are responsible for the enhanced ionic conductivity observed**.**

9.1 Introduction

Rechargeable lithium ion cells find a wide variety of applications ranging from consumer electronics to very large scale energy storage systems.[1, 2, and 3] The performance of a battery depends significantly on the characteristics of its integral parts, the cathode, anode and the electrolyte, which in turn depend on the materials used. Many research groups are involved in developing new electrode and electrolyte materials to enhance the overall performance efficiency of the battery. One of the challenges is to develop new electrolyte materials with high ionic conductivity and excellent thermal and hydrolytic stability.[4, 5, and 6]

Currently explored electrolytes for Li ion battery applications are in liquid or gel form, which makes well-defined sealing essential. The use of solid electrolytes eliminates the need for containment of liquid electrolytes, which will certainly simplify the cell design and improve the safety and durability. Inorganic ceramics and organic polymers constitute the two general classes of materials used as solid electrolytes. Main difference between these classes is related to the mechanical properties. Ceramics based electrolytes are suitable for rigid battery design due to the high elastic moduli.[7-10] Conversely, the low elastic moduli of polymers are useful for flexible battery designs. Polymers can be easily processed, which reduces the fabrication costs.[11-14] However, polymer based electrolytes are not suitable for high temperature operation and they fail under aggressive environments where, ceramic based electrolytes are more reliable.[7, 8, 9 and 15]

The other advantages of polymer electrolytes include dimensional stability, safety and the ability to prevent lithium dendrite formation. In some polymer electrolytes, lithium salts are solvated by the polymer chains, while in others a solvent is added to form a polymer gel. In general, the former is mechanically stronger, so that a free-standing film can be formed. Polymer gels, on the other hand, require mechanical support from other battery components, but typically

have higher ionic conductivities. The polymer most commonly used for lithium-ion conducting electrolytes is poly-(ethylene oxide) (PEO).[16] PEO is effective in solvating lithium salts, which are added to provide the lithium-ion conduction. The good ionic conductivity of PEO is due to ionic transport in the amorphous region, and hence the conductivity decreases with increasing the degree of crystallization. [12, 13, and 14]

The ionic conducting properties of PEO, doped with different salts like lithium perchlorate ($LiClO_4$), lithium bis(oxalato)borate ($LiB(C_2O_4)_2$) etc. are discussed in literature.[1] But the capability of *n*-Butyllitium(*n*-BuLi) which is a strong base and a comparatively much cheaper dopant material, in enhancing the ionic conductivity of PEO has not been explored so far. The present work is hence directed to investigate in detail the effects of *n*-BuLi doping on the structural and transport properties of PEO. It is interesting to see that, the crystallinity of PEO decreases with increasing the dopant concentration while the ionic conductivity is showing an increasing trend. The room temperature ionic conductivity obtained for the *n*-BuLi doped PEO is comparable and even higher than the reported ionic conductivity of PEO, doped with other Li salts. It is expected that further optimization of the doping process will result in much enhanced ionic conductivity for *n*-BuLi doped PEO.

9.2 Materials and methods

9.2.1 Synthesis

Precursors (1.6 M *n*-Butyllithium solution in hexane [$CH_3 (CH_2)_3Li$] (*n*-BuLi) and Poly (ethylene oxide) [(-CH_2CH_2O-) n], powder (PEO) of average molecular weight 200,000 were purchased from Sigma Aldrich with premium purity. 1 g of PEO was taken in a conical flask and 5 ml of *n*-BuLi was added drop wise using a glass syringe and stirred at a rate of 500 rpm using a magnetic stirrer (IKA) till the solvent hexane completely gets evaporated. The whole process was carried out in an argon (99.999 % pure) filled glove box (MTI Corporation, USA). The procedure was repeated for two other concentrations, 10 ml and 15 ml of *n*-BuLi. The powder samples so obtained were found to be free of the solvent hexane and quite stable in air and were again dried in a vacuum oven for 2 hours to ensure complete evaporation of

the solvent hexane. It is observed that, upon Li doping the colour of PEO changes from white to pale yellow. The *n*-BuLi doped PEO samples are found to be quite stable in air for a period of six months and even more. Pure PEO and the three doped samples were named as PEO, Li-PEO 1, Li-PEO 2 and Li-PEO 3 respectively and taken for various types of characterization.

9.2.1 Characterizations

X-ray diffraction technique employing the Rigaku Dmax C diffractometer with Cu Kα radiation of 1.54 Å was used for structural characterization of the samples. The JASCO 4100 model FTIR spectrophotometer was used to get the IR spectrum of the samples in the wavenumber range 450–4000 cm^{-1}. Microstructure imaging was done by Field Emission Scanning Electron Microscope (FESEM-Carl Zeiss, Supra 40 VP). Perkin Elmer, Diamond TG/DTA was employed to study the weight loss of the samples with temperature in nitrogen atmosphere. The cyclic voltammetry (CV) characterization of the samples was done using Biologic SP300. The powder samples were pelletised using a hydraulic pellet press at 5 tons pressure. Ionic conductivity studies were done on these pellets, employing Agilent E4980A impedance analyzer (20Hz-2MHz) and Agilent 16451B dielectric material test fixture.

9.3 Results and Discussions

9.3.1 X-Ray Diffraction Study

The X-ray diffraction patterns of the four samples are shown in figure 9.1. When PEO is doped with Li- ions, along with the normal PEO diffraction peaks at 18.16^0 and 22.24^0 [17], some additional diffraction peaks around 25^0, 26^0, 28^0, 31^0, 40^0, 44^0, 46^0 are also observed. These peaks correspond to the formation of additional polymer chain interlinked planes due to the presence of the dopant. Since the crystalline material is formed at the expense of the amorphous phase, the scattering intensity of the amorphous phase will be proportionately reduced on crystallization and vice versa. On reviewing the XRD spectrum of the samples, it is evident that, on increasing the *n*-BuLi concentration, the signature peaks of PEO are getting diminished in intensity

and on reaching the maximum doping concentration, the characteristic peaks of PEO are hardly seen. In the doped samples, the various diffraction peaks correspond to the short range ordering of polymer chains formed due to the influence of the dopant. Since these diffraction peaks originate from the planes which are formed at random, the phase analysis and indexing of these peaks is rather a cumbersome work.

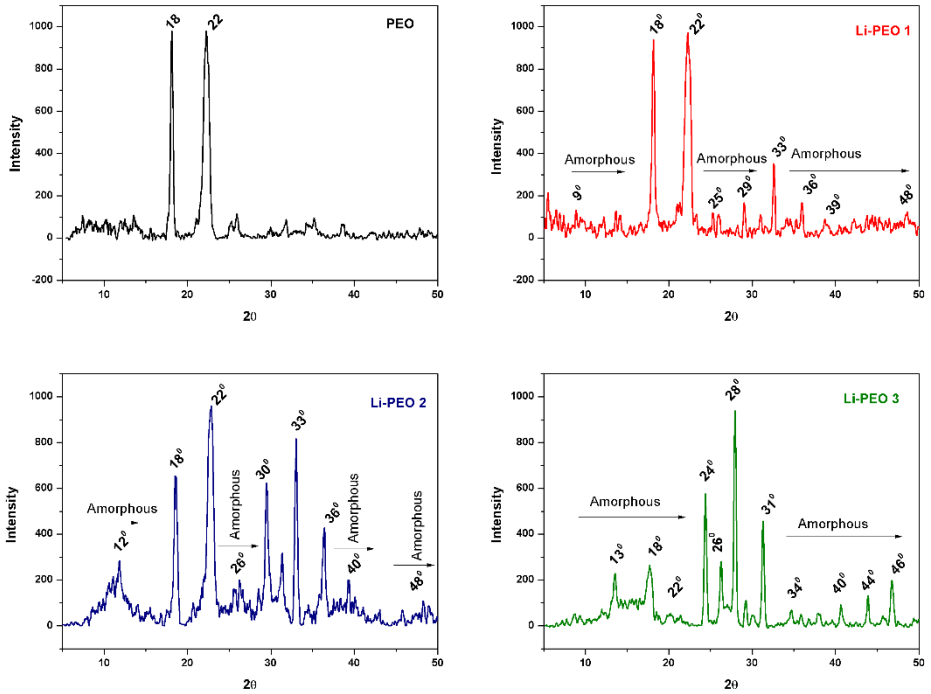

Figure 9.1: X-Ray Diffraction patterns of Pure PEO, Li-PEO 1, Li-PEO 2 and Li-PEO 3

The percentage crystallinity is calculated from the diffraction pattern of each sample which corresponds to the ratio of the total area under the crystalline peaks to the total area under the crystalline and amorphous peaks. The percentage crystallinity, Pc of the samples is deduced using the relation shown by equation 9.1.

$$P_c = \frac{A_c}{A_c + A_a} \times 100 \qquad (9.1)$$

where A_c is the area under the crystalline peaks, A_a the amorphous peak area and $A_c + A_a$, the total area including crystalline and amorphous peak

regions.[18,19] The area under the crystalline and amorphous peak regions was calculated using the multiple peak fit program in Origin 9. It is very interesting to note that on increasing the dopant concentration, the crystallinity of PEO shows a decreasing trend. The calculated parameters are tabulated in Table.1 (Significant figures after the decimal point are limited to two during the calculations).

Table. 1: Percentage crystallinity data

Sample Name	Total Area under the peaks (a.u)	Area under the Crystalline region (a.u)	% of Crystalinity
PEO	1089.03	1040.16	95.51 %
Li-PEO 1	1372.04	1043.26	76.04 %
Li-PEO 2	3344.14	1731.69	51.78 %
Li-PEO 3	1483.11	685.21	46.20 %

9.3.2 FTIR Studies

The FTIR transmittance spectra of the four samples are depicted in figure 9.2. The peak at 865 cm^{-1} corresponds to the strong anti-symmetric stretching vibration of CH_2 group which is perpendicular to the PEO molecular axis. Either the symmetric rocking vibration of CH_2 group or the antisymmetric stretching vibration of the COC group gives rise to the peak at 956 cm^{-1}. The peak at 1110 cm^{-1} is characteristic of the symmetric stretching vibration of the COC group and the strong one at 1430 cm^{-1} can be related to the bending vibration of the (CH_2-CH_2) group.[20, 21] All these peaks match quite well with the standard IR spectrum of PEO. It is amazing that on increasing the Li dopant concentration, the intensity of these characteristic peaks gets intensified, indicating that the intensity of the characteristic frequencies get improved much, which means that the system becomes more flexible and the damping of the vibrational modes due to rigid crystalline structure gets decreased. It is evident from the IR spectrum that on enhancing the Li doping concentration, the intensity of the characteristic peaks gets enhanced by a maximum amount of 30%. This is a rich evidence for the decreasing crystalline nature of PEO on doping with *n*-BuLi.

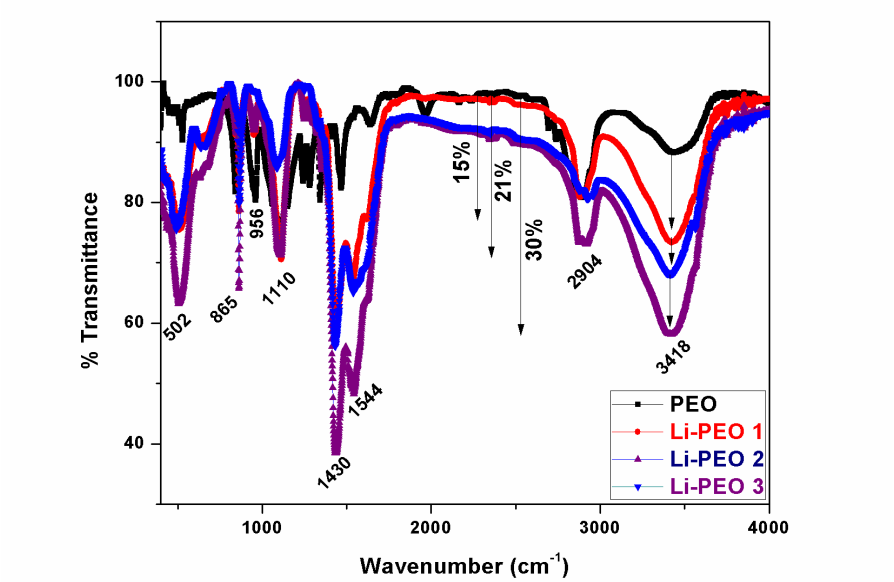

Figure 9.2: The FTIR transmittance spectra of PEO, Li-PEO 1, Li-PEO 2 and Li-PEO 3.

9.3.3 Thermo-gravimetric Analysis

The TGA curves of PEO and Li doped PEO samples are shown in Figure 9.3. The weight loss of the samples with temperature was studied under nitrogen atmosphere. For the pure PEO sample, there is a plateau extending up to 315^{o}C indicating good thermal stability of the sample with apparently no weight loss. For the Li doped PEO samples, there are two weight loss regions. The first region lies at the temperature range of 60^{o}C to 115^{o}C and indicates the decomposition of the solvent residues present in the samples and the second one is above 350 ^{0}C, corresponding to the decomposition of the PEO-dopant membrane. It can be clearly seen that all the samples exhibit only marginal weight loss until the temperature is around 150^{o}C. It can also be inferred that the PEO-*n*-BuLi is stable up to 350^{o}C before decomposition. The decomposition temperature observed in the present work for the Li- doped PEO electrolyte is considerably higher than that of the liquid/gel electrolytes currently employed in lithium secondary batteries.[22] The results of weight-loss ratios for all the samples between 50 and 800^{o}C are summarized in Table 9.2. For pure PEO, the data is given only upto 400^{0}C, since the weight loss for PEO is almost hundred percentage, on reaching 400^{0}C.

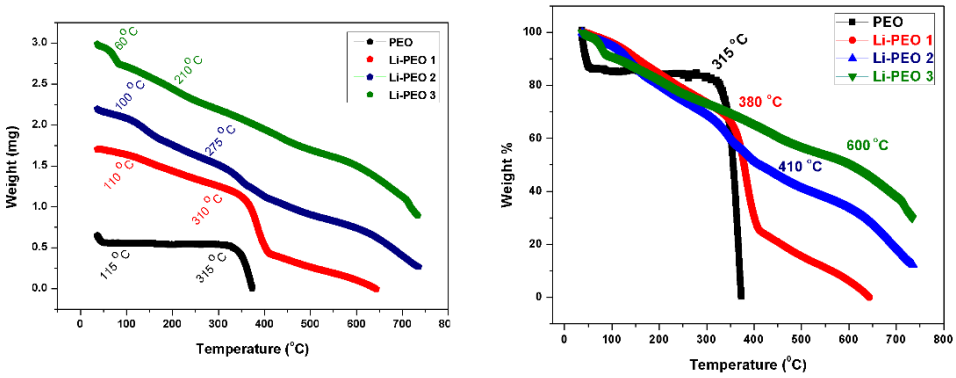

Figure 9.3: The TGA curves of PEO, Li-PEO 1, Li-PEO 2 and Li-PEO 3

Table 9.2: Initial weight loss temperatures with percentage of weight loss for PEO, Li-PEO 1, Li-PEO 2 and Li-PEO 3

Sample Name	Initial Weight loss Temperature (^{o}C)	Weight Loss
PEO	---	Nil
LIPEO 1	110	4.8 %
LIPEO 2	100	5.2 %
LIPEO 3	60	1.8 %

Rate of weight loss is more for Li-PEO 2 and Li-PEO 3 samples which may be due to lesser crystallinity of these samples compared to the other two. The weight loss process of the solid polymer electrolytes is gradual rather than abrupt, contrary to the case for liquid electrolytes [23]. For this reason, solid polymer electrolytes are more thermally stable than liquid electrolytes for applications in lithium ion batteries.[3]

9.3.4 FE-SEM Microstructure Analysis

The FESEM images are shown in figure 9.4. It is quite evident that the ordered structure of PEO is getting diluted on the addition of Li salt in to its matrix. On doping with *n*-BuLi the Li-ions get intercalated into the PEO structure and displace the polymer chains, leading to a decrease in

crystallinity. Sheet like long range ordered morphology is transformed into randomly short ordered structures which is clear from the 200 nm scaled image. This again supports the reduction in crystallinity of PEO upon Li doping which in turn improves the ionic conductivity of the whole composite structure.

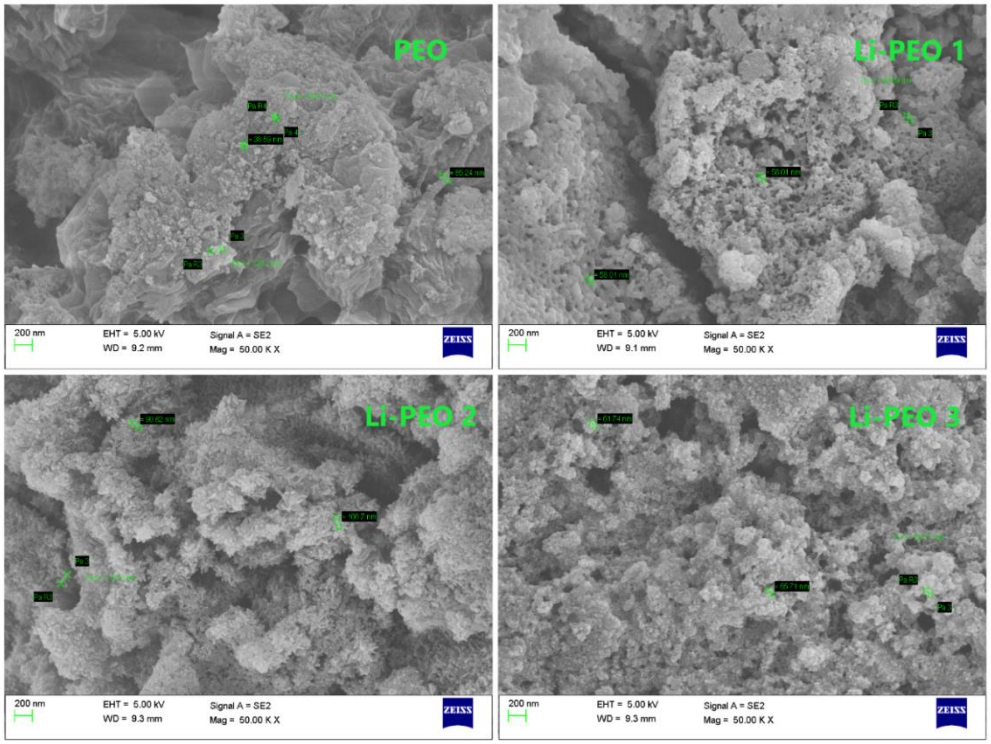

Figure 9.4: The FESEM images of PEO, Li-PEO 1, Li-PEO 2, and Li-PEO 3

9.3.5 Cyclic Voltammetry

Small current voltammetric responses of PEO and Li doped PEO samples were studied using Biologic SP300 unit for five cycles (Scan rate: 0.1 mV/s). All the samples show repeatability and electrochemical stability and the CV curves are shown in figure 9.5. Although oxidation and reduction peaks can be recognized, it is apparent that they are very misty and that the redox process takes place only to a marginal extent. A small peak during oxidation process (the anodic current) can be observed at 3.5 V, and this may be due to the oxidation of the polymer host PEO, which becomes more observable as the Li-doping concentration increases.

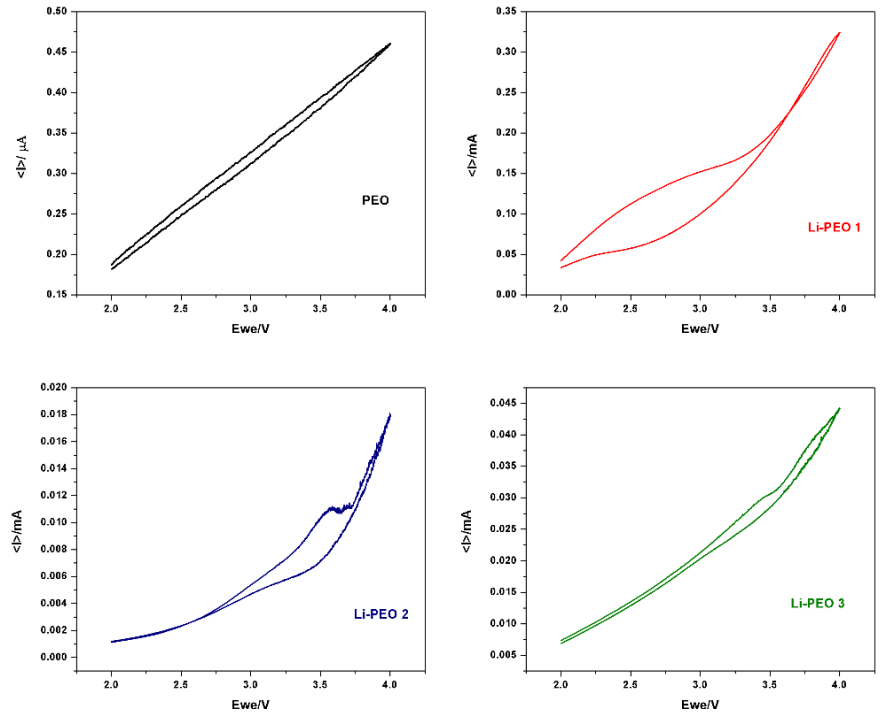

Figure 9.5: The Cyclic Voltammograms of PEO, Li-PEO 1, Li-PEO 2, and Li-PEO 3

The purity as well as the electrochemical stability of the samples can be established by the reproducible and clear nature of the cyclic voltammetry curves.

9.3.6 Impedance Analysis

The room temperature ionic conductivity of the four samples in the form of pressed pellets was evaluated using the relation shown in equation 9. 2

$$\sigma_{ac} = 2\pi\upsilon\varepsilon_0\varepsilon_r \tan\delta \qquad (9.2)$$

where $2\pi\upsilon$ is the angular frequency of the ac source, ε_0 is the dielectric permittivity of free space, ε_r the dielectric constant of the material and tan δ , the tangent loss factor.[24,25] The experiment was done in the frequency range 20 Hz to 2 MHz. The variation of ionic conductivity of pristine PEO and Li-

doped PEO samples with the frequency of applied ac source is shown by the logarithmic curve depicted in figure 9.6.

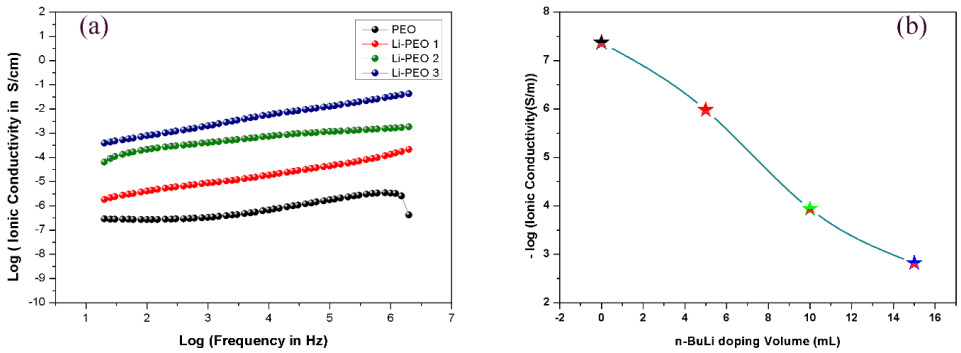

Figure 9.6: (a) Logarithmic plot for the variation of ionic conductivity of PEO and Li-doped PEO with frequency (b) The variation of ionic conductivity of PEO with *n*-BuLi doping concentration

It can be seen that, for a dielectric material, tan δ increases on increasing the frequency, then passes through a maximum value and thereafter decreases. For pure PEO, this behavior is reflected in the ionic conductivity (in SI units) curve shown in figure 9.7. This can be attributed to the variation of dielectric constant with frequency. At low frequency range, the dipoles in PEO orient in the direction of the applied field. As the frequency of the applied electric field increases, the dipoles are unable to follow the field variations to get oriented in the direction of the field, which in turn increases the loss factor and consequently decreases the dielectric constant of the medium. Such a behavior is however not observed in Li-doped PEO samples for the current frequency scan range. It can be inferred that Li doping in PEO results in the creation of mobile Li^+ ions which are solely responsible for the improvement in ionic conductivity of the doped PEO samples. With the increase in the dopant concentration in the PEO matrix, the Li salt dissociation increases which results in the reordering of the PEO matrix with lesser crystallinity and higher flexibility. The counter ions produced, being much massive compared to the Li^+ ions have only negligible contribution towards the ionic conductivity. The maximum room temperature ionic conductivity for pure PEO observed in the present work is around 4.22×10^{-8} S/cm. With Li doping there is significant enhancement in ionic conductivity and for maximum Li

doping the ionic conductivity gets enhanced to 1.53×10^{-3} S/cm which is about five orders higher than that of pure PEO. The ionic conductivity data is summarized in table 9.3.

Table 9.3: Ionic conductivity data

Sample	Li-Dopant Used (mL)	Maximum Ionic Conductivity at room temperature (S/cm)
PEO	Nil	4.22×10^{-8}
Li- PEO 1	5	1.05×10^{-6}
Li-PEO 2	10	1.15×10^{-4}
Li-PEO 3	15	1.53×10^{-3}

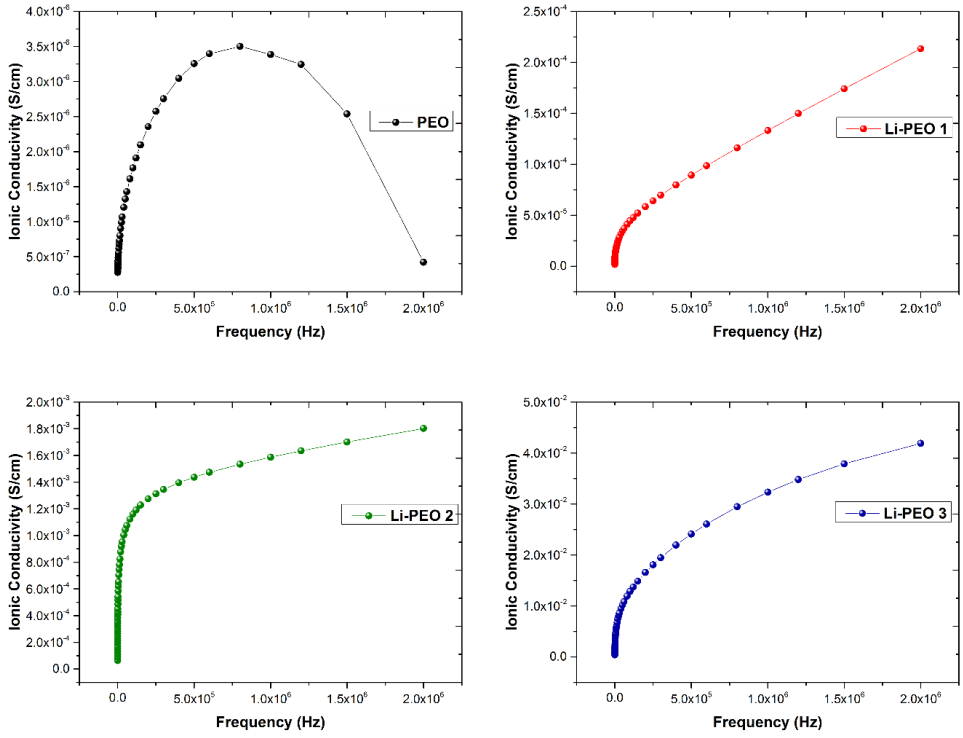

Figure 9.7: Plots showing the behavior of variation of ionic conductivity of pristine and Li doped PEO with frequency

For Li doped PEO samples using other dopants such as lithium bis(oxalato)borate ($LiB(C_2O_4)_2$) (LiBOB)) and $LiClO_4$, the room temperature ionic conductivity obtained is of the order of 10^{-5} S/cm [26,27,28,29,30] which is

much less than the value obtained in the present work using *n*-BuLi as the dopant. Another advantage of using *n*-BuLi is that it is a much cheaper dopant material compared to the conventional dopants like LiBOB and $LiClO_4$. The increase in the ionic conductivity observed for the Li-doped PEO samples in the present work can be ascribed to the increase in the number density of mobile Li^+ ions with improved Li ion diffusion. The Li doping in PEO brings about lesser crystallinity and higher flexibility for the composite material structure which in turn is responsible for the improved ionic mobility and transport and enhanced ionic conductivity.

9.4 Conclusions

In the present work, a basic study has been carried out on the structural and transport properties of undoped and *n*-Butyllithium doped PEO samples. The dopant concentration is varied to study the dopant effect on the structural and ionic conducting properties. From the X-ray diffraction and FTIR studies, it is inferred that the crystallinity of PEO samples decreases on increasing the dopant concentration. FESEM images show that sheet like long range ordered morphology of PEO is transformed into randomly short ordered structures upon Li doping. The Li-ions, in the doped PEO samples, get intercalated into the PEO structure and displace the polymer chains, leading to a decrease in crystallinity. From the thermal studies it can be inferred that the Li-doped PEO samples are thermally stable up to 150 ^{0}C which is quite significant when designing Li-ion cells for high temperature applications. The purity and electrochemical stability of the Li doped PEO samples have been established on the basis of the CV studies. The ionic conductivity studies reveal quantitatively that, the ion transporting properties get improved on increasing the Li-dopant concentration. It is observed that by increasing the dopant concentration, it is possible to decrease the crystallinity, enhance the flexibility and improve the ionic permeability considerably. In the present work, the improvement in ionic conductivity with *n*-BuLi doping is remarkable and the results have opened up novel means to correlate the polymer crystallinity with the dopant concentration and ionic transport properties. The maximum ionic conductivity observed in the present work of the order of 1.53×10^{-3} S/cm for Li doped PEO solid electrolyte is quite close to that of liquid electrolytes and

hence offers high prospects of developing all solid state Li-ion cells with *n*-BuLi doped PEO as the electrolyte. It is also anticipated that the ionic conductivity of *n*-BuLi- PEO system can further be enhanced by optimizing the doping concentration.

References

1. B. Scrosati., Application of Electroactive Polymers, *Chapman and Hall*, London (1993).
2. F.M. Gray., Polymer Electrolytes, *The Royal Society of Chemistry*, HN, Letchworth (1997).
3. Suriani Ibrahim, Mohd Rafie Johan, Int. *J. Electrochem. Sci*., **7**, 2596 – 2615 (2012).
4. Jeffrey W. Fergus, Review, J. Power Sources., **195,** 4554–4569 (2010).
5. B. Scrosati, J. Garche, *J. Power Sources*., **195,** 2419–2430 (2010).
6. J.B. Goodenough, Y. Kim, Chem. Mater., **22 (3)** 587–603 (2010).
7. V. Thangadurai, W. Weppner, *Ionics*, **12**, 81–92 (2006).
8. V. Thangadurai, W. Weppner, *Ionics*, **8**, 281–292 (2002).
9. P. Knauth, *Solid State Ionics*, **180**, 911–916 (2009).
10. N.A. Anurova, V.A. Blatov, G.D. Ilyushin, O.A. Blatova, A.K. Ivanov-Schitz, L.N. Dem'yanets, *Solid State Ionics*, **179**, 2248–2254 (2008).
11. A.K. Ivanov-Shitz, *Crystall. Rep*., **52 (2)** ,302–315 (2007).
12. F. Gray, M. Armand, in: T. Osaka, M. Datta (Eds.), Energy Storage Systems for Electronics, Gordon and Breach Sci. Publ., Amsterdam, The Netherlands pp. 351–406 (2000).
13. S. Ahmad, *Ionics*, **15**, 309–321 (2009).
14. J.Y. Song, Y.Y. Wang, C.C. Wan, *J. Power Sources*, **77**, 183–197 (1999).
15. A.M. Stephan, K.S. Nahm, *Polymer*, **47**, 5952–5964 (2006).
16. G.B. Appetecchi, M. Montanino, A. Balducci, F.L. Simon, M. Winterb, S. Passerini, *J. Power Sources*., **192** ,599 (2009).

17. Riclzard A. Vuia, S. Visudeevan, Wlodzimierz Krawiec, Lawrence G. Scunlon, and Emmanuel P. Giannelis, *A d. Mater*., **7,** 2 (1995).
18. Sreekanth J Varma et al. *Polym. Int*., **61** 743–748 (2012).
19. Sinha S, Bhadra S and Khastgir D, *J Appl Polym Sci.*, **112,** 3135–3140 (2009).
20. V. M. Da Costa, T. G. Fiske, and L. B. Coleman, Farinfrared reflection, *J. Chem. Phys.*, **101** ,2746 (1994).
21. T. Yoshihara, H. Tadokoro, and S. Murahashi *J. Chern. Phys*., **41** 2902 (1964).
22. Y. Kong, J.N. Hay, *Polymer*., **43** 3873 (2002).
23. Y. S. Lee, W.K. Lee, S.G. Cho, II Kim, C.S. Ha., *J. Anal. Appl. Pyrolysis*., **78** 85 (2007).
24. Dillip K. Pradhan, R. N. P. Choudhary, B. K. Samantaray, Int. *J. Electrochem. Sci*., **3,** 597 – 608 (2008).
25. Suriani Ibrahim et al. ,*Solid State Commun*.,**152** 426–434 (2012).
26. N. Li, L. Wang, X. He, C. Wan, C. Jiang, *Ionics*, **14**, 463–467 (2008).
27. S.Y. An, I.C. Jeong, M.-S. Won, E.D. Jeong, Y.-B. Shim, *J. Appl. Electrochem*., **39**,1573–1578 (2009).
28. G. Derrien, J. Hassoun, S. Sacchetti, S. Panero, *Solid State Ionics*, **180,** 1267–1271 (2009).
29. C. Shen, J. Wang, Z. Tang, H. Wang, H. Lian, J. Zhang, C.-N. Cao, *Electrochim.Acta,* **54** 3490–3494 (2009).
30. H.H. Sumathipala, J. Hassoun, S. Panero, B. Scrosati, *Ionics*, **13**, 281–286 (2007).

Chapter 10

Summary and Future Prospects

10.1 Summary and Conclusions

The work presented in the thesis is focussed mainly on exploring the versatile roles of polyaniline (PANI), one of the highly sought after conducting polymers, in enriching the research arenas of current technological significance. The first phase of the work encompasses the detailed structural, morphological and electrical characterisation of highly crystalline, homogeneous and conducting films of acid doped polyaniline, cast on glass substrates with the aid of a level surface. With suitable modification of the synthesis conditions it was possible to realise free standing, thicker films of polyaniline with prospects of application as conducting wires in electrical circuits.

The synthesis of polyaniline, embedded with metal nanoparticles, both in powder and thin film forms and their detailed linear and nonlinear optical studies constitute another major part of the first phase of investigations. The second phase of the work is devoted to exploring the energy storage capabilities of polyaniline and its composites. To start with, Li enriched polyaniline samples were synthesized and were used as cathodes for assembling Li ion cells. To improve the cell performance, composites of PANI with conventional inorganic cathode materials including $LiFePO_4$ and $LiMn_2O_4$ were synthesized and their electro chemical capabilities were studied. With the ambition of making all solid state, flexible Li-ion cells, lithiated PEO based solid electrolyte with good Li ion conductivity was synthesized and the Li-ion transport studies in this system were carried out. A detailed summary of these investigations follows.

The acid doped polyaniline, synthesized in the present work is found to be a highly conjugated system in which nonlinear optical effects are expected to be prominent. The nanocomposite samples of PANI, embedded with metal (Au and Ag) nanoparticles are found to show plasmonic properties such as surface plasmon resonance (SPR) and surface enhanced Raman scattering (SERS). The nonlinear optical studies on these nanocomposite samples (in powder and film forms), carried out using the Z-scan technique suggest that even in the presence of saturable absorption(SA), the PANI-Au nanocomposite powder sample shows about 50% optical limiting behaviour, compared to the 37% of pure PANI in which SA is absent. The highlight of the present work is the observation of the switching behavior from saturable absorption (SA) to reverse saturable absorption (RSA) in PANI-Ag and PANI-Au films as the laser fluence is increased and this observed switching extends ample scope for applications in optical switching devices. These composite samples are also found to be quite stable, since the structural and optical properties are found to remain the same over a period of more than six months.

The second phase of the research work highlights the investigations carried out to assess the suitability of using *n*-Butyllithium, a cost effective substitute for expensive counterparts like $LiPF_6$ and $LiBF_4$, for synthesizing Li substituted polyaniline to be used as the cathode active material in rechargeable Li ion cells. The structural analysis confirms the enhanced crystallinity/order in Li substituted PANI samples compared to pure PANI. The coin cells assembled using Li substituted PANI as cathode active material show quite good electrochemical behaviour. Specific capacity close to the expected theoretical capacity has been obtained for all the assembled cells. All the cells show excellent columbic efficiency around 98% and stable charge discharge cycling behaviour up to 50 cycles. The pouch cells assembled using lithiated PANI as cathode are found to hold the open circuit voltage (OCV) even when bent up to 90^0 from the initial state. This will open up a new methodology to realize all solid state, flexible and environmentally friendly, polymer-based lithium ion cells. The capacity of the lithiated PANI based cells has to be improved still further to meet the current industrial standards. For that, lithiated PANI (LIPO) - $LIFePO_4$ (9:1 ratio) and LIPO- $LiMn_2O_4$ (9:1 and 8:2 ratios) composite electrodes based Li-ion cells were assembled and

detailed electrochemical characterization was carried out. The average voltage of these cells is around 3.3 V. The cells are found to show the highest discharge capacity around 52 mAh/g and columbic efficiency around 97% and have got tremendous capacity retention over 50 cycles. Unlike pure $LiMn_2O_4$ based cells with poor cyclability due to Jahn–Teller distortion, LIPO-$LiMn_2O_4$ (LiMO) based cells have been found to be free of this distortion to a significant extent and show healthy cycling stability, due to the presence of lithiated PANI in the composite cathode material. The present work highlights a novel but simple approach to nullify the Jahn Teller distortion in $LiMn_2O_4$ by properly mixing it with lithiated PANI to function as the cathode material. On optimizing the *n*-BuLi doping concentration and LIPO- $LiFePO_4$/ $LiMn_2O_4$ mixing ratios, polymer-based Li-ion hybrid cells having promising energy density, capacity retention and eco friendliness with structural flexibility can be realized.

With the vision of assembling all solid state Li-ion cells, attempts were carried out to develop a solid polymer electrolyte with ionic transport properties comparable with those of conventional liquid electrolytes. Lithium enrichment was achieved in the polymer PEO by doping with the solution of *n*-Butyllithium in hexanes (*n*-BuLi). On doping with *n*-BuLi the Li-ions get intercalated into the PEO structure and displace the polymer chains, leading to a decrease in crystallinity which in turn improves the ionic conductivity considerably. The improvement in Li-ion conductivity with increase in *n*-BuLi doping concentration is found to be quite remarkable and the maximum ionic conductivity obtained is around 1.53×10^{-3} S/cm which is close to that of conventional liquid electrolytes. The present results have opened up novel means to correlate the polymer crystallinity with the dopant concentration and ionic transport properties and highlight the prospects of developing all solid state Li-ion cells using *n*-BuLi doped PEO as the solid electrolyte.

10.2 Future Prospects

Nonlinear optical studies of PANI-Au/Ag nanocomposite samples offer ample scope for further investigations by changing the atomic percentage of gold/silver in the nanocomposites and the synthesis conditions of PANI. By optimizing these parameters it may be possible to get optical limiting

efficiency close to 80%. It is generally difficult to obtain nanocomposite film samples with sufficient transparency to carry out nonlinear studies. The observed switching from SA to RSA in the PANI-Au/Ag nanocomposite films extends application prospects in the design of optical switching devices. The switching behavior detected, specifically in the nanocomposite film samples is of high technological relevance, since it offers the possibility of direct application of these films as optical switches.

The cells assembled out of lithiated PANI cathodes are found to be capable of showing stable cycling behaviour over 50 cycles and it may not be surprising if these cells are found to withstand 1000 - 2000 charge discharge cycles without significant capacity loss. The lithiated PANI based pouch cells are capable of holding the open circuit voltage even when they are bent up to 90^0 from the initial state. This opens up a new methodology to realize all solid state, flexible and environmentally friendly, polymer-based lithium ion cells. The observation that with 10% addition of $LiFePO_4$ to lithiated PANI, it is possible to obtain impressive charge discharge curves resembling those of the cells based on transition metal oxide cathodes highlights the prospects of designing polymer-based cells with improved capacity and charge discharge behaviour with the added advantage of constructional flexibility in cell design. The capability of lithiated PANI to arrest the inherent Jahn-Teller distortion associated with $LiMn_2O_4$ cathode, established through the present work, points out that, $LiMn_2O_4$ can be welcomed back in to the category of potential cathode materials for realising commercial grade, eco-friendly Li-ion cells.

The *n*-BuLi doping concentration can be optimized further to get Li enriched PEO based solid electrolyte samples with still higher ionic conductivity. Complete impedance characterisation starting from μHz frequencies and the temperature variation studies of ionic transport can be carried out in Li enriched PEO samples to assess the application prospects in the design of all solid state Li-ion cells capable of operation at elevated temperatures.

The combination of organic-inorganic hybrid cathode materials and solid polymer electrolytes can be suitably utilised to realise all solid state, flexible and environment friendly Li-ion cells with desired energy density and excellent cycle life.

It seems appropriate to conclude the thesis with the following quote about polyaniline.

> "Polyaniline, after its rediscovery in the 1980's has travelled the arduous route from laboratory benches to commercial markets in less than a decade's time. The possibilities disclosed by its unique characteristics are challenging, fascinating and farsighted. The time may not be that far, before the versatile and vast potential of this unique polymer is genuinely established and effectively utilized in the designing of smart and functional devices to reign the future consumer markets with authenticity".

Appendix

Standard battery terminology

In order to study and evaluate the properties of the electrodes used in a secondary battery, International Union of Pure and Applied Chemistry (IUPAC) has introduced some standards and guidelines. Brief descriptions of these guideline are given below.

Charge capacity Q (SI unit: mAh or C)

The charge capacity is the total amount of charge obtainable from a cell.

$$Q = \int I(t)dt$$

Specific charge q (SI unit: mAh g^{-1} or Ah kg^{-1} or C kg^{-1})

The specific charge is the total charge obtainable under specified discharge conditions from a practical cell in one discharge cycle divided by the total mass of the cell (m_b).

$$\left|\frac{Q}{m_b}\right|$$

The specific charge is often incorrectly called charge density/ specific capacity.

Specific energy w (SI unit: Wh kg^{-1} or J kg^{-1})

The specific energy is the total electrical energy (W_c) obtainable from a cell in one discharge cycle divided by the mass of the respective cell (m_b). This quantity is often incorrectly called energy density.

$$w = \frac{W_c}{m_b}; \qquad W_c = \int U(t)\, I(t) dt$$

Energy density W_V (SI unit: Wh dm^{-3} or J dm^{-3})

The energy density is the total electrical energy obtainable (W_c) from a cell under specified discharge conditions divided by the volume of the cell.

$$W_V = \frac{W_c}{V}$$

Specific power *p* (SI unit: W kg^{-1})

The specific power is the capability to deliver power per mass of a primary or secondary battery. The specific power of a cell depends on the discharge current and decreases during discharge. The specific power is often incorrectly called power density.

$$p = \frac{IU^o}{m_b}$$

Power density P_v (SI unit: W dm^{-3})

The power density is the power divided by the volume of the cell

$$P_V = \frac{IU^o}{V}$$

Coulombic Efficiency, Φ_Q (SI unit: %)

For secondary cells, the Coulomb efficiency represents the ratio of charge released during the discharge (Q_{dis}) to the charge necessary for charging the battery (Q_{ch}).

$$\mathbf{\Phi}_Q = \frac{Q_{dis}}{Q_{ch}} \times 100$$

Both Q_{dis} and Q_{ch} are obtained by integrating the respective currents over the discharging and charging time, respectively. They depend on the conditions for charging and discharging.

The charge-discharge rate C-rate (SI unit: h^{-1})

When electrochemically cycling a cell, the term charge-discharge rate or C-rate ($C/\Delta t$) is often employed to explain the time frame for either one full charge or discharge. C denotes either the theoretical charge capacity of a cell or battery (Ah) or the nominal capacity of a cell or battery. A 'C' rate of C/10 means that the cell is charged/discharged with a current which theoretically allows a full charge/discharge of the cell in 10 hours.

Irreversible capacity loss (SI unit: %)

It is also important to define how much capacity is lost after each cycle. Irreversible capacity loss is therefore explained by the following equation:

$$Irreversible\ Cap.Loss = \frac{Char.cap.(n) - dischar.cap.(n)}{charge\ cap.(n)} \times 100$$